BRNO UNIVERSITY OF TECHNOLOGY
VYSOKÉ UČENÍ TECHNICKÉ V BRNĚ

FACULTY OF CHEMISTRY
FAKULTA CHEMICKÁ

INSTITUTE OF PHYSICAL AND APPLIED CHEMISTRY
ÚSTAV FYZIKÁLNÍ A SPOTŘEBNÍ CHEMIE

NOVEL ANTIBACTERIAL COLLAGEN SCAFFOLDS FOR REGENERATIVE MEDICINE
NOVÉ ANTIBAKTERIÁLNÍ KOLAGENOVÉ NOSIČE PRO REGENERATIVNÍ MEDICÍNU

MASTER'S THESIS
DIPLOMOVÁ PRÁCE

AUTHOR
AUTOR PRÁCE
Bc. Jana Dorazilová

SUPERVISOR
VEDOUCÍ PRÁCE
doc. Ing. Lucy Vojtová, Ph.D.

BRNO 2018

VYSOKÉ UČENÍ TECHNICKÉ V BRNĚ
FAKULTA CHEMICKÁ

Zadání diplomové práce

Číslo práce:	FCH-DIP1126/2017
Ústav:	Ústav fyzikální a spotřební chemie
Studentka:	**Bc. Jana Dorazilová**
Studijní program:	Chemie pro medicínské aplikace
Studijní obor:	Chemie pro medicínské aplikace
Vedoucí práce:	**doc. Ing. Lucy Vojtová, Ph.D.**
Akademický rok:	2017/18

Název diplomové práce:

Nové Antibakteriální kolagenové nosiče pro regenerativní medicínu

Zadání diplomové práce:

1. Lite. rešerše na téma kolagen a antibakteriální aditiva
2. Příprava 3D kolagenových pěn s antibakteriálním činidlem
3. Fyzikálně–chemické a biologické testování připravených vzorků
4. Vyhodnocení, diskuze a závěr

Termín odevzdání diplomové práce: 7.5.2018

Diplomová práce se odevzdává v děkanem stanoveném počtu exemplářů na sekretariát ústavu. Toto zadání je součástí diplomové práce.

Bc. Jana Dorazilová student(ka)	doc. Ing. Lucy Vojtová, Ph.D. vedoucí práce	prof. Ing. Miloslav Pekař, CSc. vedoucí ústavu

prof. Ing. Martin Weiter, Ph.D.
děkan

V Brně dne 31.1.2018

ABSTRACT

This master's thesis deals with the characterisation of 3D porous collagenous sponges enriched with selected antibacterial agents. The literature part of the thesis focuses on the overview of biomaterials and biopolymers with the emphasis on collagen and chitosan, outlines the antibacterial properties of nanoparticles and reviews current aspects of using selenium nanoparticles as an antibacterial agent.

For the purpose of this work, two types of antibacterial additives were used – biopolymeric chitosan and selenium nanoparticles. Preparation of 3D porous structure was achieved using the freeze-drying method. Mechanical properties of prepared biopolymeric matrices were improved by chemical crosslinking in the presence of carbodiimide.

Predominantly physiochemical methods were used for characterization of prepared collagenous sponges. For microstructure analysis, pore size determination, visualisation of nanoparticles and their distribution inside the porous structure, scanning electron microscopy (SEM) with energy dispersive x-ray optical analysis (EDX) was used. Parameters such as total porosity, swelling ratio, weight loss during degradation in water and enzymatic environment were evaluated by suitable gravimetric methods. Fourier-transformed infrared spectroscopy with attenuated total reflectance (ATR-FTIR) was used to determine changes in the chemical structure of collagenous matrices before and after addition of the antibacterial agents. Percentage release of nanoparticles was evaluated using optical emission spectroscopy with inductively coupled plasma (ICP-OES). Evaluation of antibacterial properties of tested samples was carried out mainly by the agar diffusion disk method and the macrodilution broth method.

In the conducted research we were able to determine the influence of selected antibacterial additives on the physiochemical properties of 3D collagenous matrices. Their antibacterial activities showed a positive effect on bacterial inhibition of both chitosan and selenium nanoparticles with respect to their concentrations. The designed materials could be further utilized for bio-medicinal applications, especially in the field of soft tissue regeneration.

KEYWORDS

Regenerative medicine, collagen, EDC/NHS crosslinking, freeze-drying, antibacterial agents, chitosan, selenium nanoparticles.

ABSTRAKT

Tato diplomová práce se zabývá charakterizací 3D porézních kolagenových pěn obsahující vybraná antibakteriální činidla. V literární části jsou shrnuty dosavadní poznatky o biomateriálech a biopolymerech se zaměřením na kolagen a chitosan. Dále jsou v ní popsány antibakteriálních vlastnosti nanočástic v kontextu s využitím selenových nanočástic jako antibakteriální činidla.

Pro potřeby této práce byla vybrána antibakteriální aditiva dvojího typu – biopolymerní chitosan a selenové nanočástice. 3D porézní struktury bylo dosaženo metodou lyofilizace. Mechanické vlastnosti biopolymerní matrice byly podpořeny síťováním v prostředí chemického síťovadla na bázi karbodiimidu.

K charakterizaci připravených kolagenových pěn byly použity především fyzikálně-chemické metody. Na analýzu mikrostruktury a velikosti pórů, vizualizaci nanočástic a jejich distribuci v testovaných materiálech byla využita rastrovací elektronová mikroskopie (SEM) spolu s energiově disperzní analýzou (EDX). Parametry jako je porozita, botnací poměr, úbytek hmotnosti při degradaci ve vodném prostředí a v prostředí enzymů byly zjištěny vhodnými gravimetrickými metodami. Ovlivnění chemické struktury kolagenové matrice před a po přidání antibakteriálních aditiv bylo sledováno za pomocí metody zeslabeného úplného odrazu infračervené spektroskopie s Fourierovou transformací (ATR-FTIR). Procentuální uvolnění nanočástic z testovaných vzorků bylo sledováno pomocí optické emisní spektroskopie s indukčně vázanou plazmou (ICP-OES). K zhodnocení antibakteriálních vlastností testovaných materiálů byly použity především difúzní agarová disková metoda a makrodiluční bujónová metoda.

Provedeným výzkumem jsme zjistili vliv přídavku antibakteriálních činidel na strukturu a některé vlastnosti 3D kolagenových matric. Výsledky antibakteriálních testů ukázaly pozitivní vliv chitosanu i selenových nanočástic na inhibici růstu bakterií v závislosti na koncentraci přidaných aditiv. Navržené materiály mohou být využity pro biomedicínské aplikace především v oblastech zabývající se regenerací měkkých tkání.

KLÍČOVÁ SLOVA

Regenerativní medicína, kolagen, EDC/NHS, síťování, lyofilizace, antibakteriální činidla, chitosan, selenové nanočástice.

DORAZILOVÁ, J. *Novel Antibacterial Collagen Scaffolds for Regenerative Medicine*. Brno: Brno University of Technology, Faculty of chemistry, 2018. 92 s. Supervisor doc. Ing. Lucy Vojtová, Ph.D.

DECLARATION

I declare that the diploma thesis has been worked out by myself and that all the quotations from the used literary sources are accurate and complete. The content of the diploma thesis is the property of the Faculty of Chemistry of Brno University of Technology and all commercial uses are allowed only if approved by both the supervisor and the dean of the Faculty of Chemistry, BUT.

.....
student's signature

ACKNOWLEDGMENTS

I would like to express my sincere gratitude to my supervisor doc. Ing. Lucy Vojtová, Ph.D. and her research team for the continuous support of my master's thesis and related research. Besides my supervisor, I would like to thank my advisor Ing. Johana Babrnáková, for her patience, motivation and guidance during the research. My sincere thanks also go to Ing. Kristýna Šmerková, Ph.D. and Ing. Silvia Kočiová for antibacterial testing and doc. Ing. Pavel Diviš, Ph.D. for ICP-OES measurements. This work was supported by the CEITEC 2020 (LQ1601) with financial support from the Ministry of Education, Youth and Sports of the Czech Republic under the National Sustainability Programme II.

CONTENT

1 INTRODUCTION

Regenerative medicine has the potential to replace traditional ways of medicine in recovering damaged tissue. Chronic organ failure is one of the main challenges in current medicine. The reasons behind this are the increasing number of patients on transplantation waiting lists, the shortage of graft tissue donors, the postoperative limitation of the patient with the need for lifelong use of immunosuppressive and clot-thinning medicaments, and the chance of getting transmitted disease. Among the most transplanted organs are kidneys, livers, and hearts, respectively.[1] Lack of donors is also critical in the field of skin transplantation. Donors of autologous skin tissue are needed when the defect exceeds 50–60 % of the total body surface area. Example of such a severe injury could be third-degree burn damage.[2] These injuries are connected with life-threatening complications such as hypovolemia (decrease in the volume of blood and body fluids) and infection. There are a lot of drawbacks in traditional medicine that could be resolved by the methods of regenerative medicine.

One of the approaches within the field of regenerative medicine involves the fabrication a 3D porous material, which would imitate the physiological environment of the body tissues. Collagen as the most abundantly represented biopolymer in the extracellular matrix is profusely used to fulfill the needs of regenerative medicine. With the proper treatments, the resulted scaffold can exhibit suitable mechanical properties, stability and a certain biocompatibility required for regeneration of damaged tissue. By collagen scaffold modification using antibacterial agents, the scaffold is able to provide not only a supportive environment for cell proliferation and differentiation but also is able to resist microbial invasion. Preventing the microbial invasion could accelerate the healing process of wounded tissue.

Using nanoparticles as antibacterial agents has proven to be one of the effective ways to deal with the existence of superbugs – bacteria strains that are resistant to antibiotics. Currently the most used types of nanoparticles are metal-based, e.g. silver or gold nanoparticles. Using metal nanoparticles has raised some concerns since metal is a foreign element to the human body and could interfere with the physiological environment. Therefore, using more biogenic types of nanoparticles, e.g. selenium, could lower the potential toxicity of nanoparticles.

2 THE CURRENT STATE OF THE ART

2.1 Regenerative Medicine

Although no official definition has been given as to what one should imagine under the term regenerative medicine (RM), it is an interdisciplinary field of science whose main point of interest is through the manipulation of cells, natural or artificial scaffolding materials, growth factors, gene manipulation, or combinations of these elements to restore or re-establish, maintain or improve normal tissue function.[3−5] The process of body part regeneration can occur *in vivo* or *ex vivo*.[3] RM can be further divided into three main fields (Figure 1) – tissue engineering, cellular therapies and gene therapies. Tissue engineering is specific for using natural and artificial materials to create carriers mainly for cells, so-called scaffolds. Cells are ex vivo placed onto the scaffold, where they proliferate and differentiate. The prepared scaffold is then inserted into the body.[3] Cellular therapies use autologous (from the patient) or allogenic cells (from another individual of the same species) for the treatment of a disease. Stem cells can be either obtained from bone marrow, umbilical cord blood and other sources, or can be "reprogrammed" from skin fibroblasts or adipocytes (known as induced pluripotent stem cells). Gene therapies are based on the modification of the expression of an individual's genes, or repair of the abnormal genes by manipulation with specific nucleic acid (DNA or RNA). Carriers of the nucleic acids are called vectors and may be of a viral or non-viral nature.[6]

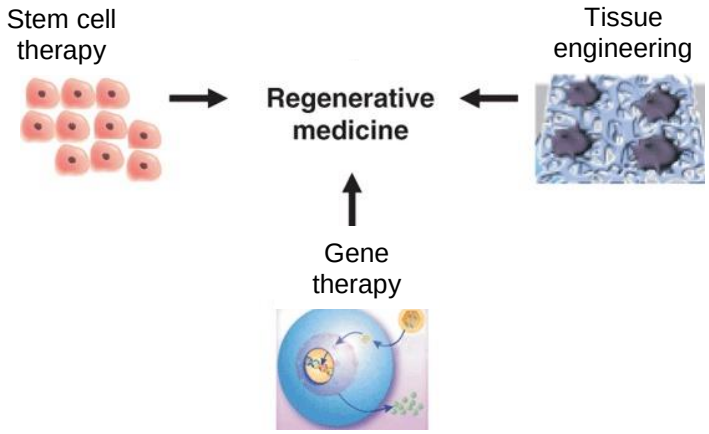

Figure 1: Fields of regenerative medicine.[7] (Modified)

2.1.1 Structure of Human Skin

Skin is the largest organ of the human body covering on average an area of 1.8 m2 (varying from person to person based on their weight and height) with thickness ranging from 1.5 to 40 mm and weight about 5 kg. The main function of the skin is protection against microbial invasion, and thermal, chemical, mechanical and osmotic damage. The skin also plays an important role in regulation and sensation. The two main cellularised layers of skin separated by a base membrane are known as epidermis and dermis. Underneath these two layers, the hypodermis is located. The epidermis is formed of stratified squamous epithelium, which ranges from 0.1 to 1 mm in thickness, and consists mainly of keratinocytes (95 %). The remaining 5 % belong to melanocytes, Merkel cells, and Langerhans cells. The stratified squamous structure is made by a process of keratinocyte stratification, where keratinocytes are pushed upwards from the base membrane after differentiation to form an integrated keratin. The second most represented cells in the epidermis, melanocytes, are primarily responsible

for the coloration of the skin. The primary function of the epidermis is protection against microorganisms and electrolyte loss. The dermis is a vascularised and innervated layer of the skin and is about 10 to 40 times thicker than the epidermis. The dermis consists of 80 % water, elastin and collagen fibres, glycosaminoglycans, hair shafts and sweat glands. The dermis provides tensile strength and elasticity to the skin. Its main function is thermo-regulation, sensation, and healing. The hypodermis contains a large amount of adipose tissue. Its main function is thermoregulation and mechanical properties.[8, 9]

2.1.2 Skin Tissue Regeneration *in vivo*

In vivo wound healing is a long-term process that goes through a series of phases, namely haemostasis, inflammation, proliferation and remodelling (Figure 2). Once the skin is injured, clot formation through haemostasis occurs to stop the blood flow. The clotting mechanism is elicited by platelets, whose production is activated primarily by thrombin. Due to the accumulation of chemicals and immunity cells (mostly macrophages and neutrophils), the inflammation process occurs in the wound, killing microbes and preventing further infection. The proliferative phase involves the proliferation of epidermal cells about 3 cm from the point of origin in all directions. Fibroblasts infiltrate the wound and start the synthesis of collagen to activate the formation of new tissue.[8, 10, 11] Wound closure is the most problematic stage of skin tissue regeneration causing wound contraction and scar formation. Wound contraction is mainly caused by contractile cells, such as myofibroblasts. In the presence of alpha smooth muscle actin, fibroblasts differentiate into myoblasts containing actin filaments that are primarily responsible for wound contraction.[11] These cells also produce highly oriented collagen fibres leading to the formation of a scar in the macroscopic view.[12] In scar tissue, collagen aligns in a single direction parallel to the basement membrane, with loosely packed fibrils of uncontrolled diameter, unlike the basket weave-like pattern with normal fibril characteristics in fully healed tissue.[13, 14] Stages of wound healing may alter due to varying severity of the wound, e.g. bedsore and burn wounds may have infection, necrosis, and agglutination. In healthy individuals, the wound should heal within 2–3 weeks followed by the remodelling phase which may last up to two years. Chronic wounds may occur if there is a loss of balance in the physiological mechanism of healing. A period of 6–8 weeks is the cut off time beyond which the wound is categorized as a chronic or non-healing wound.[11] Overall, the larger the defect is, the more difficult is the healing of the wound. When a deep wound (involving epidermis and dermis) exceeds 4 cm in diameter, it will never heal by itself and a graft needs to be used.[9]

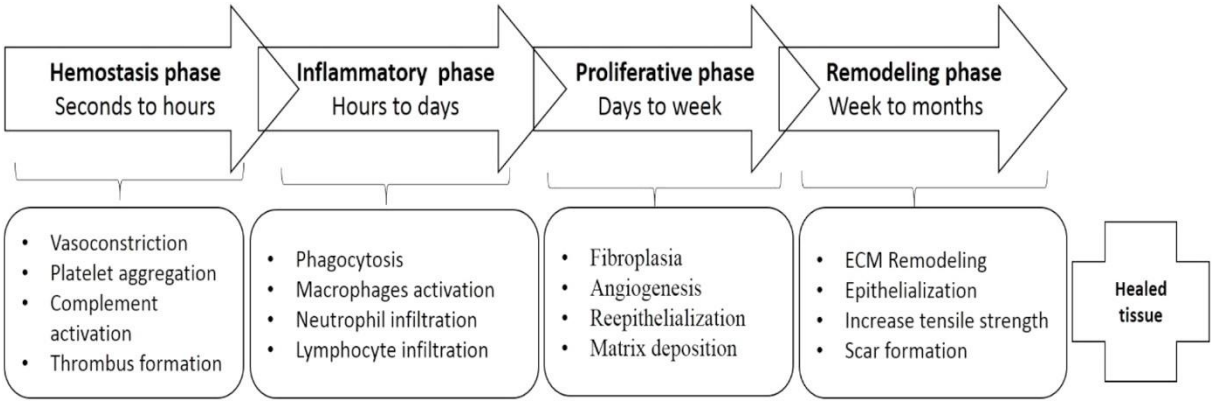

Figure 2: Stages of normal wound healing.[11]

2.2 Overview of Biomaterials

Biomaterials are defined as materials whose primary intention is to interface with biological systems to evaluate, treat, augment or replace any tissue, organ or their function.[15] Three individual groups can be distinguished: natural polymers, synthetic polymers, and composites. Each of these groups finds a quite different use in RM, according to the damaged tissue.

2.2.1 Types of Biomaterials

Natural polymers include proteins such as collagen, gelatin, elastin, actin, keratin, and albumin. A highly used group of natural polymers are also polymeric saccharides and their derivatives; chitin, cellulose, silk and hyaluronic acid are the most used ones. Using natural polymers offers many advantages. These polymers possess excellent biocompatibility, the products of biodegradation are non-toxic metabolites and overall, they are easily accepted by biological systems. However, their structure and mechanical properties are poor compared to synthetic polymers and often further modification (e.g. crosslinking) is needed to stabilize the prepared material. Moreover, interference with surrounding tissues can cause a reaction of the immune system.[5, 16]

The most used synthetic polymers include poly(glycolic) acid, poly(lactide) acid, copolymers above-mentioned, polycaprolactone and polyethylene. They are easily processable into different sizes and shapes. Their physiochemical properties (crystallinity, molecular weight, etc.) can be easily modified by incorporating functional groups, selecting different monomers, and alternating reaction conditions. Overall, they can be designed to fulfill specific needs.[5,16] *In vivo,* synthetic polymers undergo hydrolytic degradation, which is easier to simulate and operate with than enzymatic degradation of natural polymers.[16] Products of degradation are the main disadvantage synthetic polymers have, as they are responsible for a local decrease of pH. Low pH accelerates degradation and most importantly induces a local inflammatory reaction.[16, 17]

Composites are biomaterials consisting of two or more materials mentioned above. These types of materials are taking the advantage from each of the composed materials to produce a better scaffold.[16]

2.2.2 Properties of Biomaterials

One of the key parts of RM is creating a functional scaffold, with sufficient 3D structure suitable for the proliferation and differentiation of cells, made of a material properly imitating the environment that is natural for cells. The majority of mammalian cell types are anchorage-dependent, meaning they will die if an adhesion substrate is not provided. Therefore, the scaffold must provide a suitable substrate for cell attachment, proliferation, differentiation, and migration, and must not permit the transport of nutrients and biological signaling factors. Great emphasis must also be put on the properties of scaffolding materials. The key properties are mentioned below. [4, 5, 16]

- *Biocompatibility*. The scaffold inserted in the body integrates with surrounding tissue, thus should perform its function without causing a harmful immune or inflammatory reaction, and should not be cytotoxic. If the scaffold is nontoxic and degradable, new tissue will eventually replace it. When the scaffold is toxic, rejection of the scaffold and cell apoptosis in the surrounding tissue may occur.

- *Biodegradability*. In a reasonable amount of time, every material used in RM should disintegrate without the need for surgical removal. Products of the degradation should be non-toxic and should be eliminated from the body through natural metabolic processes. Ideally, the degradation rate is set to match the rate of tissue regeneration. Two different models of biodegradation are distinguished *in vivo*: hydrolytic degradation mediated by physiological water and enzymatic degradation mediated by specific enzymes.
- *Mechanical and structural properties*. The mechanical properties of the scaffold should match those of the tissue at the implantation site. It is important to produce a scaffold with defined parameters of the porous structure, such as pore size, distribution, and interconnectivity. Pore size mainly determines the efficiency at which cells proliferate into the scaffold. If the pores are too small, cells do not penetrate the structure, in opposite cases the pores are too large, and cells do not attach to the scaffold. Moreover, the right porous structure enhances vascularisation and metabolite transport, thus it helps tissue to fully regenerate.
- *Imitating a natural environment for cells*. Mimicking the native extracellular matrix (ECM), an endogenous substance that surrounds cells, allows cells to bind into tissues and provide signals that aid cellular development and morphogenesis.

2.2.3 Design and Methods of Fabrication

Different designs of polymeric scaffolds have been used in the field of RM. Each of these designs is used in a different way according to the damaged tissue (Figure 3).[4]

- *Three-dimensional (3D) porous matrix*. A 3D porous matrix is the generally used design in the field of regenerative medicine. Serving as an ECM analogue, it provides a suitable microenvironment for optimal cell growth and function. Suitable porous and interconnected networks are essential for cell penetration and nutrients, and waste transportation. Factors including porosity and pore morphology influence cellular colonization rate, organization, angiogenesis and the release of biofactors.[18, 19]
- *Nanofibre mesh*. Structures of fibre meshes are typically non-woven membranes composed of consecutive layers of randomly aligned nanofibers with porosities comparable to the diameters of the fibres. The production of fibres with smaller diameters significantly increases the surface area to volume ratio and allows superior mechanical performance (stiffness and tensile strength) to be obtained. In fact, the smaller the dimension is, the lower the probability of occurrence of a local defect is. This is the reason that nanofibres possess such good mechanical properties.[20]
- *Hydrogel*. 3D networks composed of hydrophilic polymers held together via chemical or physical intra- or intermolecular interactions are called hydrogels. Their key property is the ability to absorb huge amounts of water or biological fluids without dissolving. High hydrophilicity is caused by the existence of hydrophilic functional groups such as carboxyl, amide, amino and hydroxyl groups. In tissue repair applications, these hydrogels have attracted increasing attention because of their similarity to the ECM and their injectable capability. Injectable hydrogels can fit any shape of target defects and entrap cells or other biological molecules easily.[21]

– *Microspheres*. Microspheres are defined as organic or inorganic, spherical particles ranging from 1 to 1 000 μm in diameter. They can be used for drug or bioactive molecule encapsulation. Microspheres have been extensively used in drug delivery applications largely because of their ability to serve as excellent controlled release vehicles. They can be packed together, alone or in combination with other materials, to yield porous 3D structures that can serve the purpose of RM.[22]

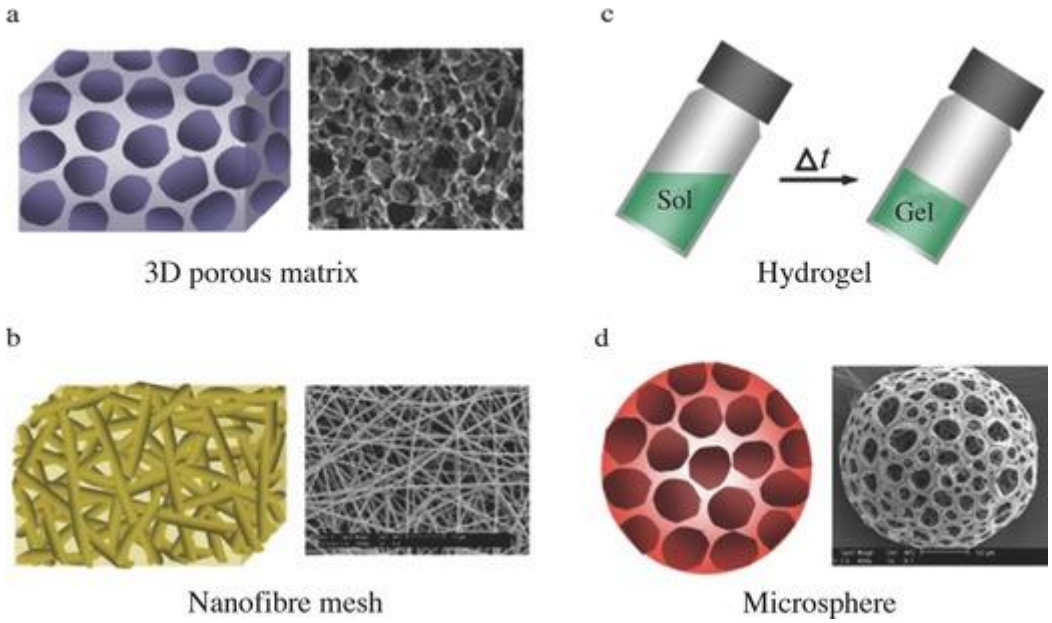

Figure 3: Different forms of polymeric scaffolds.[23]

These designs of polymeric scaffolds can be obtained through a variety of techniques. The most used ones are summarized below.

– *Freeze-drying*. The technique of freeze-drying is based on dissolving biomaterial in water followed by freezing the material, thus ice crystals are formed within the material. Ice crystals serve as porogens and their size can be controlled by the freezing rate (the faster the freezing is, the smaller the pores that are formed), and pH. Ice crystals are then removed by sublimation. The freeze-drying process involves three major steps: (1) Freezing the solution to low temperatures (-70 °C to -80 °C). (2) The primary drying process involves lowering the pressure to a few millibars through partial vacuum and removing of ice within the material by direct sublimation. (3) The secondary drying process involves removal of the unfrozen water within the material by desorption. The advantages of the freeze-drying method are in the usage of water and ice crystals as porogens instead of organic solvents. The disadvantages are in the expense and in the relative impossibility to prepare a defined porous structure. Through the freeze-drying method, 3D porous scaffolds are made.[24, 25]
– *Phase separation*. This technique works on the same principle as the freeze-drying method, with the difference that an organic solvent is used instead of water. Thereby it is necessary to add the extra step of leaching the organic solvent out of the scaffold. Without the leaching step, it would not be possible to incorporate bioactive molecules or cells into the scaffold.[25]

- *Salt leaching*. The principle of this method is in preparing a biomaterial solution with salt crystals of a specific diameter. Salt crystals serve as porogens. After evaporation of sufficient solvent, the biomaterial-salt matrix is immersed in water, where the salt crystals are dissolved, leaving empty pores behind. The pore size and porosity are easily controlled by varying the sizes and the number of salt particles, respectively. The product of this method is a 3D porous scaffold.[24]
- *Gas forming*. This method of preparation uses high-pressured CO2. The biomaterial is saturated by CO2 at high pressure. Lowering the pressure back to atmospheric level after saturation creates pores within the scaffold resulting in the creation of a 3D sponge-like porous scaffold. Just like the freeze-drying method, the main advantage is in the elimination of organic solvent usage and the main disadvantage is the relative difficulty of creating the intended pore connectivity and size. By the gas forming method, scaffolds with porosity of up to 93 % and pore sizes of up to 100 μm can be fabricated.[24]
- *Electrospinning*. The technique of electrospinning is used for fabrication of fibres with diameters ranging from 10 to 1000 nm. Fibres are made via the effect of an electric field. High voltage is applied to a capillary tube filled with polymer solutions. When the intensity of the electrical field is increased, the charge repulsion will overcome the surface tension to form a jet. The solvent evaporates to form fibres as the jet travels to the collector. Fibres can be modified by regulating parameters including viscosity and conductivity of the solution, hydrostatic pressure, the distance between the tip and the collector, etc. The high voltage makes it an unsuitable technique for natural polymers.[25, 26]

2.3 Collagen

Collagen is the most abundant protein of the ECM in mammals and plays a dominant role in maintaining the biological and structural integrity of ECM.[5] Collagen forms one-third of total proteins in humans and accounts for three-quarters of the dry weight of skin.[27] Considering collagen is a major component of ECM, it makes collagen an ideal material for application in RM. Being the most widespread protein in nature, there are many sources of extraction.[5] Collagen can be extracted from rats, cattle and pigs. Each source of collagen gives the protein different mechanical and physical properties. Bovine collagen has been the most used source of collagen, however, in recent years there has been an increasing number of studies using a different source of collagen, e.g. fish collagen.[28, 29]

Collagen is highly versatile in terms of physical forms as reviewed in [5]. Collagen-based materials can be fabricated into, for example, injectable gels, films, meshes, and fibres. Applications of collagenous scaffolds prepared in these ways include 3D cell culture, bone and cartilage repair, vascular and cardiovascular grafts, skin grafts, corneal defects and wound dressing.

2.3.1 Structure and Constitution

Collagen is a group of proteins with similar structure and properties. To this day, at least 22 different collagens composed of at least 46 distinct polypeptide chains have been distinguished.[5, 27] In the human body, 80–90 % of the collagen belongs to types I, II and III. These are fibrillar collagens about 300 nm long.[30]

The structure of collagen consists of three parallel polypeptide α-chains in a left-handed, polyproline II-type (PPII) helical conformation coil about each other to form a right-handed triple helix with a pitch approximately 8.6 nm.[5, 27, 31] These α-chains consist of more than 1000 amino acids each.[31] Glycine is a key amino acid in the structure, stabilizing PPII helices. Due to its stabilizing effect glycine makes up every third amino acid in a repeating sequence of XaaYaaGly, where XaaYaa can be any amino acid.[27] Amino acids in given places are frequently proline (28 %) and hydroxyproline (38 %). The most common triplet is proline, hydroxyproline, glycine (10,5 %), respectively.[27, 31] Another important amino acid member of the collagen primary structure is hydroxylysine. Hydroxylysyl residues are making it possible for sugar components to be attached to the structure.[31]

The individual triple helices described above are known as tropocollagen and are considered as a tertiary structure of the collagen molecule.[27] Tropocollagen has an average molecular weight of approximately 300 kDa, a length of 300 nm with a diameter of 1.5 nm.[31] The quaternary structure of collagen is considered to be tropocollagen molecules arranged into fibrils with distinct periodicity. The self-assembly process is part of fibrillogenesis creating fibrils 10 to 500 nm in diameter. The complicated structure of collagen (Figure 4) gives it unique physiochemical and biomechanical characteristics compared to synthetic polymers.[31]

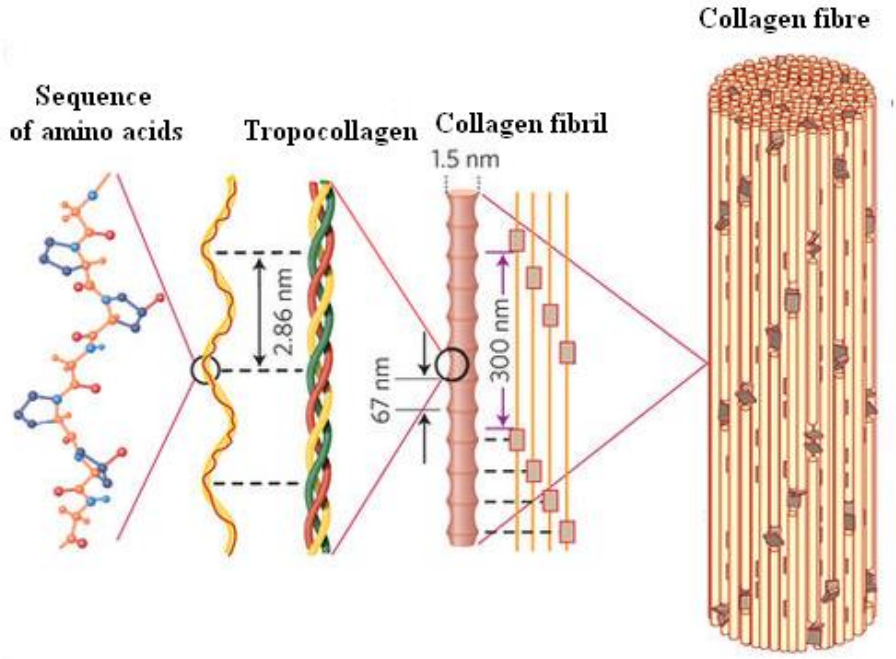

Figure 4: Hierarchical structure of collagen molecule.[32] (Modified)

2.3.2 Physiochemical and Biological Properties

Collagen type I is abundant in vertebrate tissues and is usually extracted from the skin and tendons of the source.[5] With a carbohydrate content of less than 1 %, this type of collagen can be considered as a glycoprotein. The sugar components are single galactose units or disaccharide of galactose and glucose units.[31] Because of its abundance, ubiquity, and biocompatibility, collagen type I is the most commonly used type of collagen in RM. The main advantages and disadvantages of using collagenous matrices in RM are summarized in Table 1.

Table 1: Properties of collagenous matrices used in RM.[33]

Advantages	**Limitations**
Biocompatible	No inherent rigidity
Minimal potential for antigenicity after removal of telopeptides	Potential for antigenicity through telopeptides
Adhesive	
Fibrous, cohesive and nonfriable	
Can be combined with other materials	
High porosity	

Collagen fibres appear to be the most crucial part in the induction of regeneration of tissues due to the participation of collagen fibres in communication processes between cells and the ECM. On the surface of collagen fibres several peptide motives are located. These motives mediate adhesion to cell integrins. These bindings between collagen and cells via integrins mediate changes in cell phenotype.[12]

As a structural protein and key member of EMC, collagen is resistant to proteolysis. *In vivo* collagen is degradable via enzymes called collagenases. Collagenases are enzymes from a family of Zn^{2+} matrix metalloproteinases (MMPs). Collagen types I–III are hydrolyzed by MMP-1, MMP-2, MMP-8, MMP-13, and MMP-14.[31, 34, 35] The activity of the MMPs relies on three principles: (1) the ability to bind collagen molecules, (2) the ability to unwind the three α-chains and (3) the ability to cleave each strand of the triple helix.[36] Once a collagenous structure is scattered to fragments, gelatines and non-specific proteases biodegrade the rest.[35] The rate of the biodegradation can be further modulated by crosslinking techniques. In addition, the degradation products have been shown to induce a chemotactic attraction of human fibroblasts.[36]

Collagen is known for its low toxicity and immunogenic reactions due to the similarity in the amino acid sequence between species and the low content of aromatic amino acids. Immunogenicity meaning induction of an immune response. On the other hand, antigenicity, the existence of antibodies and interaction between the antibodies and the antigenic determinants or epitopes, is worse. Animals and humans can produce antibodies to three antigenic determinants in the collagen molecule: (1) the terminal determinants located in the non-helical telopeptide region (P-determinants), (2) the central determinant presented by the amino acid sequence in the helical section and (3) the tertiary triple-helix structure known as the helical α-determinants. Nevertheless, it has been shown that selective removal of the non-helical component from the molecule can suppress collagen's antigenicity. Moreover, chemical crosslinking also reduces the antigenicity.[31, 36]

2.3.3 Crosslinking

Collagen-based materials often undergo crosslinking to improve their structural and biomechanical properties. It is also a common strategy used in the fabrication of hybrid collagenous scaffolds with other biopolymers, e.g. chitosan. Native collagen possesses multiple inter- and intramolecular crosslinks, which help stabilize the protein's structure and improve its durability.[37] Collagen is naturally crosslinked by lysyl oxidase during the process of fibril formation.[31] However, during processes of extraction and purification collagen became mechanically and thermally unstable. Prepared scaffolds are prone to disintegrate upon handling and collapse under pressure from surrounding tissue *in vivo*. To re-establish biomechanical properties additional crosslinking is used.[31, 37]

Various methods are used to enhance the structural properties of collagen. These techniques can be divided into two main groups: [31, 37]

- *Chemical methods* (aldehydes, isocyanates, carbodiimides, etc.).
- *Physical methods* (ultraviolet irradiation, dehydrothermal treatments, etc.).

Overall chemical methods offer crosslinked scaffolds with highly enhanced biomechanical properties. The disadvantage of chemical crosslinking is the fact that most of the used chemical crosslinkers are cytotoxic and a further leaching step is needed. Therefore, physical methods could be a good alternative to chemical crosslinking. However, it has been proven these methods may cause denaturation of collagen.[38]

Using EDC (1-ethyl-3-(3-dimethylaminopropyl)-carbodiimide) in the presence of NHS (N-hydroxysuccinimide) as a crosslinking agent has been proven to be one of the most successful chemical crosslinking methods utilized to crosslink the systems containing amino and carboxylic groups. EDC is used as an activator of carboxylic acid groups and NHS is used as a stabilizer to improve the crosslinking efficiency. EDC/NHS crosslinking is considered to be relatively non-cytotoxic. Cytotoxicity depends on the concentrations of crosslinking agents. Regarding these crosslinking agents' concentration, 0.5 mol/l has been proven to not reduce cell viability.[39]

The EDC/NHS crosslinking mechanism starts with the activation of the residual carboxylic acid groups by EDC to yield an O-acylisourea group. O-acylisourea groups alone in water environment undergo fast hydrolysis to regenerate the original -COOH group.[41] NHS is used to prevent this unwanted reaction. In the presence of NHS, O-acylisourea forms an NHS activated carboxylic acid group, which is highly reactive towards the amine group. This leads to the formation of an amide bond, so-called zero-length crosslinks. EDC is not incorporated in the matrix but it is converted to 1-ethyl-3-(3-dimethyl-aminopropyl)-urea.[40−42] Schematic view of the EDC/NHS crosslinking process is shown in Figure 5.

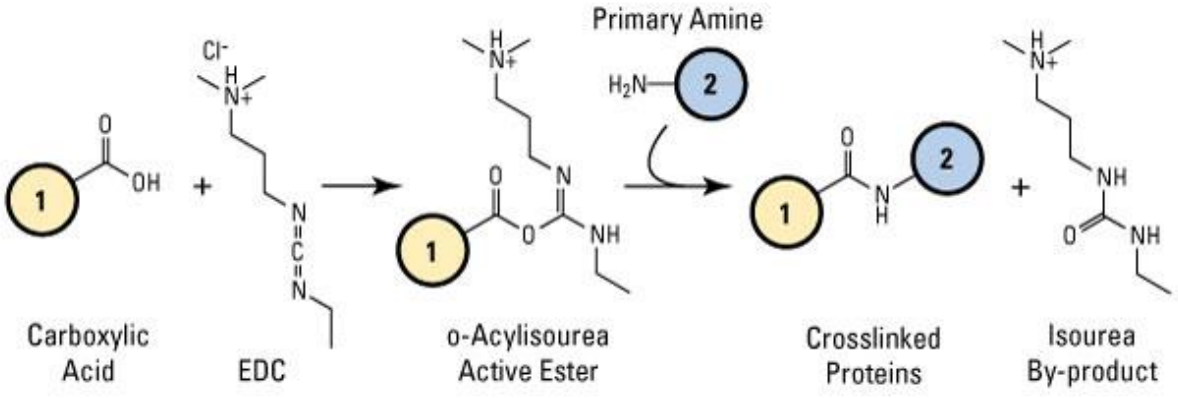

Figure 5: Schematic representation of crosslinking process with the EDC/NHS agent.[43]

2.3.4 Collagenous Materials in Skin Tissue Regeneration

Two fundamental approaches are used in obtaining collagen as a suitable biomaterial for regenerative medicine. (1) Using a decellularized collagen matrix and preserving its original tissue shape and ECM structure. Tissue decellularization can be accomplished by using physical (snap freezing or high pressure), chemical (ionic detergents, acid and alkaline treatments, chelation with EDTA) or enzymatic (digestion with trypsin) methods. For the best result, a combination of the above-mentioned techniques is used. (2) Extraction, purification, and polymerization of collagen and its diverse components to form a functional scaffold. Collagen extraction can be achieved by solubilisation methods in acid, neutral salt or proteolytic solutions. Acid extraction with slight pepsin solubilization has proven to be the most effective technique in terms of yields. The latter method of collagen extraction followed by proper treatment has recently become the preferred single technique to approach collagen tissue engineering.[36]

Preparation of a suitable scaffold design usually follows after the treatments mentioned above. Collagen gels are usually prepared with a very low concentration of collagen (around 0.2 % weight per unit volume) compared to the amount of collagen present in native tissue (around 20 %).[44, 45] Lowering the concentrations compensates cell contractions, the capability of the seeded cells to modify and remodel the surrounding collagenous matrix.[46] Due to cell contraction, the final concentration of collagen in thus prepared scaffolds can reach 1.5 %.[45] It has been shown that collagen sponges made from 0.5% suspensions, lyophilized to maintain a porous surface, and crosslinked by suitable techniques have interconnected pores suitable for cellular in-growth and histogenesis. They are highly porous (>95%) with pore diameters in the range of 120–200 μm (Figure 6).[33]

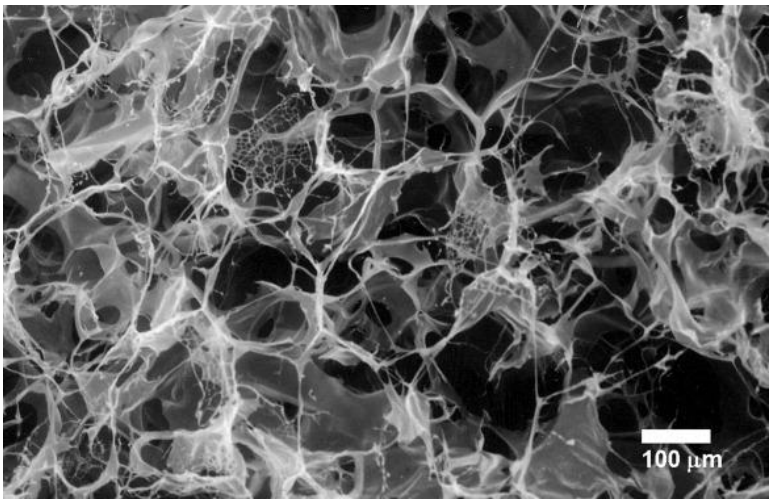

Figure 6: Porosity of 0,5% collagen lattice sponges.[33]

Collagen can be used independently or as a one part of a composite. George *et al*. [47] fabricated a collagen scaffold with a honeycomb structure for dermal tissue engineering with pore sizes of about 300 μm, which they suggested are the most suitable for adhesion, proliferation, and multiplication of fibroblasts. A UV crosslinked collagen scaffold was prepared from atelocollagen molecules with removed telopeptides lowering the antigenicity of the scaffold. A fibroblast cell culture medium showed a significant increase in total cellular DNA and procollagen type I content on a collagen scaffold in comparison with a control cell culture (Figure 7). The specific honeycomb structure and the porosity of the honeycomb walls allow transportation of nutrients to the cells and removal of waste products as in a dynamic culture environment. Overall, the 3D environment of the honeycomb collagen scaffold provides the natural ECM environment with the necessary mechanical support and biochemical interplay as in living systems for the formation of a dermal substitute.

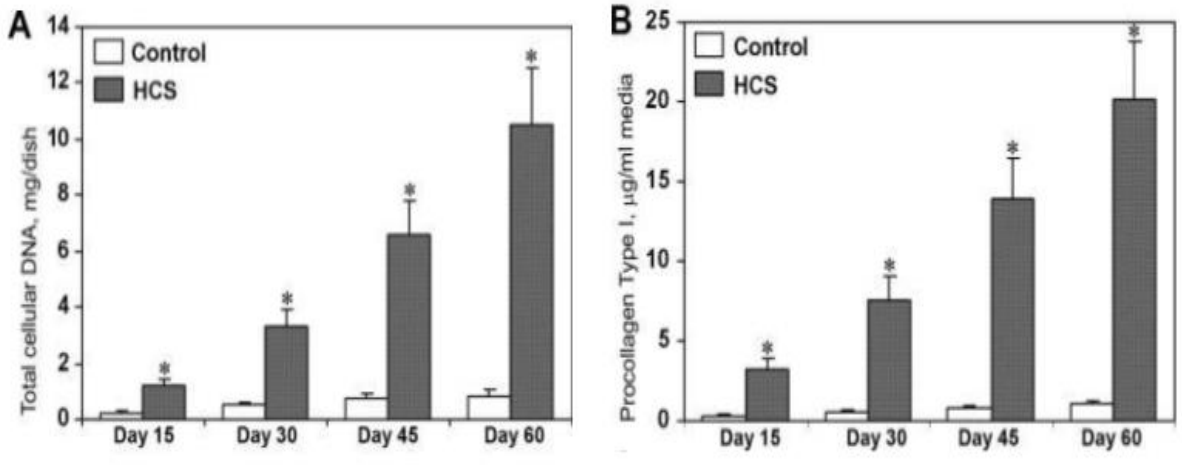

Figure 7: Total cellular DNA content of control cultures and cultures with honeycomb collagen scaffold on days 15, 30, 45, and 60 after placing the honeycomb sheet (A). Procollagen Type I C-peptide present in the media of control cultures and cultures with honeycomb collagen scaffold on days 15, 30, 45, and 60 after placing the honeycomb collagen sheet (B).[47]

In the study [48] tri-polymer polycaprolactone (PCL)/gelatine/collagen type I was fabricated. PCL/gelatine scaffolds were fabricated through the electrospinning method, and were later modified by collagen (0.2–1.5%) through grafting in an EDC/PBS solution. Adding collagen to the composite enhanced proliferation of cells (L929 mouse fibroblasts), especially in composites modified with 1% collagen.

On one hand, the three-dimensional proteinaceous structure of collagen provides cell-cell and cell-matrix interactions with the fibroblasts, and is shown to be effective in absorbing wound exudates. However, on the other hand, it can be an easy target for the invasion of exogenous microorganisms. Thus, it is highly recommended that antimicrobial agents are added within the structure of the scaffold.[10]

2.4 Chitosan

Collagen-based materials are often reinforced with different biomaterials to emphasize structural and biomechanical properties and to add additional properties to the composite.[5] Chitosan is a derivative of polysaccharide chitin, that can be found in the exoskeletons of crustaceans and insects. It can be isolated from various sources, from the above-mentioned animals, mushrooms, the cell walls of green algae and fungi. Chitin is considered to be as one of the most abundant polysaccharides in nature and ranks second to cellulose in terms of abundance. Focusing on structure, chitin is a derivate of cellulose with the same sugar backbone but with its hydroxyl groups replaced by acetylamino groups (2-(acetylamino)-2-deoxy-D-glucose).[34] Generally, chitosan can be produced via enzymatic hydrolysis by chitin deacetylase or chemical hydrolysis under alkaline conditions (Figure 8).[50] The incorporation of chitosan into various scaffolds can be done by various techniques – lyophilization, gas foaming, electrospinning, etc. Chitosan forms stable scaffold with both natural and synthetic polymers.[34]

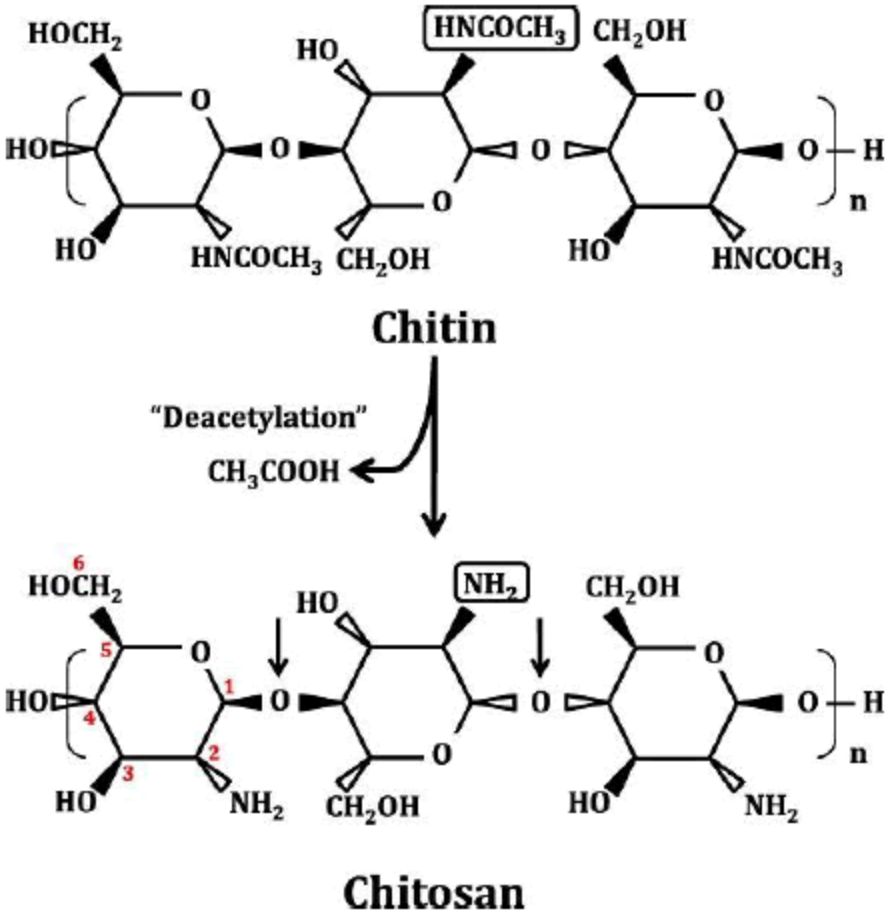

Figure 8: Chemical structure of chitin and chitosan and schematic representation of the process of deacetylation.[49] (Modified)

2.4.1 Physiochemical and Biological Properties

Chitosan is a natural linear carbohydrate biopolymer that exhibits structural similarity to the glucosaminoglycans of the ECM, that have an important role in cell-cell adhesion. Its hydrophilic structure promotes cell adhesion, proliferation, and differentiation and may attract fluids and cells to the defect site. The physiochemical properties mainly depend on two factors – molecular weight and degree of deacetylation (DDA).[50, 53, 54]

Chitosan is considered to be a biodegradable polymer and its biodegradation rate can be easily moderated by the DDA. Biodegradation of chitosan *in vivo* is highly dependent on the presence of enzymes – proteases, chitinases and in mammals mainly lysozyme. Products of biodegradation are non-toxic oligosaccharides of variable length composed mostly of aminosaccharides that are further incorporated into glycosaminoglycans and glycoprotein metabolic pathways or excreted.[54, 55]

One of the characteristic properties of chitosan is its antibacterial nature. Although the exact mechanism of the antimicrobial activities is unknown, two theories have been stated. The first claims that electrostatic interactions between the polycationic structure of chitosan and the anionic bacterial wall structure alter its permeability. The second considers binding chitosan via protonated amino groups with the cell DNA, inhibiting synthesis of microbial RNA.[49, 55] Antibacterial activity is closely linked with the pH of the environment, the lower the pH is the more protonated the amino groups are.[55]

Its cationic character gives chitosan unique properties. Not only is it considered to be part of the antibacterial mechanism, but its cationic nature also helps to form polyelectrolyte complexes with anionic glycosaminoglycans, such as heparin and chondroitin sulfate. These polyelectrolyte complexes influence the activity of growth factors and cytokines, and find their usage in bone and cartilage regeneration. The cationic character also explains chitosan's analgesic effect. Amino groups protonate in the presence of proton ions that are released in the inflammatory area, resulting in an analgesic effect. Additionally, release of N-acetyl-β-D-glucosamine as a product of degradation causes fibroblast proliferation and increases the level of natural hyaluronic acid synthesis in the wound region.[50, 55, 57] Worth mentioning are mucoadhesive properties and haemostatic activities which are also in direct relationship to its polycationic character, with its dependence on DDA.[52] Its haemostatic properties are based on binding to red blood cells to facilitate clot-formation and stimulating the release of transforming growth factor with palette-derived growth factor.[50]

2.4.2 Application as an Additive for Wound Healing

Due to its remarkable properties, chitosan has been highly used in wound healing [52] and overall skin tissue engineering. Chitosan-based materials have been showing promising results in controlling evaporative water loss and maintaining a moist environment which is necessary for fast and effective wound healing. Furthermore, due to its antibacterial properties, there is no need to be cautious about the invasion of exogenous microorganisms. Oxygen permeability, promoting fluid drainage and a significant increase in the epithelialization are other useful properties chitosan possess.[50]

Various fabrication strategies and forms of chitosan have been used in wound healing. Chitosan-gelatin-hyaluronic acid scaffolds fabricated by freeze-drying methods were characterized by Haifeng *et al*.[58]. Chitosan-hyaluronic composite was prepared by Sanad and Abdel-Bar [59] These sponges were enriched with andrographolide lipid nanocarriers. Andrographolide is a naturally occurring diterpene lactone showing wound healing activity in rats.[60] Scaffolds for dermal tissue engineering consisting of gelatine and carboxymethyl-chitosan prepared by lyophilization technique were reviewed in the Agarwal *et al*.[61] study. In the Patel *et al*.[62] study, chitosan-gelatin hydrogel films were characterized. These films were crosslinked with glutaraldehyde and enriched with Lupeol, which is a pentacyclic triterpene naturally occurring in fruits (fig, mango, and more) and in medicinal plants (Shea butter plant, Tamarindus indica, and more). Lupeol possesses anti-inflammatory properties.[63]

2.5 Antibacterial Nanoparticles

The reason behind adding antibacterial agents in scaffolds is to stop microbial contamination. It can be helpful in healing deep dermal injuries, e.g. venous ulcers and third-degree burn injuries, and for adjusting scaffolds that are implanted in the body. As mentioned above, ideal biomaterials possess a 3D structure to simulate a suitable structural environment for cells. Cells are too large to occupy the whole structure of the scaffold and smaller pores are often filled with bacteria. Implanting these scaffolds can be lethal for the patient.

The most used current antibacterial agents are either of natural origin (aminoglycosides), chemically modified compounds (β-lactams), or synthetic antibiotics (sulfonamides). These agents have been showing great results. However, due to their broad use and abuse, there has been an increase in the number of resistant strains of bacteria lately.[64] Such antibacterial resistance contributes to the emergence of diseases that were under control for many years, e.g. tuberculosis.[65] Hence there is a place for new antibacterial agents to replace those mentioned above. As reviewed in [10], over the last few years there have been a lot of different approaches in regenerative medicine to solve this problem by using a wide range of antibacterial additives – hyaluronic acid, chitosan, alginate fibres with silver nanoparticles and gellan gum are some of the examples. For the purpose of this work, only the antibacterial activity of nanoparticles will be further discussed.

Nanomaterials are defined as ranging in size from 1 to 100 nm. Their properties are easily adjustable mainly by increasing or decreasing surface to volume ratio. Nanoparticles (NPs) proved to be very useful in the bio-medicinal field of interest, not only as antibacterial agents but also for drug delivery systems, nanoelectronics, biosensors and *in vivo* imaging.[11]

2.5.1 Antibacterial Effect of Nanoparticles

Although silver nanoparticles are highly used in all kinds of applications, the exact mechanism of NP antibacterial activity has not yet been understood completely. The main problem with understanding the antibacterial effect is its variety. In general, antibacterial effect of NPs is based on electrostatic interaction with the membrane of bacteria, causing disruption of its integrity and inducing the oxidative stress that leads toward producing reactive oxygen species (ROS). ROS are responsible for the further disruption of DNA and protein structure. (Figure 9). The mechanism of NP toxicity towards bacteria depends on the properties of bacteria (surface modification, intrinsic properties, bacterial strain) and on the physiochemical properties of NPs.[64] Though there is a generalized mechanism, in reality, the mechanism is much more complex. For example, TiO_2 and ZnO induce frameshift mutation in *Salmonella typhimurium* [66]. TiO2 is toxic towards *Escherichia coli*, *Staphylococcus aureus*, *Pseudomonas aeruginosa* and *Enterococcus hire* only under UV illumination, due to TiO_2 photocatalysis that can increase peroxidation of the polyunsaturated phospholipid component of the lipid membrane.[67]

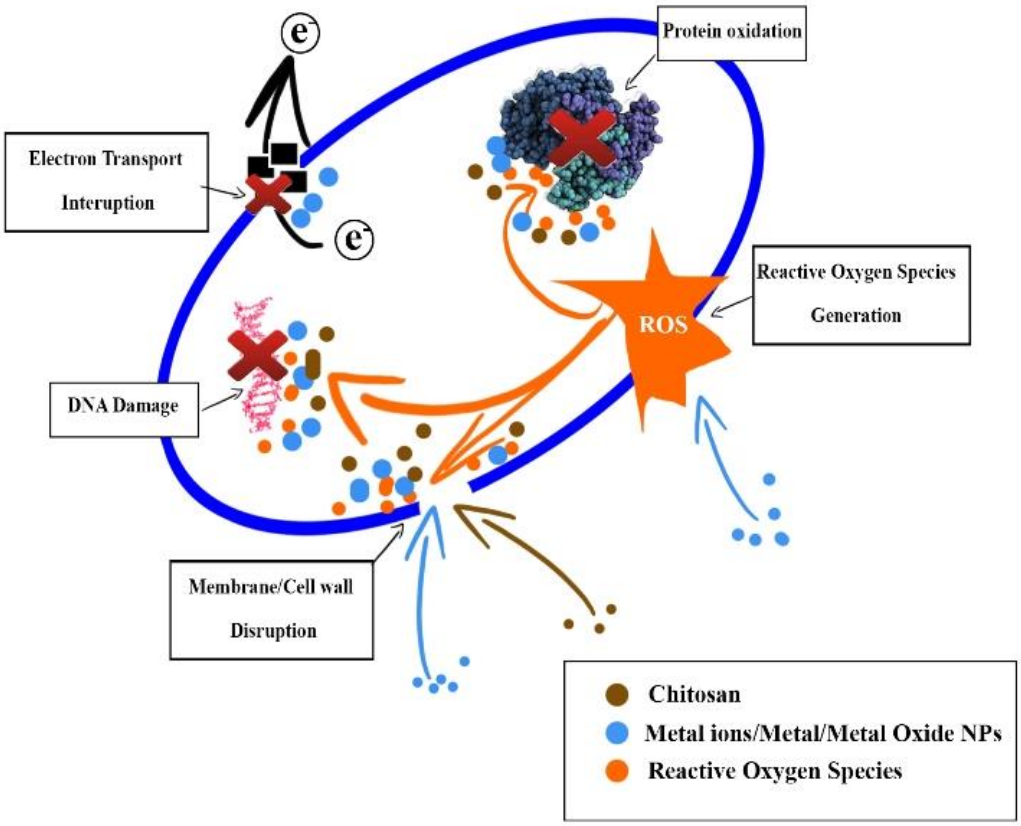

Figure 9: Schematic representation of the generalized antibacterial mechanism of chitosan and metal nanoparticles.[64]

2.5.2 Factors Lowering Efficiency of an Antibacterial Effect

The structure of the cell wall plays an important role in the tolerance or susceptibility of bacteria in the presence of NPs. The bacteria cell wall is designed to provide strength, rigidity and shape, and serve as a protective shield from osmotic rupture and mechanical damage. According to their structure, components, and function, bacteria can be divided into gram-positive and gram-negative. The unique structure of a gram-positive bacterial wall is a thick layer (ranging from 20 to 50 nm) of peptidoglycans, which are attached to teichoic acids. On the other hand, gram-negative bacterial walls are overall more complex, consisting of a thin layer of peptidoglycans covered by an outer membrane. Crucial factors in lowering efficiency of NP antibacterial activity are dependent on the structural motives of the cell wall and the diffusion ability of NPs.[64]

More additional parameters can influence the tolerance of bacteria towards NPs. The antibacterial effect of nanoparticles highly depends on bacterial growth rate. Studies have shown a higher toxic effect of NPs on fast-growing bacteria than on slow-growing. Presumably it is due to the expression of stress-response genes.[69] Some bacteria can produce biofilms, which are formed by the secretion of a matrix (proteins, DNA, and extra-polysaccharide) covering the bacterial cell community.[64] This biofilm formation can be very challenging for some NPs. MgF_2-NPs have shown their effectiveness in the prevention of biofilm formation in *E. coli* and *S. aureus* [70]. Superparamagnetic iron oxide NPs with a silver coating have also shown good results against biofilms using external magnetic fields.[71]

2.5.3 Potential Hazards of Using Metal Nanoparticles

With the growing application of metal NPs in the bio-medicinal field, a number of concerns about the safety of inserting metal nanoparticles into living organisms with the emphasis on interaction between cells and NPs, is starting to increase. Overall, the most used metal nanoparticles in bio-medicinal applications are silver and gold NPs.

As reviewed in [72] gold is highly used in the medicinal field in stents, pacemakers, dental fillings, etc., showing its great biocompatibility. In nanoform, gold nanoparticles possess anticancer properties and enhance the antibacterial properties of other antibacterial agents. For these reasons, gold nanoparticles are mainly used for tissue regeneration, targeted drug delivery, and wound healing. Most of the time gold nanoparticles are need to be crosslinked with biomaterials such as collagen or chitosan, to be able fully to integrate with bioactive molecules like polysaccharides, growth factors, peptides and others.[11] However some of the *in vitro* and *in vivo* studies have shown gold nanoparticle toxicity towards various cell lines.[73] It has been reported that gold nanoparticle toxicity towards cells is dose-dependent and depends on the properties of NPs. The size of gold nanoparticle is a key parameter, since particle size plays a big role in endocytosis, cellular localization and accumulation *in vivo*.[73−75] Size-dependent gold nanoparticle toxicity has been studied in [75], where gold nanoparticles with sizes between 0.8–15 nm were used. Connective tissue fibroblast, epithelial cells, macrophage and melanoma cells were the most sensitive cell lines toward 1.4 nm gold nanoparticles with IC50 values (half maximal inhibitory concentrations) ranging from 30 to 56 μM. The IC50 values of 0.8, 1.2, and 1.8 nm gold nanoparticles were 250, 140 and 230 mmol/l, respectively. At contrast, the 15 nm gold nanoparticles were nontoxic even at 60-fold higher concentrations than the smaller particles.

Silver is well-known for its antibacterial properties. The ability to slow or even inhibit growth of microorganisms has been known for a very long time, as colloidal silver has been used since the 20th century. As reviewed in [76], the antibacterial effect of silver persists in nanoform, as silver nanoparticles are highly used in wound healing. Silver nanoparticles have the ability to disrupt bacterial membranes causing damage to the microorganism and accelerating the healing process.[76] Silver nanoparticles have been also showing a promising dose-dependent anticancer effect towards colon and breast cancer cell lines.[77] However, recent studies have been showing silver nanoparticles toxicity towards various cells. Yue *et al*.[78] studied the *in vitro* toxic effect of silver nanoparticles on algae and fish cells. Silver nanoparticles have been showing cytotoxicity to both types of cells. More serious cytotoxicity has been determined towards fish cells, where silver nanoparticles entered cells via endocytic pathways and disrupted processes inside the cell. *In vitro* cytotoxicity of silver nanoparticles causing oxidative stress in human liver cells (HepG2 cell type) has been shown in [79]. However, in comparison to ionic silver, silver nanoparticles have IC50 values 100-fold higher, meaning ionic silver is even more toxic than silver nanoparticles.[79] Overall *in vitro* toxicity of silver nanoparticles mainly depends on the cell type and the size of the nanoparticles.[80]

Nevertheless, a recent study on human epithelial cells (type A549) presented results suggesting the presence of silver nanoparticles can create hormesis.[81] This means that exposure to a low non-toxic dose of silver nanoparticles might protect against a second toxic dose. Although this study could lessen the caution about using silver nanoparticles, it is still good choice to find alternatives to metal nanoparticles.

2.6 Selenium Nanoparticles

Selenium is an element of the chalcogenide group. Besides its use in electronics, ceramics, metallurgy and other applications, it has also quite a big potential in bio-medicinal applications, since selenium is considered as a biogenic element. Selenium is important for proper cellular and metabolic functioning in all animals, at least 25 human selenoproteins and enzymes contain this element.[82−83] Normal selenium levels in adults are around 81 µg and the dietary requirement is 55 µg per day with an upper limit of 400 µg.[84]

2.6.1 Antimicrobial Properties of Selenium Nanoparticles

Due to their properties, selenium nanoparticles (SeNPs) may be used in a wide range of applications ranging from electronics to medicine. The extent of the perspective use of SeNP is summarized in Figure 10. Crucial properties that make SeNPs suitable agents for medicinal application are their antimicrobial, antioxidant and anticancer activities.[85] Although all these properties are worth mentioning, for the purposes of this work only the antibacterial activity will be further discussed.

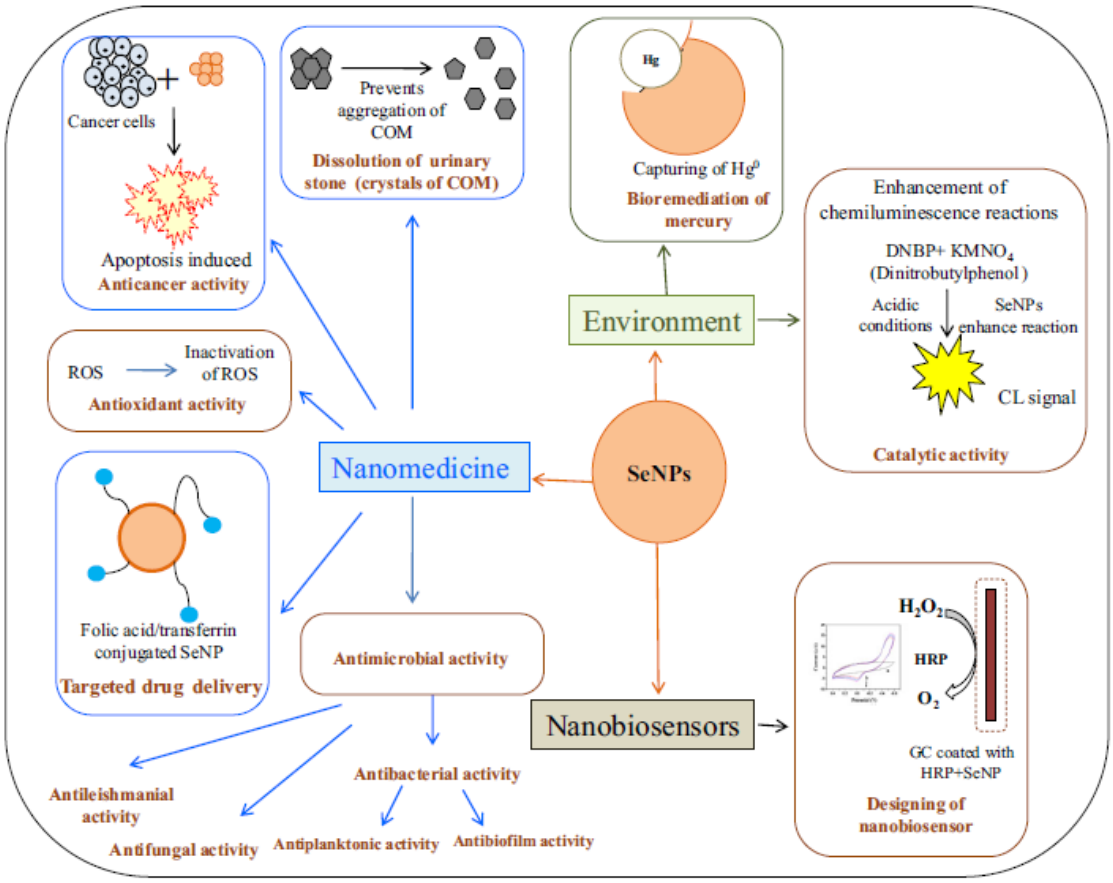

Figure 10: Applications of selenium nanoparticles in the bio-medicinal field.[85]

SeNPs appear to be effective against a large group of microorganisms, consisting of gram-positive and gram-negative bacteria and fungus, which will be further discussed. Moreover, SeNPs have shown their toxicity towards protozoa (*Trichophyton rubrum* [86] and *Leishmania major* [87]). SeNPs have been also showing promising antimicrobial activity against microorganisms forming biofilms – *Candida albicans* [88], *Proteus mirabilis* [89], *Pseudomonas aeruginosa* [89−91], *Klebsiella pneumoniae* [91] and *Acinetobacter baumannii* [91].

One of the most dreaded biofilm-forming bacteria is considered to be *Staphylococcus aureus* (*SA*). Due to biofilm formation, *SA* is resistant to a wide range of antibiotics. Methicillin is currently known as one of the effective antibiotics against *SA*. The reason behind finding new antibacterial agents against *SA* is the existence of a methicillin-resistant strain, so-called *MRSA*. As mentioned bellow, SeNPs have been showing promising results against *SA* and *MRSA*.

The mechanism of the antimicrobial effect of selenium nanoparticles is highly dependent on the physiochemical nature of NPs and the type of microorganism. SeNPs toxicity to Candida albicans is based on sulphur substitution in amino acids and disrupting biological processes.[88] In the case of Leishmania major SeNPs cause DNA fragmentation and stimulate apoptotic cell death. [87] The antimicrobial effect of SeNPs with quercetine and acetyl choline toward *E. coli* and *S. aureus* works in 3 steps: (1) compromising bacteria cell membranes, (2) increasing intracellular ROS level production, (3) entry into bacterial cells and disruption of the DNA structure.[91]

SeNPs coatings on medical devices using different materials (silicone, polyurethane (PU) and polyvinylchloride (PVC)) showed promising results in antibacterial activity against *SA* compared to the antibacterial effect of silver nanoparticle coatings.[92] In the work, SeNPs were synthesized using sodium selenite with Se at +IV oxidation state. The coating density was the highest on the PVC surface and the lowest on the PU. Corresponding to the coating density, SeNPs-covered-PVC showed better results in reducing bacterial densities compared to the other two materials. Compared to the uncoated surface as control, bacterial density values decreased to 20 % on PVC, 50 % on silicone and only 80 % on PU. The antibacterial activity of SeNPs on PVC was better compared to silver NPs. Results from the Wang and Webster study [90] showed the high effectiveness of selenium coated paper towels in inhibition of bacteria growth on the paper towel surfaces. The selenium coatings significantly inhibited *SA* growth by about 90 % after 24, 48 and 72 hours and successfully inhibited *P. aeruginosa* growth after 48 and 72 hours by 55% and 84%, respectively. In a study by Chudobova *et al*. [93], SeNPs showed positive results against *S. aureus* with inhibitory concentrations of 10 μM and a total inhibitory concentration of 300 μM. The Nguyen *et al*. study [94] showed higher inhibitory concentration values suggesting the antimicrobial effect of SeNPs may depend highly on the morphology of nanoparticles. Another interesting study dealing with the *SA* issue is from Huang *et al*.[91]. They prepared a synergistic nanocomposite consisting of SeNPS, quercetin, and acetylcholine, and used it on an above-mentioned superbug – *MRSA*. This synergistic nanocomposite showed high antibacterial activity with the inhibition zone close to 2 cm and a minimum inhibitory concentration of 2.0 μg/ml.

It is worth mentioning that SeNPs have not shown a post-antibiotic effect, which is defined as the potential of a substance to delay regrowth of a microbial population after short-term exposure and removal of an antimicrobial compound.[85]

3 GOAL OF THE WORK

The main purpose of the work is to summarize the current state of the art in the chemistry of biomaterials, as well as the application of nanoparticles as antibacterial agents. The experimental part is focused on the preparation of collagen matrices with selenium nanoparticles, the testing of the influence of selenium nanoparticles on various physiochemical and antibacterial properties of collagen matrices and the study of the release kinetics of selenium nanoparticles.

4 EXPERIMENTAL PART

4.1 Chemicals

All chemicals were used without further purification or modification.

- Bovine collagen type I. (100 %), obtained from 8% aqueous solution by freeze-drying, Výzkumný ústav pletařský a.s., Czech Republic.
- Chitosan from shrimp shells, 70 % DDA, low-viscosity, Sigma Aldrich, Germany.
- Selenium nanoparticles bonded in chitosan (SelenChitosan), Mendel University, Czech Republic.
- Selenium nanoparticles bonded in carboxymethyl-cellulose (SelenBact), Mendel University, Czech Republic.
- Ultrapure water type II according to ISO 3696.
- Collagenase from *Clostridium histolyticum* (≥ 125 CDU/mg), lyophilised powder, Sigma Aldrich, Germany.
- Lysozyme human, recombinant, expressed in rice (120 530 units/mg protein), lyophilized powder, Sigma Aldrich, Germany.
- Ethanol absolute p.a., PENTA s.r.o., Czech Republic.
- Chemicals for crosslinker preparation:
    - N-(-3-Dimethylaminopropyl)-N'-ethylcarbodiimide hydrochloride, Sigma Aldrich, Germany,
    - N-hydroxysuccinimide 98%, Sigma Aldrich, Germany,
    - ethanol 96% p.a., PENTA s.r.o., Czech Republic,
    - sodium phosphate dibasic for molecular biology (≥98,5 %), Sigma Aldrich, Germany.
- Chemicals for 0.01M phosphate buffered saline preparation:
    - disodium hydrogen phosphate dodecahydrate G.R., lach:ner, Czech Republic,
    - potassium dihydrogen phosphate G.R., lach:ner, Czech Republic,
    - sodium chloride G.R., lach:ner, Czech Republic,
    - potassium chloride G.R., lach:ner, Czech Republic,
    - hydrochloric acid, Sigma Aldrich, Germany.
- Fluorescent dye SYTO9, Thermo Fisher Scientific, United States of America.
- Fluorescent dye Propidium Iodide, Sigma Aldrich, Germany.

4.2 Characterization of Nanoparticles

Two types of nanoparticles, differing in the biopolymeric substance that they were anchored in, were used in this work. SelenBact (SeB) is a complex of selenium nanoparticles with carboxymethyl-cellulose that was prepared at Mendel University. SeB nanoparticles were formed by reduction of Na_2SeO_3 with mercaptopropionic acid in the presence of carboxymethyl-cellulose. The size of the nanoparticles determined by dynamic light scattering (DLS) and transmission electron microscopy (TEM) differs from 50 to 300 nm. Colloidal dispersion pH values ranged from 5.4 to 5.6, the content of selenium was about 278 ppm and the colour of the dispersion varied from colourless to pale orange.[95] Scanning electron microscopy (SEM) images and DLS size distributions are illustrated in Figure 11.

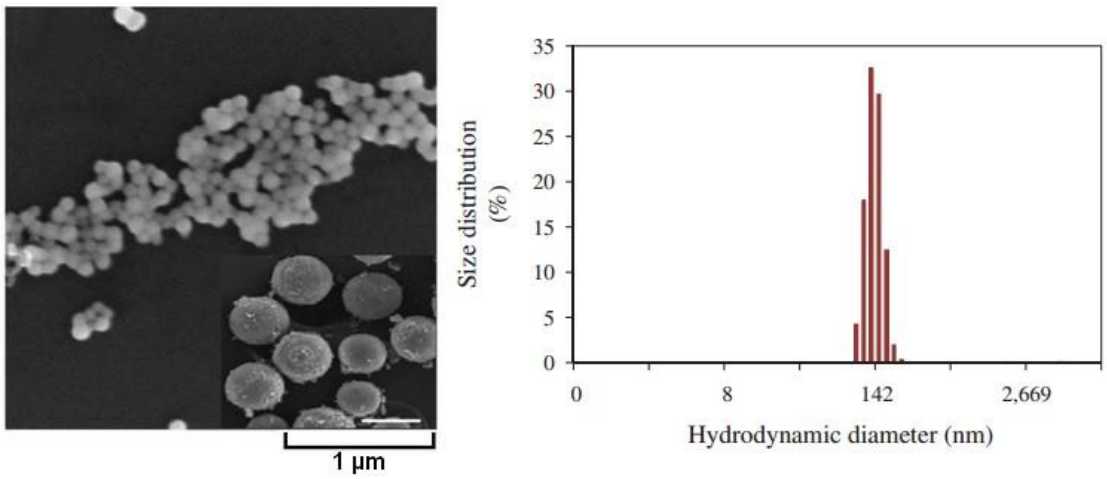

Figure 11: Selenium nanoparticles type SelenBact – SEM visualisation (left) and size distribution evaluated by DLS (right).[95] (Modified)

SelenChitosan (SeCh) is a complex of selenium nanoparticles with chitosan, prepared at Mendel University. SeCh nanoparticles were prepared by a similar process of reduction of Na_2SeO_3 with mercaptopropionic acid in the presence of chitosan. The size of the nanoparticles varies from 55 to 500 nm, the content of selenium was about 663 ppm and the colour of the dispersion was pale orange.[96]

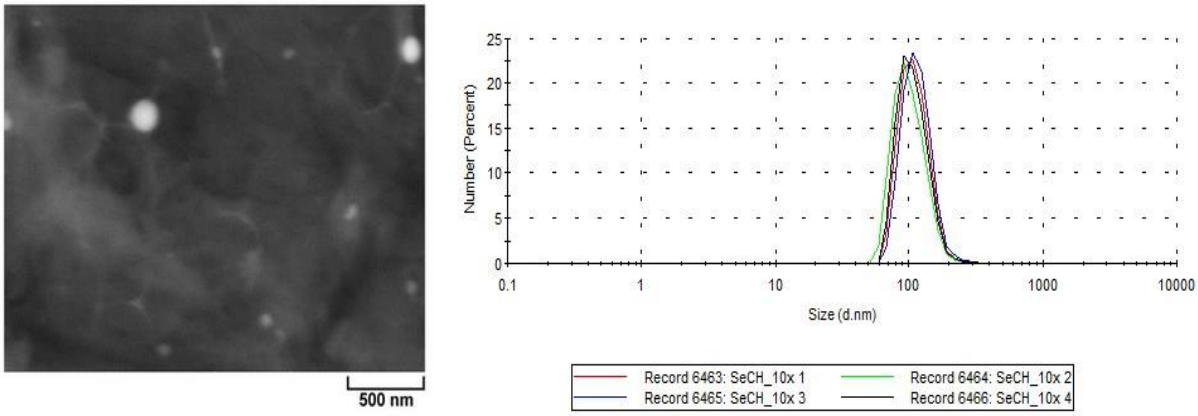

Figure 12: Selenium nanoparticles type SelenChitosan – SEM visualisation (left) and size distribution evaluated by ZetaSizer (right). Data from ZetaSizer were used with permission of Mendel University.

4.3 Equipment

- Disintegrator Ultra Turrax ® T18 basic, IKA, Germany.
- Freeze-dryer Epsilon 2-10D LSCplus, Christ, Germany.
- Analytic balance SI-234A, DENVER INSTRUMENT, United States of America.
- Incubator BPN-80CRH(UV) Series Co2, Hinotek, China.
- Water purification system Direct-Q®, Merck, United States of America.
- Pocket pH meter H138 minilab™, Hach Company, United States of America.
- Scanning electron microscope with energy dispersive spectrometer MIRA3, TESCAN, Czech Republic.
- Multipoint stirrer Cimarec™, Thermo Scientific, United States of America.
- Optical emission spectrometer with inductively coupled plasma Ultima2, Horiba Scientific, United States of America.
- Fourier transformed infrared spectroscope with attenuated total reflectance Vertex 70/70v, Bruker, United States of America.
- Spectrometer Ultrospec® 10 Cell Density Meter, Biochrom, United Kingdom.
- Inverted fluorencence microscope Olympus IX71, Olympus, Tokio Japan.

4.4 Preparation of Samples

Two series of samples were prepared. The first series of samples containing a higher concentrations of selenium nanoparticles (Table 2), was prepared for the purpose of optimization of the preparation procedure, determination of microstructure and chemical nature, characterization of swelling properties, evaluating the degradation over time and testing the release kinetics of the selenium nanoparticles. Dimensions of the smaller samples were d=8.42±0.08 mm and h=7.51±0.07 mm and dimensions of the larger samples were d=8.41±0.08 mm and h=15.53±0.09 mm, where parameters *d* and *h* stand for diameter and height, respectively. Images of the samples are enclosed in appendices – Appendix 1.

Table 2: List of samples – the first series of samples. Samples contained two types of biopolymeric matrices – collagen (Coll) and chitosan (Chit), and two types of selenium nanoparticles – SelenChitosan (SeCh) and SelenBact (SeB)

SeNPs application	Sample	Collagen content, wcoll [%]	Chitosan content, wchitosan [%]	SeNPs content, wSeNPS [ppm]
–	Coll	0.5	–	–
–	Coll/Chit	0.5	0.5	–
In situ	Coll_SeCh	0.5	–	18.5
	Coll_SeB	0.5	–	18.5
	Coll/Chit_SeCh	0.5	0.5	18.5
	Coll/Chit_SeB	0.5	0.5	18.5
Ex situ	Coll_SeCh	0.5	–	18.5
	Coll_SeB	0.5	–	18.5
	Coll/Chit_SeCh	0.5	0.5	18.5
	Coll/Chit_SeB	0.5	0.5	18.5

The second series with lower concentrations of selenium nanoparticles (Table 3) was prepared for the purpose of evaluating the antibacterial activity of selenium nanoparticles. Reduction of selenium nanoparticle concentrations followed the trends of cytotoxic studies (to be published). Dimensions of the samples were d=8.37±0.08 mm and h=1.5±0.05 mm. Image of the samples is enclosed in appendices – Appendix 2.

Table 3: List of samples – the second series of samples.

SeNPs application	Sample	Collagen content, wcoll [%]	Chitosan content, wchitosan [%]	SeNPs content, wSeNPS [ppm]
–	Coll	0.5	–	–
–	Coll/Chit	0.5	0.5	–
Ex situ	Coll/Chit_SeCh	0.5	0.5	1.0
	Coll/Chit_SeCh	0.5	0.5	5.0
	Coll/Chit_SeB	0.5	0.5	1.0
	Coll/Chit_SeB	0.5	0.5	5.0

4.4.1 Collagenous Sponges with Additives

Collagenous suspensions (0.5%) without additives were prepared by disintegration (6 000 rpm, 5 min) of swelled pure collagen in an exact volume of ultrapure water. During disintegration, collagen suspensions were cooled in an ice water bath to prevent denaturation by heating. After disintegration, exact volumes of collagenous gel were transferred into well plates by pipetting. Thus prepared samples were freeze-dried in the freeze-dryer Epsilon 2-10D LSCplus (Christ) for two days.

Collagenous samples with chitosan were prepared by weighing an exact amount of chitosan and mixing with ultrapure water. The prepared chitosan suspension was added dropwise to the disintegrated suspension of collagen. Further workflow followed the same pattern as the preparation of collagenous sponges without additives.

Collagenous sponges with the addition of selenium nanoparticles *in situ* were fabricated by preparing dilute solutions of selenium nanoparticles in ultrapure water and adding them to the collagen suspension (with or without chitosan) after disintegration. Further workflow followed the same pattern as the preparation of collagenous sponges without additives.

Collagenous sponges with the addition of selenium nanoparticles *ex situ* were prepared by adding dilute solutions of selenium nanoparticles to wet collagen sponges (with or without chitosan) after crosslinking. Thus prepared samples were freeze-dried for two days.

4.4.2 Crosslinking of Samples

Sample preparation was followed by a crosslinking procedure. Crosslinking was carried out to stabilise samples, enhance biomechanical properties and prolong the degradation rate. *In situ* selenium nanoparticles were added before the crosslinking and *ex situ* selenium nanoparticles were added after crosslinking and before the second freeze-drying. The chemical crosslinking agent EDC/NHS (1-ethyl-3-[3-(dimethylamino)-propyl]-carbodiimide/N-hydroxysuccinimide) diluted 2:1 in 96% ethanol was used. The prepared crosslinking agent was poured into each well with the freeze-dried sample and let react for two hours. After two hours, the crosslinking agent was removed cautiously, followed by two washes in 0.1M Na_2HPO_4 and three washes in ultrapure water. Then fresh ultrapure water was added, and samples were freeze-dried for two days. Samples prepared *ex situ* were freeze-dried in a dilute solution of selenium nanoparticles instead of ultrapure water.

4.5 Physiochemical Characterisation

The physiochemical characterisation was carried out by the following methods. The morphology, microstructure, content, and homogeneity of the distribution of selenium nanoparticles in the samples were studied using scanning electron microscopy (SEM) with energy-dispersive electron X-ray spectroscopy (EDX). Porosity was measured by liquid replacement method using Archimedes principle. Swelling behaviour and degradation in an environment of ultrapure water and PBS with sufficient enzymes were observed using gravimetric methods. Fourier transformed infrared spectroscopy with attenuated total reflection (ATR-FTIR) was carried out to observe the characteristic functional groups of prepared collagenous samples and their alternation after the addition of additives. The release kinetics of the selenium nanoparticles were followed by using optical emission spectroscopy with inductively coupled plasma (ICP-OES)

4.5.1 Scanning Electron Microscope Analysis with Energy Dispersive Spectrometry

The morphology and microstructure of the prepared samples were studied using SEM. Lyophilized collagen sponges were carefully sliced into 1 mm slices using a scalpel and placed on the metallic target with double-sided tape. Before measurement, samples were coated with a thin gold layer to obtain better resolution. Samples were observed using a scanning electron microscope MIRA3 (Tescan) at 10.0 kV acceleration voltage obtaining SEM images and EDX elemental mapping.

4.5.2 Porosity and Pore Size Distribution Measurements

Porosity measurements were carried out using Archimedes principle.[97] Absolute ethanol was used as a probe, because of its ability to fully penetrate the microstructure of the scaffold without swelling. Briefly, dry samples with similar weight (d=8.41±0.08 mm, h=15.53±0.09 mm) were weighed on analytic balances (w_d). 5 ml of absolute ethanol were added to each of the glass vials, which were weighed afterwards (w_1). Then the dry scaffolds were immersed in 5 ml of absolute ethanol and let rest for 5 minutes. After 5 minutes, vials with absolute ethanol and wet scaffolds were weighed, obtaining the w_2 value. The value of w3 was obtained by weighing vials with absolute ethanol after removal of the wet scaffolds. Porosity was calculated by the following equation (1), where ρ_e stands for the density of absolute ethanol:

$$P\ [\%]=\frac{\frac{(w_2-w_3-w_d)}{\rho_e}}{\frac{(w_1-w_3)}{\rho_e}}\cdot 100=\frac{(w_2-w_3-w_d)}{(w_1-w_3)}\cdot 100 \quad (1)$$

Pore size analysis was carried out by the software ImageJ, using images obtained from SEM. Cropped SEM images of 50× magnification and 2 mm scale were used with dimensions of 3.70×3.70 mm2. Every measurement consists of four measurings obtaining 400 values of the pore sizes in total (one measuring consists of 100 values).

Graphs were created in Microsoft Office Excel.

4.5.3 Swelling and Degradation in Hydrolytic Environment

Swelling kinetics and degradation over time were observed using the gravimetric method. Briefly, dry samples of similar weight (d=8.42±0.08 mm, h=7.51±0.07 mm) were properly weighed on analytical balances, placed in clean vials into which 5 ml of ultrapure water was added. At regular time intervals (1, 3, 5, 10, 15, 20, 30, 45, 60, 150 and 180 min), swelled samples were removed from the vials, carefully dried on filtrate paper and weighed on the analytic balance. Swelling behaviour was evaluated through appropriate parameters – swelling ratio *Q* (2) and water content *WC* (3), which are expressed by the following equations, where w_w is the weight of the wet samples and w_d is the weight of the dry samples.

$$Q\ [-]=\frac{w_d}{w_w} \quad (2)$$

$$WC\ [\%]=\frac{w_w-w_d}{w_w}\cdot 100 \quad (3)$$

Hydrolytic degradation followed swelling measurements. After swelling measurements, the samples were put into vials containing fresh ultrapure water. The hydrolytic degradation was simulated in an incubator at 37 °C. After regular time intervals (1, 2, 3, 6, 7, 14, 21, 28 and 35 days) the samples were removed, dried carefully on filtrate paper and weighed on an analytic balance. Afterwards, samples were put into fresh water to prevent microbial contamination. Degradation was evaluated through the parameter of weight loss D, where the w_D parameter is the weight of the wet scaffold on the appropriate day and w_{60} is the weight of the swelled sample after 60 minutes when the swelling kinetics value has become stable.

$$D\ [\%]=100-\left(\frac{w_D\cdot 100}{w_{60}}\right) \quad (4)$$

Figures were created in Microsoft Office Excel. Each value was averaged from three parallel measurements.

4.5.4 Degradation in Enzymatic Environment

In vitro degradation measurements followed degradation of samples in environment of two enzymes – collagenase of *Clostridium histolyticum* (c=2.2 mg/l) and human recombinant lysozyme (c=0.4 mg/ml). The concentrations of both enzymes were chosen according to [98, 99], the collagenase concentration was respected to the physiological concentration of the enzyme in human skin, and the lysozyme concentration was chosen according to the determined lysozyme concentration in human tears.

Enzymatic degradation measurement was carried out in a 0.1M phosphate buffered saline (PBS) at 37 °C. 0.01M PBS was prepared by weighing appropriate amounts of NaCl, KCl, Na_2HPO_4, and KH_2PO_4 into a beaker with 800 ml of ultrapure water. After the proper dissolving of the chemicals, the pH was measured with a pocket pH meter H138 minilabTM (Hach Company) and adjusted with 0.1M hydrochloric acid to the proper pH. For the measurement with collagenase, PBS with a pH value of 7.4 was prepared. The experiment with lysozyme was carried out in PBS with pH values of 7.4 and 6.0.

Samples (d=8.42±0.08 mm, h=7.51±0.07 mm) were left to swell in the PBS without enzymes for one hour and afterwards weighed, obtaining w_D. 10 ml of PBS with the corresponding enzyme were poured into glass vials. Swelled samples were immersed in PBS solutions enriched by enzymes. At regular intervals (2, 4, 8, 24, 48, 72 and 144 h), samples were removed, dried carefully on filtration paper and weighed on an analytical balance. Collagenase and lysozyme degradation were performed separately.

The enzymatic degradation was evaluated by the same equation as the hydrolytic degradation (4). Graphs were created in Microsoft Office Excel. Each value was averaged from three parallel measurements.

4.5.5 Fourier Transformed Infrared Spectroscopy with Attenuated Total Reflectance analysis

Fourier transformed infrared spectroscopy with attenuated total reflectance (ATR-FTIR) was performed on ATR-FTIR spectroscope Vertex 70/70v (Bruker). Prepared sponges were sliced to thin slices (1 mm) using a scalpel and placed on a germanium diamond carefully. ATR-FTIR spectra were measured in an evacuated environment in a MIR spectral range of 4300–800 cm^{-1} with 32 scans per sample. Spectra were evaluated using OPUS and Microsoft Office Excel.

4.5.6 Release Kinetics of Selenium Nanoparticles

The release of selenium nanoparticles was studied in an environment of ultrapure water. For every analysis samples were prepared days ahead. Each sample (d=8.41±0.08 mm, h=15.53±0.09 mm) was immersed in 25 ml of ultrapure water. At regular time intervals (30 min, 1, 4, 8, 24, 48 h) 3.5 ml of solution with released selenium nanoparticles were removed for further analysis. After 48h, when the last sample had been removed, only 4.0 ml of solution remained in the vial. The whole experiment was performed at lab temperature (25 °C). To imitate a dynamic body environment, a magnetic stirrer was used, stirring at 250 rpm.

The selenium nanoparticles release study was performed on an optical emission spectrometer with inductively coupled plasma Ultima2 (Horiba Scientific). A five-point calibration curve method was used for the determination of the concentration of selenium nanoparticles in the samples. Calibration solutions were prepared by pipetting corresponding volumes of solutions with selenium nanoparticles into volumetric flasks and filled in the rest with ultrapure water.

Graphs were created in Microsoft Office Excel. Each value was averaged from three parallel measurements.

4.6 Biological Characterisation

The biological characterisation was carried out by the following methods. Quantification of antibacterial activity was performed using the agar diffusion disk method and broth macrodilution method. Bacterial cell viability was observed in live/dead assay.

4.6.1 Antibacterial Properties

The antibacterial properties of prepared scaffolds were tested on three bacterial strains, which represented both gram-positive and gram-negative bacteria: *Escherichia coli* (*EC*), *Staphylococcus aureus* (*SA*) and Methicillin-Resistant *Staphylococcus aureus* (*MRSA*)

Evaluation of antibacterial activity through inhibition zones was performed using the agar diffusion disk method. Briefly, the bacterial medium was diluted in a PBS, obtaining the a value of absorbance equal to 0.5 McFarland (600 nm). A diluted suspension was applied onto an agar plate using a cotton stick. Afterwards, the scaffolds (d=8.37±0.08 mm, h=1.5±0.05 mm) were placed onto agar plate. Every agar plate held four to five scaffolds and one antibiotic in the centre as a positive control. Agar plates were incubated for 16 h at 37 °C before measuring inhibition zones.

Live/dead assay was performed on the samples that were removed from the agar plate. The samples were stained with fluorescent dyes – SYTO9 (green) and Propidium Iodide (red) and observed with inverted fluorescence microscope Olympus IX71 (Olympus) using a 460–495 nm excitation wavelength for SYTO9 and 545–580 nm for Propidium Iodide. Cells with a compromised membrane that were considered to be dead or dying stained red, whereas cells with an intact membrane stained green.

Evaluation of antibacterial activity through absorbance was performed by the broth macrodilution method. Briefly, the bacterial medium was diluted to the value of absorbance in 0.5 McFarland (600 nm) in PBS. The diluted bacterial suspension was further diluted 1:100 in the broth medium. The requisite volume of diluted bacterial suspension was added to Eppendorf tubes. Afterwards the scaffolds (d=8.37±0.08 mm, h=1.5±0.05 mm) were inserted into the tubes. Absorbance values were measured after 16 h. Antibacterial activity was also observed at predetermined time intervals – 0, 3, 6 12, 15 and 24 h.

5 RESULTS AND DISCUSSION

5.1 Visualisation and Distribution of Nanoparticles

Scanning electron microscopy with energy-dispersive electron X-ray spectroscopy was used for the confirmation of successful sample preparation with selenium nanoparticles. As was mentioned above, two methods of sample preparation were used (*ex situ* and *in situ* addition of selenium nanoparticles). The EDX spectrum (Figure 13) shows that carbon, oxygen and nitrogen (gold and palladium excluded) contributed to the three major elements of the collagenous matrix. This is in agreement with the chemical composition of the proteinaceous matrices. The existence of the sodium peak resulted from the use of disodium phosphate during the crosslinking treatment. Disodium phosphate is used for binding EDC after the crosslinking process is over and removing it from the sample. It is possible that some unbound sodium phosphate was left behind in the structure. With a very low value, selenium is also represented in the spectrum. The low percentage representation of selenium may be caused by measuring EDX in a non-specific area of the sample without closer zooming.

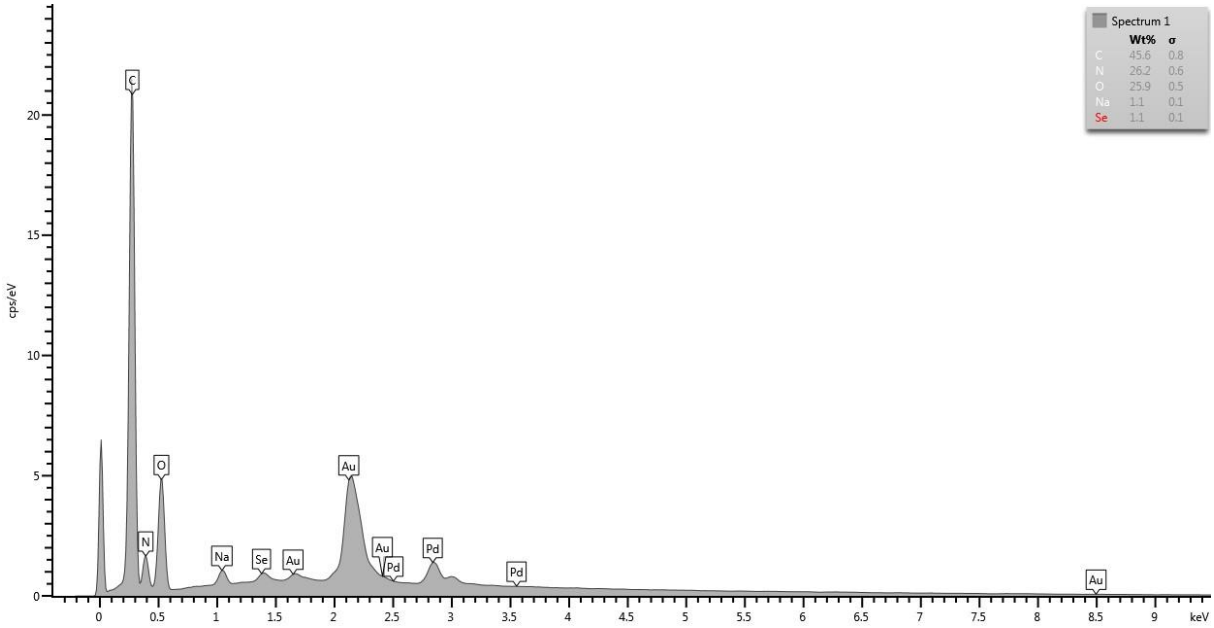

Figure 13: Representative EDX spectrum of ex situ prepared collagenous scaffold with SeCh nanoparticles (Coll_SeCh). The predominant components were found to be carbon (C), oxygen (O), and nitrogen (N). With 1.1 % of total intensities, selenium is also represented.

The summarised quantitative results obtained using the EDX method (Table 4) give an insight into the chemical composition of different samples and can be used to compare the differences in the content of selenium in the samples prepared by different preparation procedures. The trend of the predominant intensity of carbon, oxygen and nitrogen elements can be observed in all of the samples. The percentage representation of other elements (excluding selenium) ranged from 0.00 to 4.56 % depending on the sample. As has been discussed above, sodium and phosphor were detected in the structure because of the application of sodium diphosphate during crosslinking procedure.

To compare the effectiveness of binding nanoparticles into the structure of scaffolds, noncrosslinked samples were used as a control. Comparing the percentage representation of selenium to the other detectable elements, selenium occupied only a small fraction of total content of detectable elements. Almost all of the *in situ* prepared samples did not beam the signal for the element selenium. One of the reasons why the *in situ* method might yield such dissatisfying results could be in the usage of the chemical crosslinker during the process of sample preparation. The selenium nanoparticles were not crosslinked into the structure of collagenous matrices through the biomaterial carriers (carboxymethyl-cellulose and chitosan) as we assumed. The selenium nanoparticles were leached out along with the EDC/NHS crosslinker during the crosslinking procedure. A small percentage representation of selenium could be spotted in *in situ* prepared collagenous samples containing SeCh nanoparticles (IN_Coll_SeCh), suggesting that the idea of crosslinking selenium nanoparticles into the structure of collagenous matrices could work but with a very low efficiency. On the other hand, in *ex situ* prepared samples, elemental selenium was relatively abundantly detected. From the results of the EDX analysis, we assumed that further using *in situ* prepared samples would not serve the purpose of this work. Therefore, we only used the *ex situ* prepared samples for further analysis.

Table 4: Summary of EDX elemental mapping of the samples containing selenium nanoparticles. Three series of samples were tested – non-crosslinked (labelled as NO_name of the sample), in situ prepared (labelled as IN_name of the sample) and ex situ prepared (labelled as EX_name of the sample). The total elemental content of the samples is 100 %. The value for each element represents its percentage relative to the total content of detectable elements.

Sample	**C [%]**	**N [%]**	**O [%]**	**Se [%]**	**Other elements (Na, K, Ca, P, S, Cl) [%]**	**Total [%]**
NO_Coll_SeCh	58.30	17.02	18.45	0.23	6.00	100
NO_Coll/Chit_SeCh	56.68	17.55	23.94	0.16	1.68	100
NO_Coll_SeB	70.52	0.00	22.35	0.26	6.86	100
NO_Coll/Chit_SeB	69.53	0.00	27.24	0.09	3.14	100
IN_Coll_SeCh	58.25	17.12	22.69	0.07	1.87	100
IN_Coll/Chit_SeCh	58.99	15.04	22.28	0.00	3.69	100
IN_Coll_SeB	56.47	16.76	25.52	0.00	1.25	100
IN_Coll/Chit_SeB	56.77	14.51	26.49	0.00	2.22	100
EX_Coll_SeCh	42.83	27.19	27.92	0.92	1.14	100
EX_Coll/Chit_SeCh	43.69	24.96	26.29	0.22	4.83	100
EX_Coll_SeB	57.65	21.16	15.24	0.35	5.61	100
EX_Coll/Chit_SeB	49.84	20.88	27.64	0.04	1.59	100

The SEM and EDX analyses were further used for the visualisation and determination of selenium nanoparticle distribution in the samples. Figure 14 represents the view of the collagen sample containing SeCh nanoparticles (Coll_SeCh) at a 25.0k× magnification, which corresponds to an area of 22.0×16.5μm2. Around the examined area, spherical particles with a very small diameter were spotted.

The average size of the nanoparticles obtained by analysis from the software ImageJ was 180±20 nm. The sizes corresponded to the sizes of selenium nanoparticles mentioned above (see chapter Characterization of Nanoparticles). From the SEM image, selenium nanoparticles seemed to be spread out evenly without any visible agglomerates. Unfortunately, due to the difficulties connected with getting higher magnification, we were unable to examine a closer view of the nanoparticles.

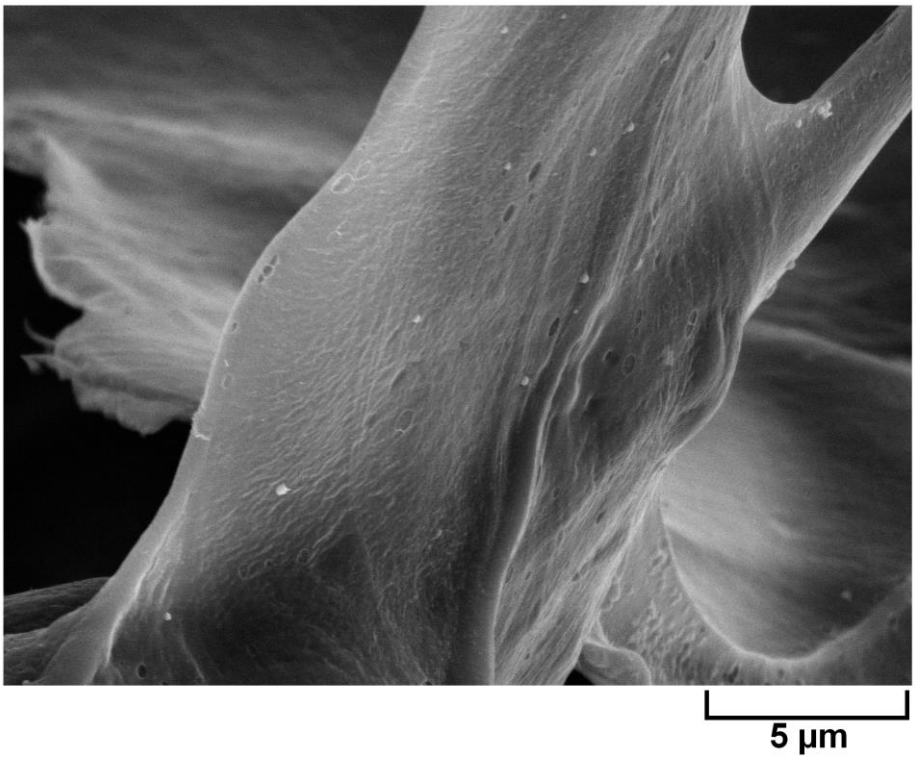

Figure 14: SEM visualisation of nanoparticles on the sample Coll_SeCh (ex situ prepared).

The homogenous distribution of selenium nanoparticles was further determined by EDX visualisation on SEM images. Figure 15 shows the EDX visualisation of selenium nanoparticles type SeCh on the collagen scaffold (Coll_SeCh). Selenium EDX signals were merged with carbon signals, which serves the purpose of depicting the microstructure of the scaffold. Selenium nanoparticles were spread out evenly in the whole structure of the scaffold. The rest of the SEM images with EDX visualisation can be found in the appendices (Appendix 3–4).

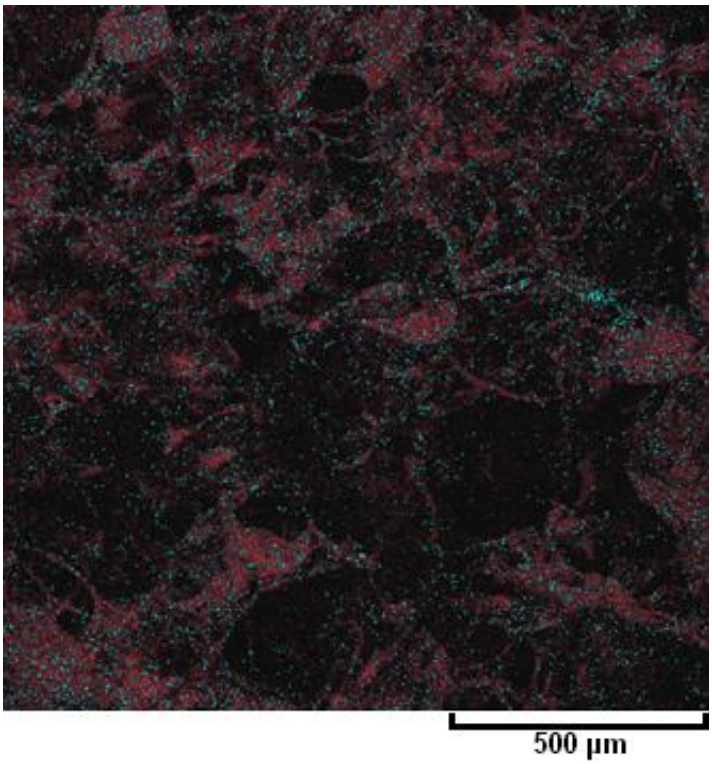

Figure 15: Representative image of EDX distribution of selenium element (blue) and carbon element (red) in the Coll_SeCh sample (ex situ prepared).

5.2 Microstructure and Porosity

One of the requirements for a scaffold is to be easily accepted by the body environment, meaning that the scaffold should have sufficient microstructure imitating the microenvironment, where cells could proliferate and differentiate. The characteristics of such a microenvironment include sufficient pore shapes, pore sizes, pore distribution and porosity.

The interconnected 3D porous structure of the scaffolds before and after addition of selenium nanoparticles is illustrated in Figure 16. The addition of selenium nanoparticles alternated the porous microstructure of the samples. Collagen samples (Coll) and collagen samples enriched only with chitosan (Coll/Chit) showed a honeycomb-like structure, which has been previously reviewed as highly suitable for cells.[47] Pore sizes and shapes seemed to bemore defined and uniform-looking. The difference between Coll and Coll/Chit microstructure could be spotted in the existence of fibres between pores, which were more visible in Coll/Chit SEM images.

The addition of solutions with selenium nanoparticles remodeled the defined honeycomb structure into a more fibrous structure. Remodeling of the structure is mainly caused by the biopolymer carriers of the selenium nanoparticles. The addition of SeCh nanoparticles interfered with the structure only slightly. In the Coll_SeCh sample, the pattern of the original the honeycomb structure was still visible. However, in the rest of the samples with selenium nanoparticles, honeycomb structure was mostly destroyed.

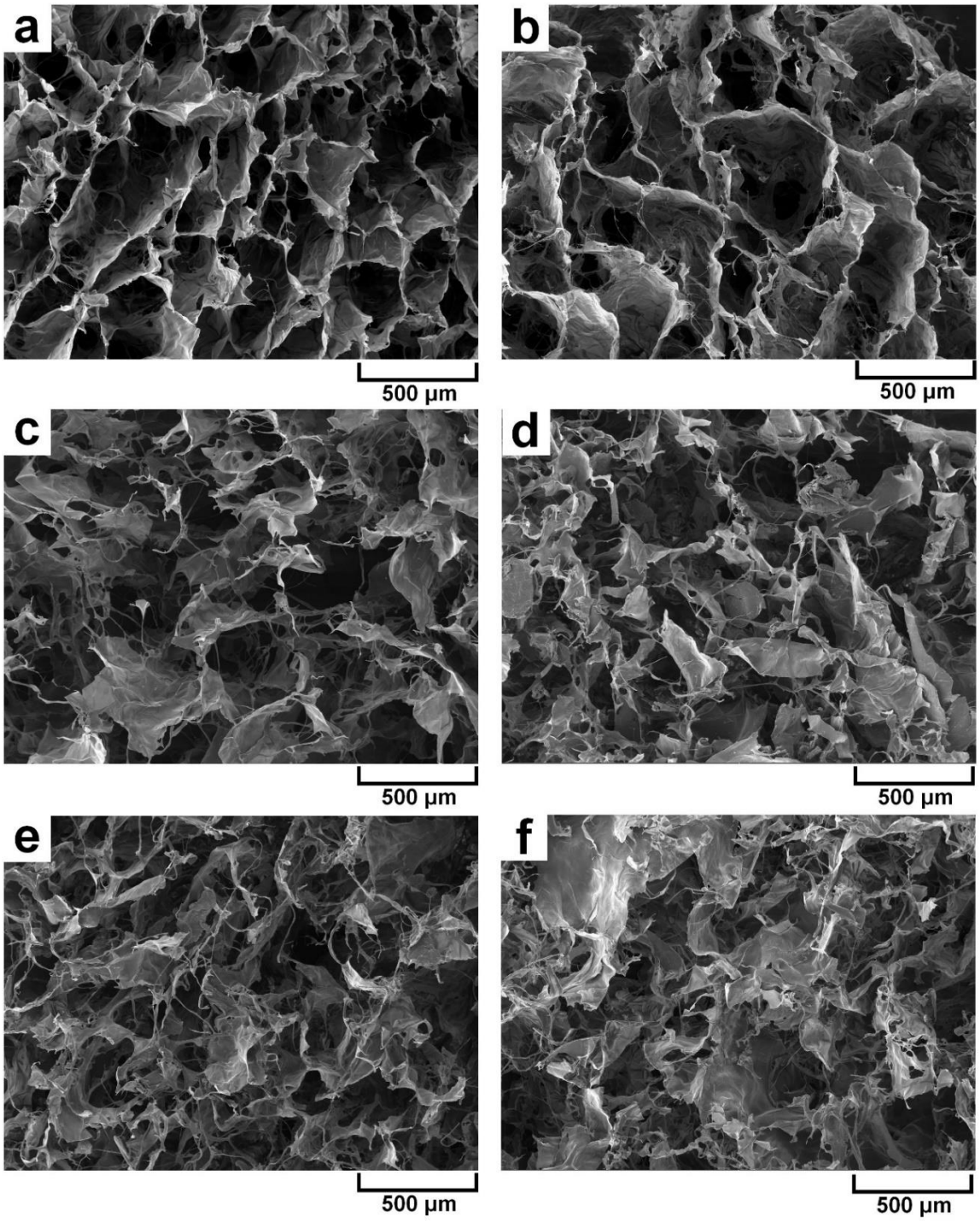

Figure 16: Cross-section SEM images of following samples - Coll (a), Coll/Chit (b), Coll_SeCh (c), Coll/Chit_SeCh (d), Coll_SeB (e), Coll/Chit_SeB (f). Samples were recorded at 175×magnification with the scale of 500 µm, displaying an area of 2×1.5 mm2.

Knowing, that there is a visual influence of selenium nanoparticles solutions on the microstructure of the samples, pore size distribution was evaluated (Figure 17). Pore sizes analysis from the SEM images revealed that the distribution of pores was decreasing to lower values with the order of samples: Coll ≈ Coll/Chit > Coll_SeCh > Coll/Chit_SeCh ≈ Coll_SeB > Coll/Chit_SeB.

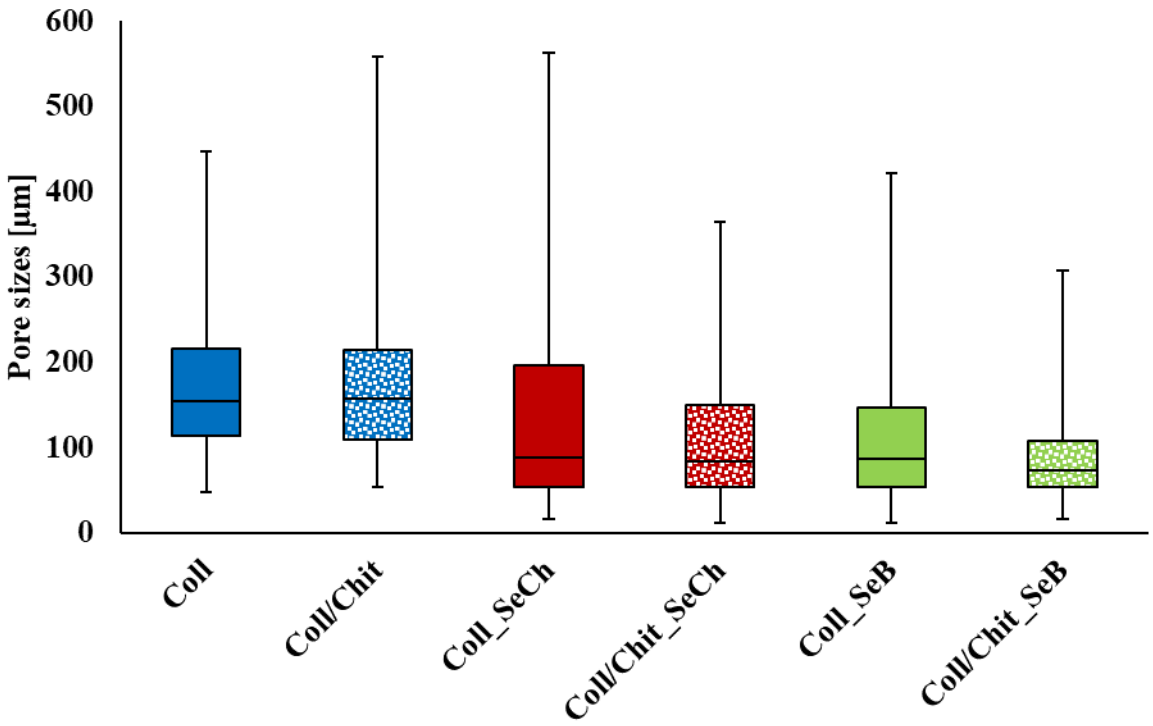

Figure 17: Pore size distribution analysis displayed by box plot. The lower error bars showing the minimum pore size values, the higher error bars showing the maximum pore size values. The bottoms and the tops of the individual boxes represent the first and the third quartiles of pore size values, respectively. The line dividing the box into the two parts stands for the median value of the pore sizes (second quartile).

Average pore sizes values are summarized in Table 5. It is debatable how the structure would influence cell proliferation *in vivo*. On the one hand, there has been a study on how pores with an average size of 300 µm and a honeycomb structure are sufficient for cells, on the other hand, there has also been a study suggesting that pores of 150 µm and lower are better for fibroblast proliferation.[47, 100] Detailed pore size distribution is enclosed in appendices (Appendix 5–7).

Table 5: Summary of average pore sizes.

Sample	**Average pore sizes [µm]**
Coll	179±19
Coll/Chit	177±18
Coll_SeCh	137±23
Coll/Chit_SeCh	118±18
Coll_SeB	118±18
Coll/Chit_SeB	94±13

Porosity was evaluated by Archimedes principle and the results are illustrated in Figure 18. Coll and Coll/Chit samples showed the highest values of porosity. One would assume that the trends of porosity would follow the trends of pore size distribution or that the samples with the smallest pores (samples enriched with SeB nanoparticles) would have the highest porosity. However, the samples cointaining selenium nanoparticles showed exactly the opposite trend to the trend of pore size distribution.

Porosity is defined as the fraction of the volume of empty spaces over the total volume. SeCh nanoparticles probably filled the collagenous sample with more material resulting in the smaller pores. On the other hand, carboxymethyl-cellulose (carrier of SeB nanoparticles) might only divide pores with its fibres without filling then in, resulting in lowering the porosity only slightly.

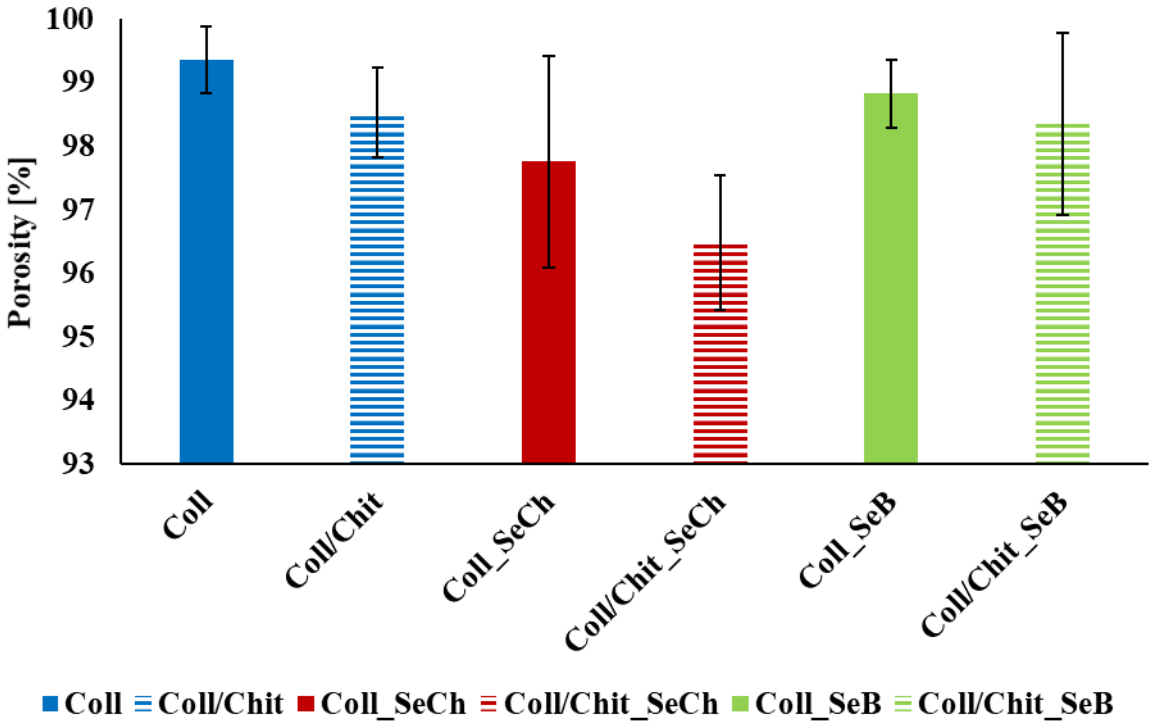

Figure 18: Porosity measured by Archimedes principle of collagen samples (full columns) and collagen-chitosan blends (dashed columns) with and without selenium nanoparticles.

5.3 Stability of Collagenous Sponges in Water Environment

Stability in a water environment and water-retaining properties are very important for the material used in skin regeneration. Material with good swelling properties could reduce the inflammation of the wound by preventing the accumulation of exudates. Swelling is characterised as the increase of sample mass after immersion in the liquid. Swelling behaviour is related to the existence of hydrophilic functional groups in the polymeric structure, which are responsible for creating hydrogen bonds with the surrounding liquid molecules. Swelling behaviour in an environment of ultrapure water is illustrated in Figure 19. All of the prepared samples showed a tendency to swell in a water environment. During the initial swelling, samples were probably absorbing more surplus water than when the swelling stabilized to the constant values, due to the liquid flow inside the scaffold. Hence the initial higher values of the swelling ratio can be observed in all of the samples. After around 20 minutes, all samples were fully swelled, and the swelling ratio became relatively constant at lower values. All samples were stable during the whole experiment and did not dissolve after immersion in ultrapure water. Stability in a water environment was greatly improved by EDC/NHS crosslinking. Crosslinking can stabilise collagenous matrices by creating new intramolecular bonds resulting in the lowering swelling ratios. This trend has been previously observed in[101].

The highest swelling ratio was noticed for collagen samples with no additives. The addition of chitosan into collagen scaffolds decreased the absorption of swelling water into the structure. This trend could be related to the creation of intramolecular bonds between collagen and the additive resulting in the decrease of free hydrophilic functional groups. A lowering of the swelling ratio in collagen-chitosan blends has been observed before.[102, 103] The addition of selenium nanoparticles also seems to be influencing the swelling ratios. The lowering of the values was mainly caused by the biomaterial carriers of selenium nanoparticles. Higher values of the standard deviation of the Coll, Coll_SeB and Coll/Chit_SeB samples are due to the fact that these samples absorbed a large amount of unbonded water and drying them out evenly was difficult. On the other hand, small differences between each sample in the case of samples containing SelenChitosan nanoparticles showed how impenetrably and hydrophobically these samples acted. Water hardly got into the porous structure of these samples, which made them less swelled.

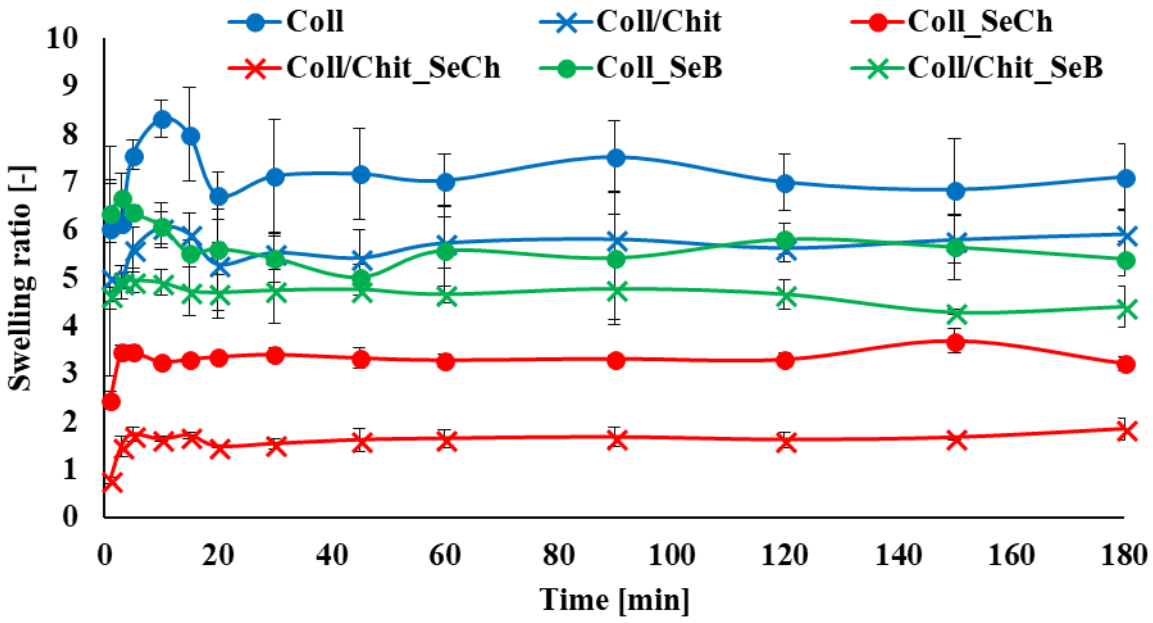

Figure 19: Swelling ratio of collagen samples (dot mark) and collagen-chitosan blends (cross mark) with and without selenium nanoparticles.

Since the addition of selenium nanoparticles alters the structure of the samples, one would assume that there is a connection between the microstructure of the samples and their swelling ratios. As could be seen in Figure 20, both porosity and swelling ratio curves follow a very similar pattern – the higher the porosity, the higher the swelling ratio of the sample is. Meaning that swelling ability could not only be related to the existence of free hydrophilic groups, but also to the porosity.

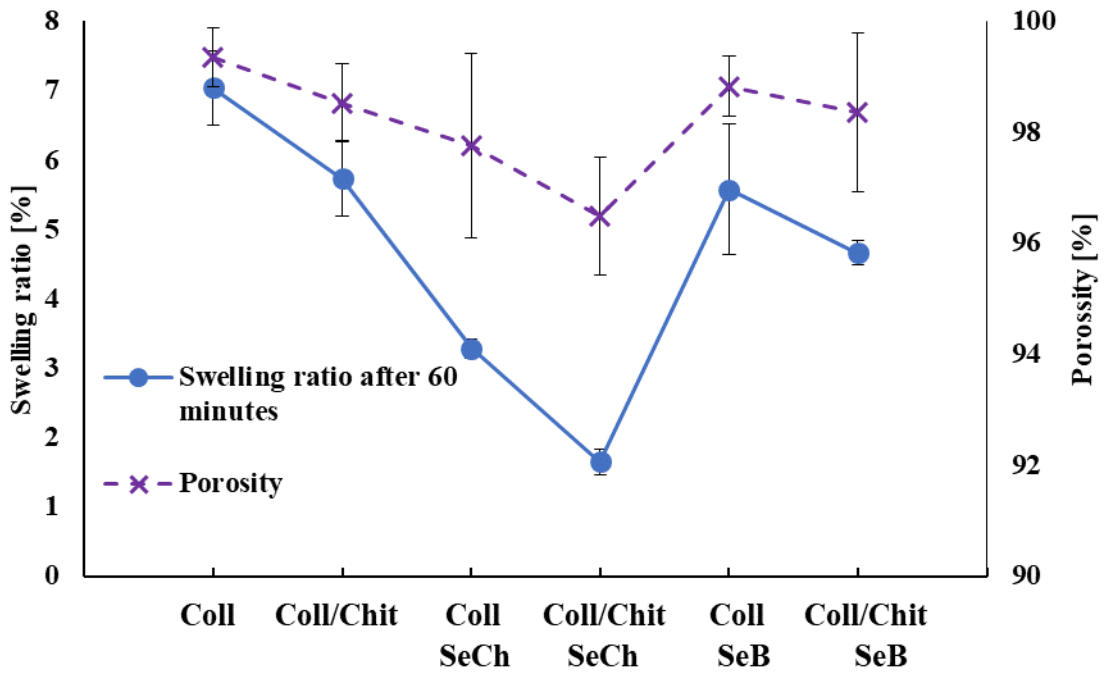

Figure 20: Trends of swelling ratio in water after 60 minutes (full line) and porosity (dashed line) of collagenous samples with and without additives.

The water content is related to the flow of water inside the sample. It is defined as the amount of water absorbed by swelling. Absorption of water into the microstructure is very important for wound healing, since the damp environment can help nutrient transportation and enhance growth and proliferation of cells. The water content values (Figure 21) copied the same trends as the swelling ratio values. The highest amount of water was absorbed by the Coll sample (85.7±1.1 %). A small decrease in the values could be seen in the Coll/Chit, Coll_SeB and Coll/Chit_SeB samples. The lowest values were measured in samples containing SeCh nanoparticles – Coll_SeCh (69.5±1.2 %) and Coll/Chit_SeCh (38.8±7.0 %). Though the values of the water content of samples containing SeCh nanoparticles were relatively low, all determined values are in agreement with the ranges of the water content of human skin. The water content of human skin ranges from 41 to 81 %, depending on the part of the body.[105]

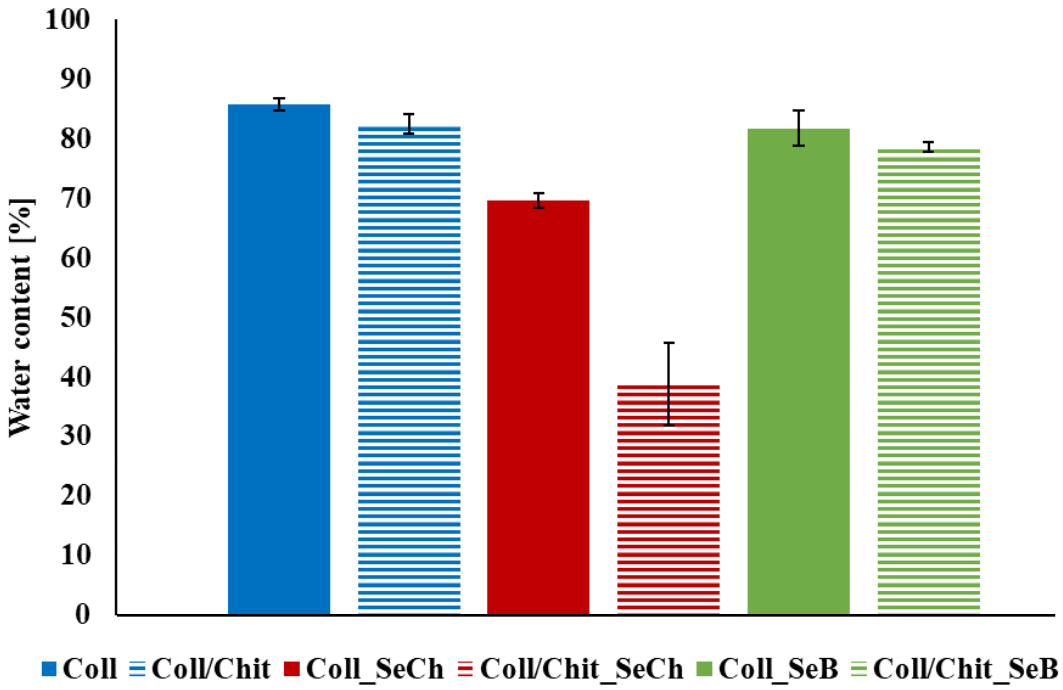

Figure 21: Water content values (after 60 minutes) of collagen samples (full columns) and collagen-chitosan blends (dashed columns) with and without selenium nanoparticles.

Stability in a water environment was further observed for a longer period of time (35 days). After one day of degradation, some samples still had the tendency to swell (Coll and Coll_SeB). All of the samples showed good stability in a water environment. After 35 days the weight loss ranged from 1.4 to 2.6 % (Figure 22).

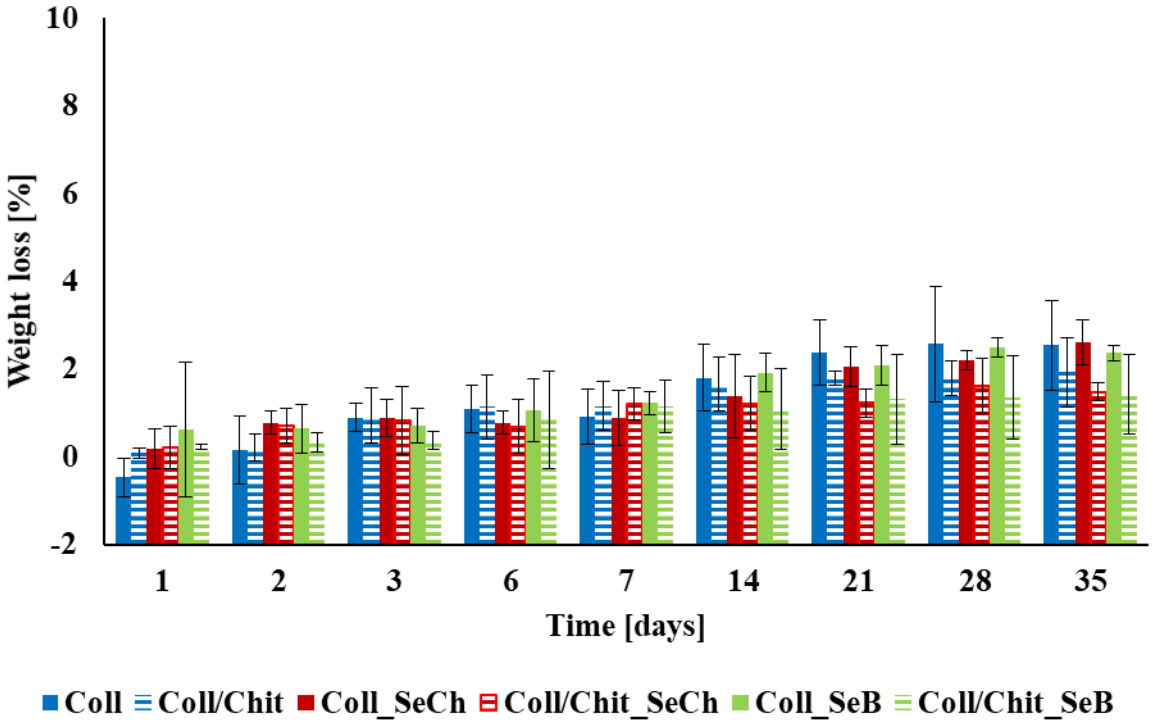

Figure 22: Degradation of collagen samples (full columns) and collagen-chitosan blends (dashed columns) with and without selenium nanoparticles in an environment of ultrapure water.

5.4 Degradation *in vitro*

Simulating *in vitro* degradation is necessary for obtaining information about material behaviour in the enzymatic environment, with the emphasis on adjusting the degradation rate to match the physiological healing of the wound tissue. Furthermore, this information is crucial to the design of systems for the controlled release of incorporated active compounds, such as selenium nanoparticles. The degradation rate of each scaffold can be easily modified by crosslinking treatment. As has been shown in [101], EDC/NHS treatment has shown a significant increase in the resistance of collagenous materials to enzymatic degradation. The increase in concentration of the chemical crosslinker decreases the amount of the weight loss.

Results of the degradation in the presence of collagenase are shown in Figure 23. A faster degradation rate of collagenous samples without the addition of chitosan was observed during day 1 of the degradation. For the rest of the days (2–6 days), the degradation of collagen without additives went through in a relatively stable manner. After two days (48 h) collagen samples with SeCh nanoparticles samples became unstable, resulting in two samples becoming completely disintegrated – no standard deviation can be observed. After three days (72 h) all of the Coll_SeCh samples disintegrated and could no longer be weighed. Coll_SeB samples followed the same trend, although they withstood the degradation for a little bit longer and fully disintegrated after 6 days of degradation (144 h). All collagenous samples enriched with chitosan did not fully disintegrate. However, observing the values of collagen-chitosan blends with selenium nanoparticles, a weight loss of around 50 % of the total mass (after 72 h) is visible, suggesting the stability of these samples was reinforced by chitosan, which held the samples together.

The increase in the degradation rate of collagenous samples with selenium nanoparticles could be related to the increase of collagenase activity caused by the existence of selenium nanoparticles in the samples. Selenium is a biogenic element, which plays important role in many physiological processes. As has been previously reviewed, some enzymes have shown different activity in the context of different concentrations of selenium. The most influenced activity has been the activity of selenoenzymes such as thioredoxin reductase.[105] Concerning collagenase activity, Broderius *et al.* [106] have found opposite trend to our findings – collagenase activity increased in muscle and heart of white muscle selenium deficient lambs in comparison with selenium supplemented lambs. However, these results were discussed with low statistical significance. To verify the hypothesis, further analysis on the dependence of collagenase activity on selenium concentration is needed.

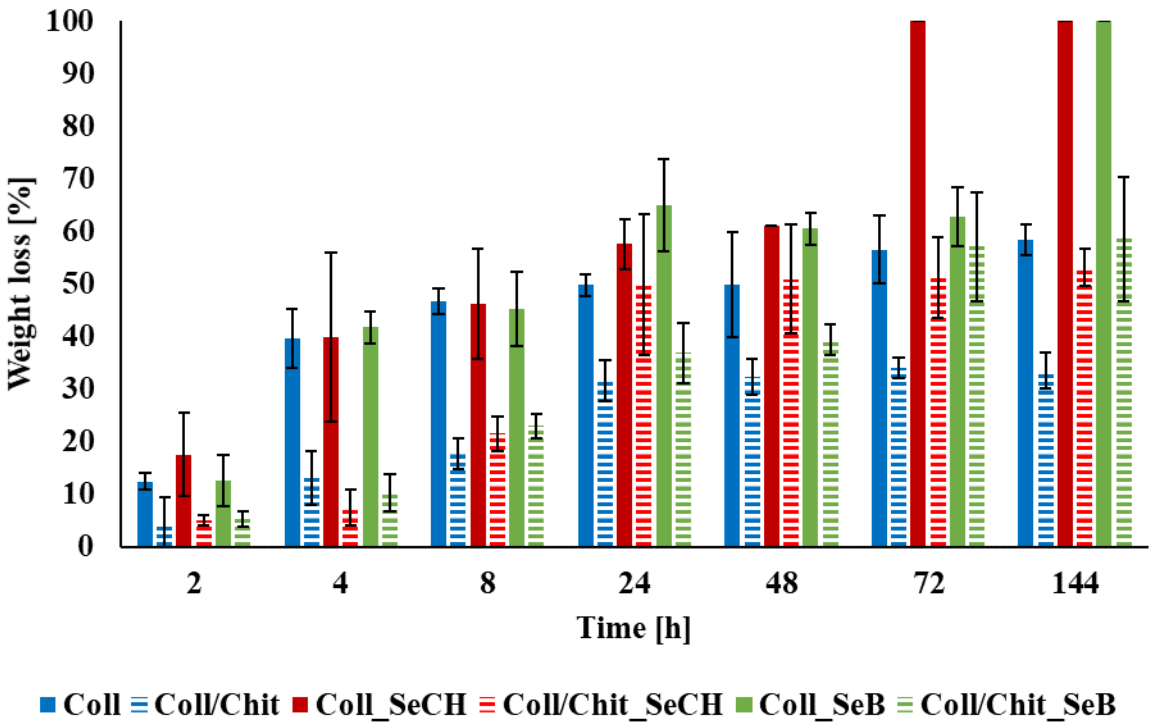

Figure 23: Degradation in the presence of collagenase (environment of PBS with pH 7.4 and 37 °C) of collagen samples (full columns) and collagen-chitosan blends (dashed columns) with and without selenium nanoparticles.

The degradation of collagenous samples enriched with chitosan in the presence of lysozyme is illustrated in Figure 24. Degradation was performed in an environment of PBS with pH adjusted to the values of 7.4 and 6.0. Lowering of the pH to more acidic values was carried out with the emphasis to the pH values referring to the highest activity of human lysozyme (around 6.0).[107] Lysozyme is mostly active in wounds, where is able to catalyse hydrolysis of 1,4-beta-linkages between N-acetylmuramic acid and N-acetyl-D-glucosamine residues in peptidoglycan, which is the major component of gram-positive bacterial cell wall. It has been shown that pH in a normal healing wound is more acidic because many of the bacteria strains are inactive under pH 6.0. It is one of the protecting mechanism of human body against bacterial infection. On the other hand, the pH of the chronic wound is more alkalic, resulting from untreated microorganism invasion.[108]

From the results that are shown in Figure 24, a higher activity of lysozyme at pH 6.0 can be observed. In comparison with the degradation rate in the presence of collagenase, lysozyme degradation followed almost the same degradation pattern with respect to the percentage of weight loss. The decrease in weight loss after 8 hours of degradation may be caused by the loosening of the intramolecular bonds between collagen and chitosan that were created during crosslinking procedure. Since collagen had proven to swell more than collagen-chitosan blends, the decrease might indicate that swelling overcomes degradation. The trend of fully disintegrated samples containing selenium nanoparticles and non-fully disintegrated samples without selenium nanoparticles after 6 days of degradation was also observed in the samples that underwent degradation in lysozyme.

A degradation study in presence of lysozyme was also carried out on collagenous samples without chitosan. However, no significant weight loss was observed. The only change that could be seen was the loss of the orange colour that collagenous samples with SeCh nanoparticles had. Figures illustrating the change in weight of collagenous samples and loss of orange colour are attached in the appendices (Appendix 8–9).

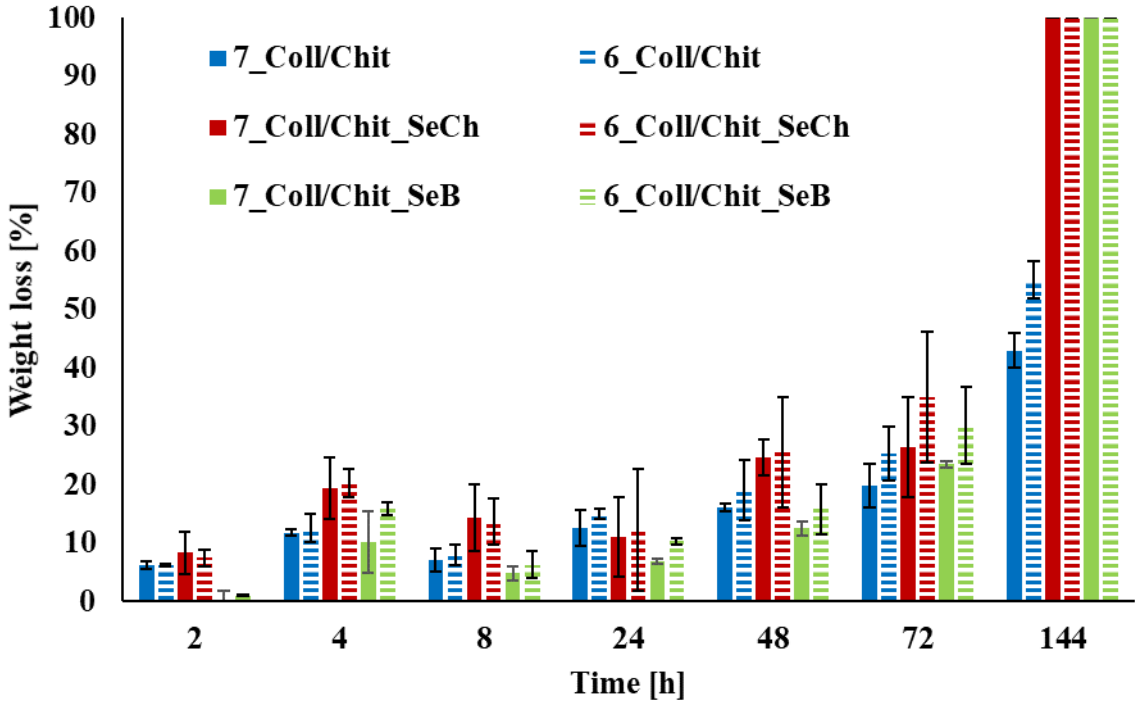

Figure 24: Degradation in lysozyme presence of collagen-chitosan blends with and without selenium nanoparticles. PBS was used as an environment with pH 7.4 (full column) and pH 6.0 (dashed column).

Samples were tested separately in the presence of each enzyme. For further studies, preparation of an environment with both enzymes is highly recommended. A mutual influence of enzymatic activity could be observed. The lysozyme concentration was chosen according to concentration of lysozyme in human tears. However, some studies have been reporting lower concentrations of lysozyme in human skin.[109] For further studies, lowering of lysozyme concentration is recommended. Degradation rates of samples were relatively high. With such a high tendency to degradation, materials would disintegrate faster than the wound would heal. There could be also a possibility that the degradation is size-dependent, so testing the enzymatic degradation on samples with larger dimensions is suggested.

5.5 Infrared Spectroscopic Analysis

The potential interaction of additives with specific functional groups and the alternation of the collagen structure after addition of antibacterial agents were observed using ATR-FTIR spectroscopy analysis. The changes in the chemical structure are reflected in the absorption spectra due to the changes in the molecular vibrations of the chemical bonds.

The spectrum of collagen without any additives can be seen in Figure 25. Five characteristic amide bands are displayed in the spectrum – amide A, B, I, II, and III. The amide A bands displayed vibration at around 3 312 cm^{-1}. This band is associated with the NH- stretching vibration and the existence of hydrogen bonds. A free NH- stretching vibration occurs in the range 3 400–3 440 cm^{-1}. When the NH- group is involved in a hydrogen bonding, the position is shifted to lower frequencies usually near 3 300 cm^{-1}.[110] Thus vibration at 3 312 cm^{-1} showed relatively strong hydrogen bonding. Amide B bands were located around 2 926 cm^{-1}. This characteristic band of collagen is related to an asymmetrical stretch of CH2- stretching vibration.[111] Amide I and II bands could be observed at wavenumbers of 1 651 cm^{-1} and 1 545 cm^{-1}. The amide I band is associated with C=O stretching vibration in the acetamide of the amide functional group.[112] The position of the amide II band is usually determined from N-H stretching vibration coupled with the C-N stretching vibration of collagen amide groups. The amide III band could be observed at 1 236 cm^{-1}.[112] The amide III band is a complex vibration of C-N stretching and N-H in-plane bending. It is also composed of absorptions arising from vibrations of CH2 groups from the glycine backbone and proline side chains.[113] Usually, amide bands I, II and III can be found at wavenumber ranges 1 600–1 690, 1 480–1 575, and 1 229–1 301 cm^{-1}, respectively. The existence of intermolecular interactions causes shifting of peaks to lower wavenumbers and could be an indication of the existence of hydrogen bonds as well. The band belonging to a wavenumber of 1450 cm^{-1} represented vibrations of CH3 groups in pyrrolidine rings of proline and hydroxyproline.[114] A wide band of vibration merging into the peak of amide A (3 447 cm^{-1}) displayed the vibrations of OH functional groups.

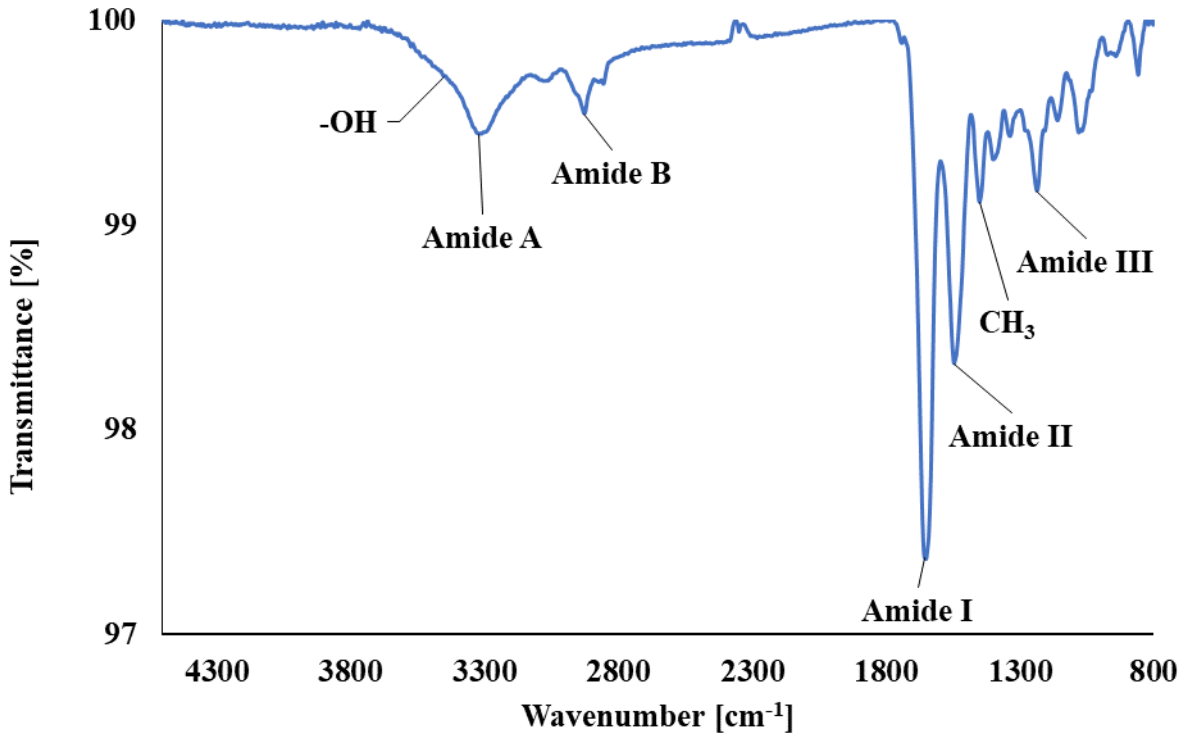

Figure 25: ATR-FTIR spectrum of collagen with no additives.

The spectrum of the collagen and chitosan blend (Figure 26) varied mainly in bands with wavenumbers of 943, 1 067 and 1 151 cm^{-1}. These characteristic bands belonged to the chemical nature of chitosan. The band of 943 cm^{-1} displays the bending of C-H groups in the polysaccharide structure. The vibration determined by C-O groups in glycosidic bondings can be observed at 1 067 cm^{-1}. The band at 1 151 cm^{-1} corresponded to the asymmetric vibration of C=O of polysaccharide.[104] The existence of the C=O peaks prove that chitosan was not fully deacetylated (DDA 70 %). The interactions between collagen and chitosan might occur by hydrogen bond formation. The -OH, -NH2 and -C=O groups in collagen are capable of forming hydrogen bonds with -OH and -NH2 in chitosan.[113] Hence slight shifts of amide bands in the spectrum of collagen-chitosan compared to the pure collagen spectrum could be seen. Also -OH functional groups (3 448 cm^{-1}) were more visible in the collagen-chitosan spectrum. Lowering of Amide I and II peak heights was displayed in the collagen-chitosan spectrum, corresponding to the trend observed in [113]. The band referring to the amide III absorption displayed a loss of intensity in the collagen-chitosan spectrum.

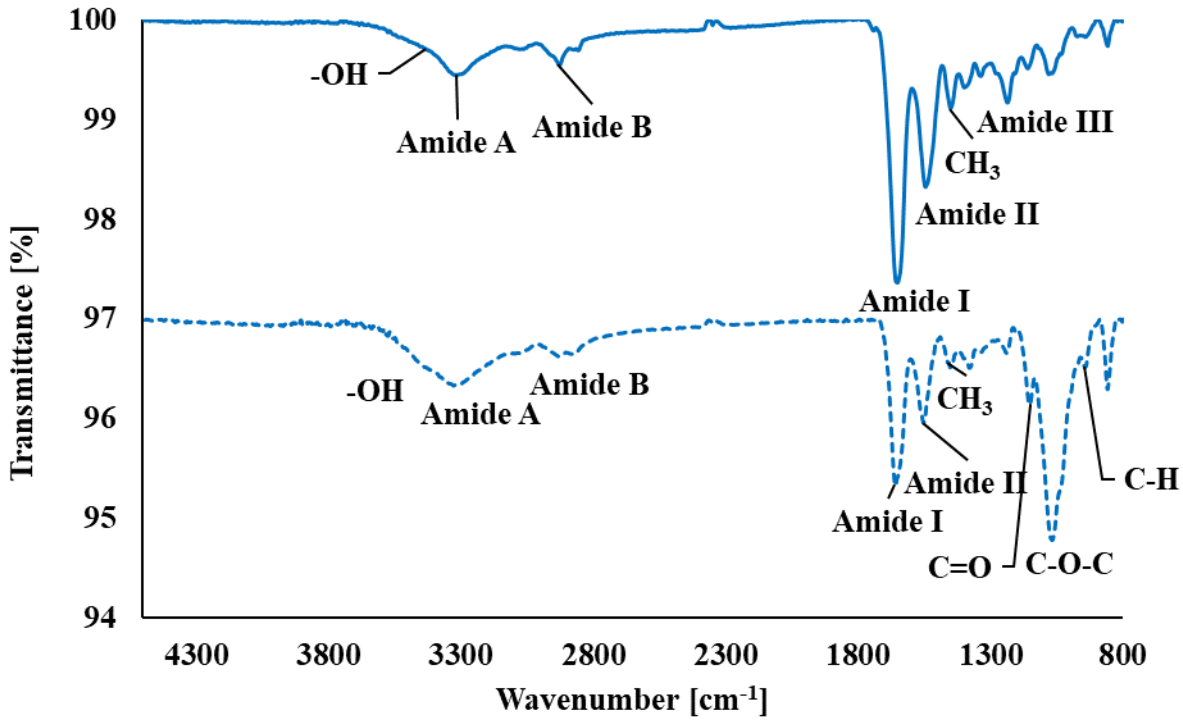

Figure 26: ATR-FTIR spectra of collagen (full line) and collagen-chitosan blends (dashed line). For a better visualisation the spectra were merged together. Therefore, transmittance values do not correspond with the measured data.

The higher structure of collagen can be evaluated with difficulty by Amide I and II band deconvolutation. However, an easy method of evaluating the transmittance ratio of pyrrolidine (CH3) and Amide III vibrations can give an insight into collagen triple helix integrity. Ratio values for denaturated collagen are around 0.5 and those for intact structures are around 1.0. The obtained triple helical structure ratio of pure collagen was 1.00, indicating that the triple helix structural motif was not destroyed during the process of sample preparation. The same ratio was obtained for the biomaterial blend of collagen and chitosan, suggesting the existence

of the triple helical structure as well. This is an important feature, since the hierarchical collagenous structure is considered to be responsible for collagen's biological and mechanical properties. The summary of characteristic bands and the triple helix ratio is given in Table 6.

Table 6: Characteristic bands and triple helix evaluation of collagen and collagen-chitosan samples.

Sample name	Wavenumber [cm^{-1}]						Triple helix ratio
	Amide A	Amide B	Amide I	Amide II	Amide III	Chitosan bands	
Coll	3 312	2 926	1 651	1 545	1 236	–	1.00
Coll/Chit	3 325	2 930	1 659	1 553	1 240	943;1 067; 1 151	1.00

ATR-FTIR spectra of collagenous matrices with selenium nanoparticles are illustrated in Figure 27 and characteristic vibrations are listed in Table 7. Small changes in the band positions might indicate the change in the hydrogen bonding. No novel bands were seen in the spectra of collagenous samples enriched with selenium nanoparticles. This may mean that selenium nanoparticles were not bonded into the structure of collagen or the concentrations of selenium nanoparticles may be too low to be detectable. The ratio determining the existence of the triple helix did not differ from the ratio of pure collagen, meaning that the triple helix was not disrupted by the addition of nanoparticles.

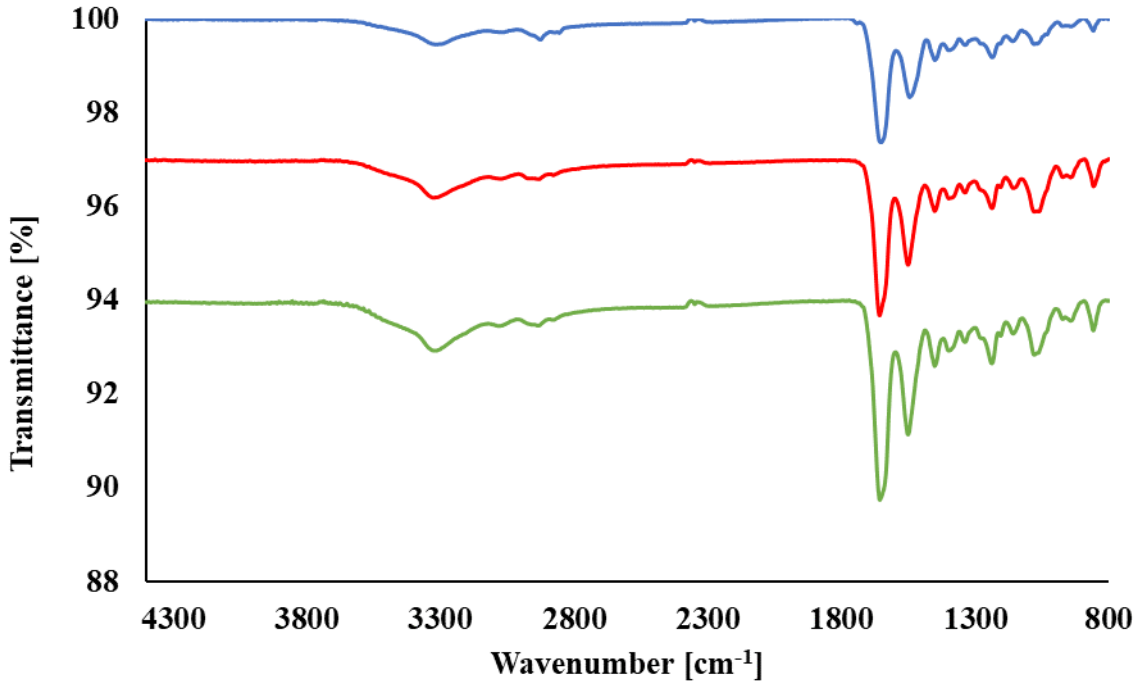

Figure 27: ATR-FTIR spectra of collagen (blue line), collagen with SelenChitosan nanoparticles (red line) and collagen with SelenBact nanoparticles (green line). For a better visualisation the spectra were merged together. Therefore, transmittance values do not correspond with the measured data.

Table 7: Characteristic bands and triple helix evaluation of collagen samples enriched with selenium nanoparticles.

Sample name	Wavenumber [cm^{-1}]					Triple helix ratio
	Amide A	Amide B	Amide I	Amide II	Amide III	
Coll	3 312	2 926	1 651	1 545	1 236	1.00
Coll_SeCh	3 325	2 932	1 657	1 551	1 236	1.00
Coll_SeB	3 319	2 935	1 657	1 551	1 238	1.00

ATR-FTIR spectra of collagen-chitosan blends with selenium nanoparticles are illustrated in Figure 28 and characteristic vibrations are listed in Table 8 The spectra yield the same results as the results discussed above − neither a distinct peak shifting, nor a new specific characteristic bands were observed in the spectra of collagen-chitosan blends enriched with selenium nanoparticles. The triple helix ratio values also remained unchanged.

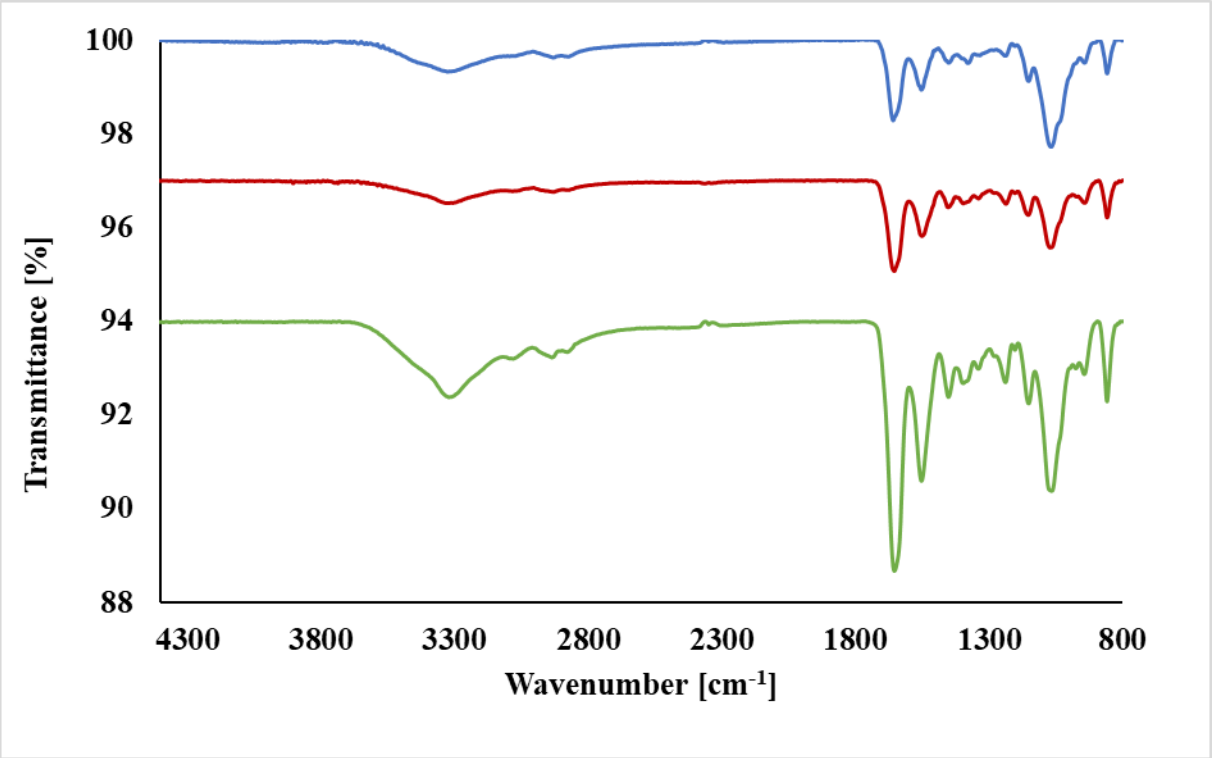

Figure 28: ATR-FTIR spectra of collagen-chitosan blend (blue line), collagen-chitosan blend with SelenChitosan nanoparticles (red line) and collagen-chitosan blend with SelenBact nanoparticles (green line). For a better visualisation the spectra were merged together. Therefore, transmittance values do not correspond with the measured data.

Table 8: Characteristic bands and triple helix evaluation of collagen-chitosan samples enriched with selenium nanoparticles.

Sample name	Wavenumber [cm^{-1}]						Triple helix ratio
	Amide A	Amide B	Amide I	Amide II	Amide III	Chitosan bands	
Coll/Chit	3 325	2 930	1 659	1 553	1 240	943; 1 067;1 151	1.00
Coll/Chit_SeCh	3 325	2 928	1 655	1 551	1 236	941; 1 072;1 153	1.00
Coll/Chit_SeB	3 321	2 935	1 655	1 553	1 238	943; 1 065;1 151	1.00

5.6 Release Kinetics Study

The release rate of selenium nanoparticles is illustrated in Figure 29. An initial burst followed by a slow release of selenium nanoparticles could be observed in all of the samples. The collagenous samples with SeB nanoparticles showed a higher release rate in the first half an hour (54.9±4.0 and 75.2±6.1 % for the Coll_SeB and Coll/Chit_SeB samples, respectively). The existence of chitosan in the collagenous matrices resulted in the increase of the amount of released SeNPs. Therefore, the collagen-chitosan matrices enriched with SeB nanoparticles released the highest amount of selenium nanoparticles. To summarize the results, the release ratio followed the order: Coll/Chit_SeB > Coll_SeB > Coll/Chit_SeCh > Coll_SeCh, where the Coll/Chit_SeB sample released the highest amount of selenium nanoparticles.

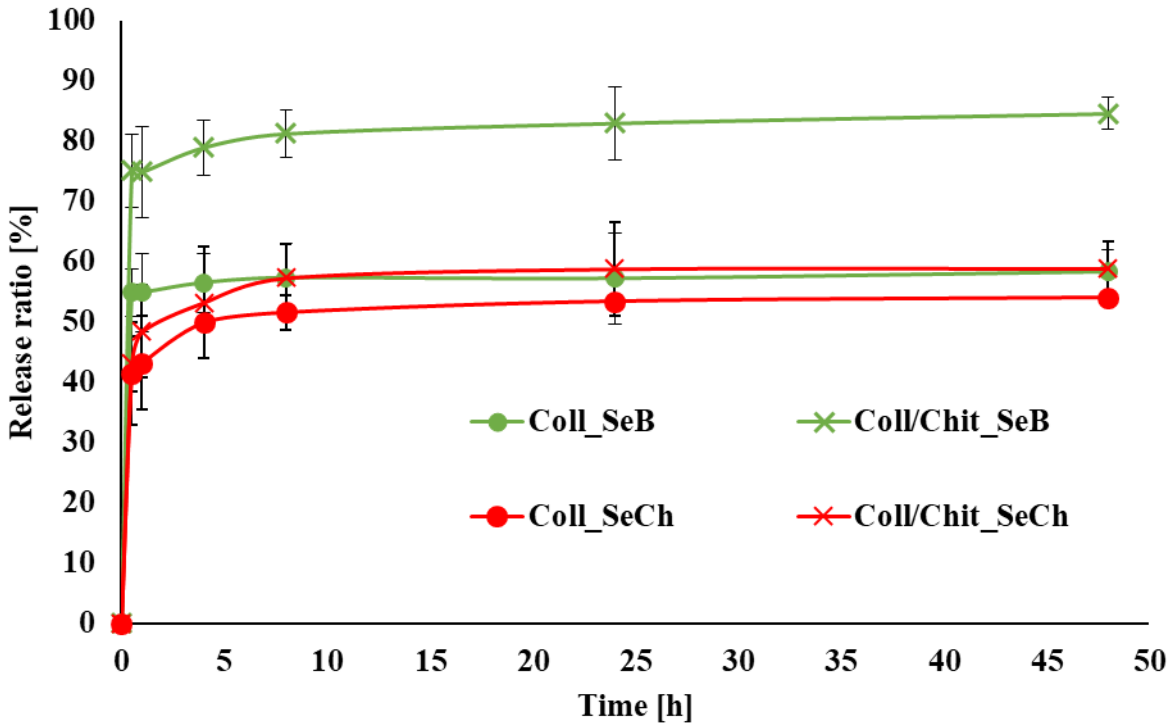

Figure 29: Time-dependent SeNPs-release profile (related to the amount of nanoparticles added during the preparation process) of collagenous samples (dot mark) and collagen-chitosan blends (cross mark).

After 8 hours, the release ratios became relatively stable on a constant value, meaning a minimum amount of nanoparticles was further released. As could be observed, a part of the total amount of nanoparticles did not release from the samples at all. This observation could be related to the pore sizes (Figure 30). The samples containing SeB nanoparticles had the smallest pore sizes and most of the selenium nanoparticles were probably attached onto the surface and did not penetrate deep into the structure. The addition of chitosan also decreased pore sizes in the microstructure, therefore it increased the amount of released SeNPs. To verify the hypothesis of the relation between the release rate and the pore sizes, further studies of the release kinetics in an enzymatic environment are recommended. Enzymes would cleave the structure of samples resulting in the release of a higher amount of nanoparticles.

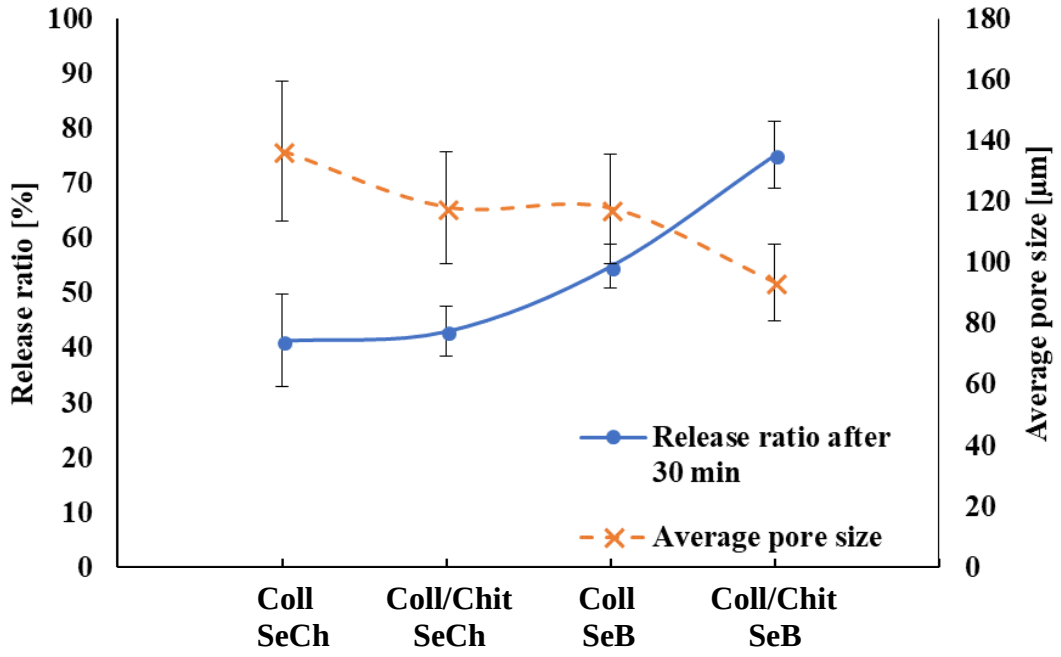

Figure 30: Trends of the release ratios of selenium nanoparticles in a water environment after 30 minutes (full line) and the average pore sizes (dashed line) of collagen-based sponges.

5.7 Antibacterial Activity Assay

According to the cytotoxicity studies, the higher the concentrations of selenium nanoparticles were, the lower the viability of fibroblasts was (Figure 31). The highest viability of fibroblast cells was observed for the selenium nanoparticles at concentrations 1 ppm. Since selenium is a biogenic element, smaller concentrations (around 1 ppm) seemed to have a positive effect on fibroblast viabilities – the results showed 152.6 % viability after 24 h and 134 % viability after 72 h compared to the positive control. Increase of the concentrations of selenium nanoparticles over 1 ppm resulted in the increase of the cytotoxicity towards fibroblasts. 5 ppm concentrations seemed to be the upper limit for the cytocompatible concentrations of selenium nanoparticles (123.8 % viability after 24 h and 66.4 % viability after 72 h). Concentrations above 5 ppm decreased viability under 100 % after 24 h and 72 hours. The cytotoxic studies were also carried out on the collagen-chitosan blends containing selenium nanoparticles. The same trend of the increasing cytotoxicity with the increasing concentrations of the selenium nanoparticles within the scaffolds was observed. More detailed assay from the cytotoxic study to be published.

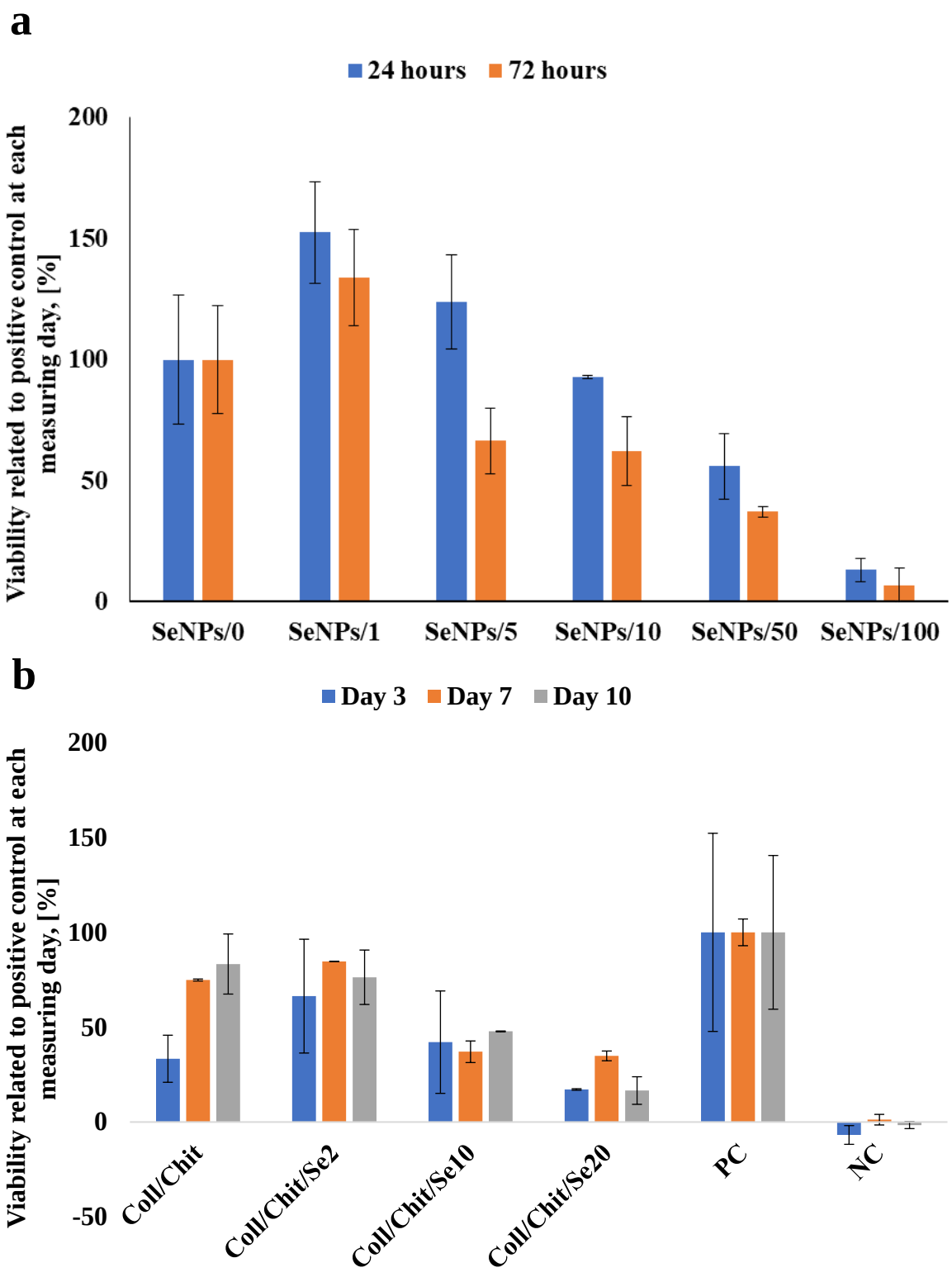

Figure 31: Viability of fibroblasts in contact with SeNPs (a) and collagen-chitosan blends enriched with SeNPs (b) The concentrations of SeNPs ranged from 0 to 100 ppm. The concentrations of selenium nanoparticles inside collagen-chitosan samples ranged from 0 to 20 ppm. Published with a permission of Ing. Johana Babrnáková.

In cooperation with Mendel University, antibacterial evaluation of prepared samples was executed. The testing of antibacterial activity followed the cytotoxic studies. For that reason, the concentrations of selenium nanoparticles were lowered, and only collagen-chitosan blends were used. The maximal concentration of selenium nanoparticles was 5 ppm. This concentration has been previously discussed as the limit concentration at which the selenium nanoparticles have been still performing any antibacterial activity.[93] The lowest examined concentration was 1 ppm.

The summarized results from the agar disk diffusion method can be seen in Table 9. The prepared samples did not exhibit any antibacterial activity towards the gram-negative bacterial strain (*E. coli*). The antibacterial activity was observed towards gram-positive bacterial strains (*S. aureus* and *Methicilin-resistant S. aureus*). The results showed that the creation of the inhibition zones was dose-dependent and the zones enlarged with the increasing concentrations of selenium nanoparticles. No antibacterial inhibition zone was found around the samples containing no selenium nanoparticles, as well around the samples containing SeNPs in the concentration of 1 ppm. The inhibition zones diameter of the5 ppm samples Coll/Chit_SeB and Coll/Chit_SeCh, were respectively 10.09 and 8.39 for *SA* and 10.79 and 8.6 for *MRSA*. Comparing the antibacterial activity of the 5 ppm scaffolds to the antibiotics (positive control), the samples demonstrated lower antibacterial activity. However, in materials, where the antibacterial agent would serve the purpose of prevention against microbial contamination, lower antibacterial activity is not a bad outcome. Also, it is important to point out that selenium nanoparticles created larger inhibition zone against *MRSA* than *SA*.

Table 9: Summary of the inhibition zone diameters.

Samples	**Inhibition zone [mm]**		
	E. coli	***S. aureus***	**Methicillin-resistant *SA***
Coll	0	0	0
Coll/Chit	0	0	0
1_Coll/Chit_SeCh	0	0	0
5_Coll/Chit_SeCh	0	8.39	8.6
1_Coll/Chit_SeB	0	0	0
5_Coll/Chit_SeB	0	10.09	10.75
Positive control	25.76	16.92	17.93

After the measurement of inhibition zones, the Coll/Chit, Coll/Chit_SeB, and Coll/Chit_SeCh samples were removed from the agar plate and used for the evaluation of live/dead assay. The purpose of the evaluation was to determine if the bacteria invade the inside structure of the material. The Coll/Chit sample was chosen to be the positive control. The samples that were exposed to *EC* were affected by the microbial invasion the most, meaning that there were found some dead cells, but the number of living ones prevailed. Regarding the samples that were exposed to *SA* and *MRSA*, the least amount of living cells was observed in the samples containing SeB nanoparticles. Nevertheless, the SeCh-samples also showed almost none living cells inside. Since the highest numbers of living cells were found in the Coll/Chit samples, one would assume that the addition of chitosan alone was not sufficient enough to obtain good antibacterial activity. Figure 32 is illustrating live/dead assay of the samples that were removed from the agar disk covered with *MRSA*. The rest of the images can be found in the appendices (Appendix 10–11).

The live/dead assay could be a good method for determining, if the bacteria cells proliferate through the scaffolds, where no inhibition zone was found. We think that inhibition zone is a great quantitative parameter for determination of antibacterial activity. However, in the materials, the prevention of microbial invasion inside the scaffold is sufficient enough. Therefore, further live/dead testing on samples containing 1 ppm nanoparticles is highly suggested.

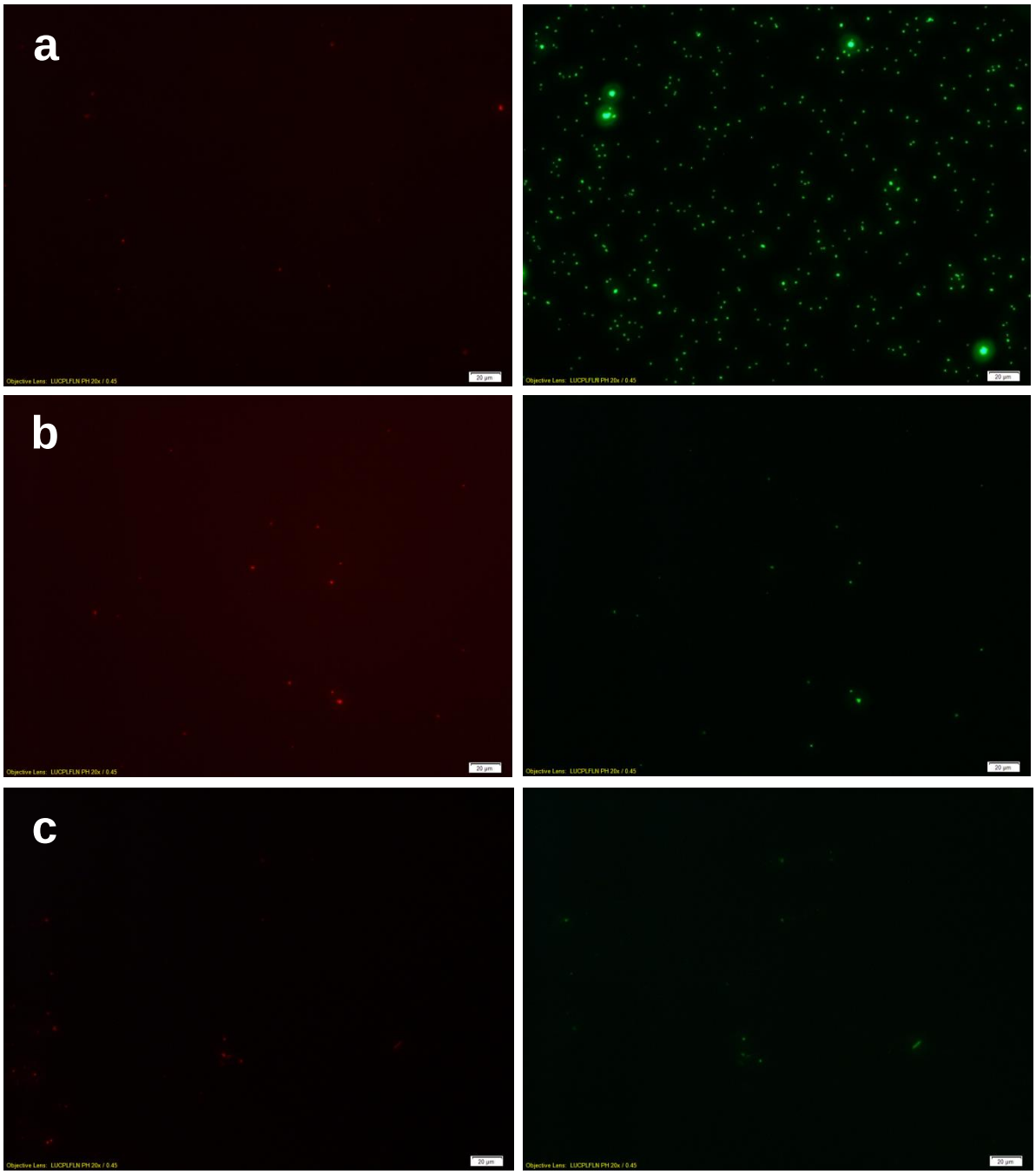

Figure 32: Representative live/dead assay image of Coll/Chit (a), Coll/Chit_SeCh (b) and Coll/Chit_SeB (c) samples after their removal from the agar plate covered with MRSA.

The antibacterial activity was further evaluated by the macrodilution broth method. The inhibition values are illustrated in Figure 33. The results obtained from the macrodilution broth method yield better insider look on the antibacterial activity of each sample. Also, in the future applications these materials might be used inside the body, which is mostly liquid environment. Therefore, the macrodillution method could yield more accurate results. In a broth environment, each of the samples exhibited some antibacterial activity resulting from the penetration of the broth through the whole porous structure. Hence bacteria were exposed to the whole structure, not just the surface. The addition of chitosan into the samples showed better antibacterial activity comparing to the pure collagen sample. The 1 ppm samples showed low toxicity towards *SA* and *E. coli*. The increase of the selenium concentrations

resulted in the increase of the antibacterial activity towards all of the tested bacterial strains, especially *MRSA*. Comparing the SeNPs-enriched samples with the Coll/Chit sample, SeNPs are definitely the agents, that grant the samples with antibacterial effect towards *MRSA*.

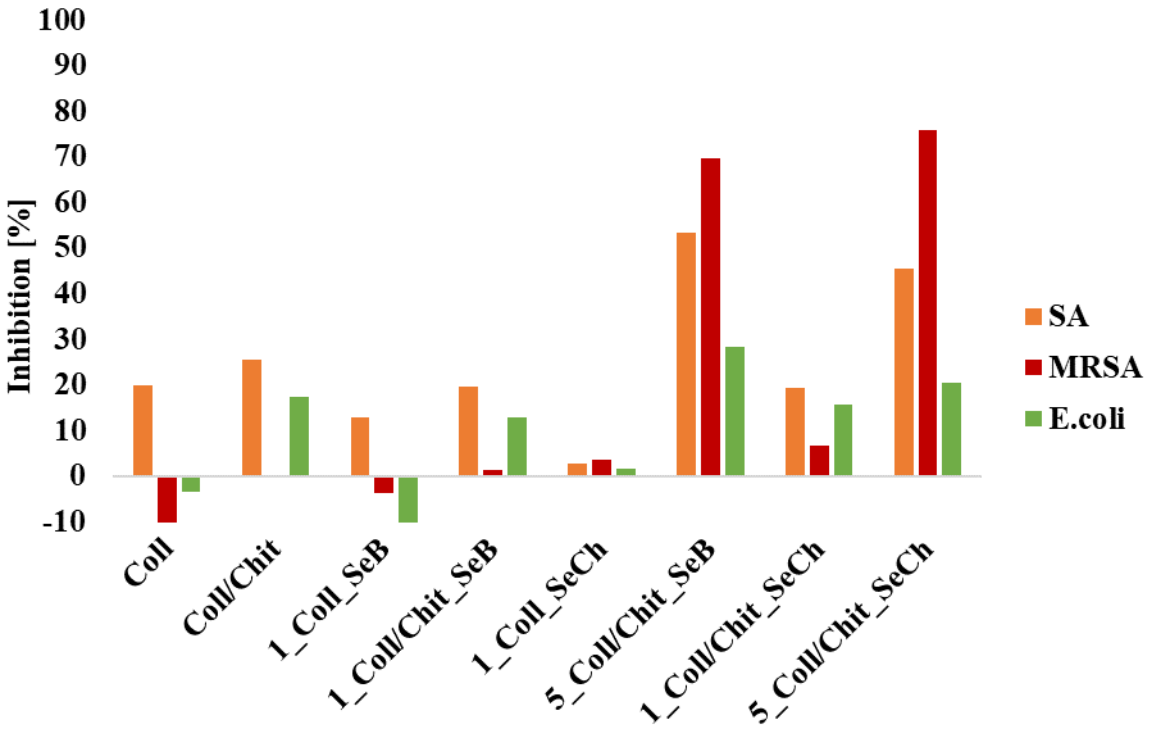

Figure 33: Inhibition of the bacterial growth of SA (orange), MRSA (red) and EC (green).

The antibacterial activity was also observed at regular time intervals, to obtain results comparable to the release kinetics curves. The results displaying bacterial inhibition of *SA* and *MRSA* compared to the release ratio profiles are illustrated in Figure 34. Since a very low bacterial inhibition of *E. coli* was observed, the results belonging to *E. coli* are attached in the appendices (Appendix 12). The time dependence bacterial inhibition curves of all the samples are also enclosed in the appendices (Appendix 13–14). According to the findings, the release of selenium nanoparticles did not copy the trends of bacterial inhibition over time. The rate of bacterial inhibition was delayed compared to the release rate of selenium nanoparticles. Even though, a burst release of selenium nanoparticles can be observed (most of the selenium nanoparticles released during the first half an hour), the bacterial inhibition proceeded with a slower rate. The selenium nanoparticles exhibited prolonged bacterial inhibition of *MRSA* compared to the inhibition of *SA*, which is corresponding with the previous findings. The released data used in these figures were obtained from the release study of the 18.5 ppm samples. Revise of the release experiment for the 5 ppm samples is highly suggested for the future work.

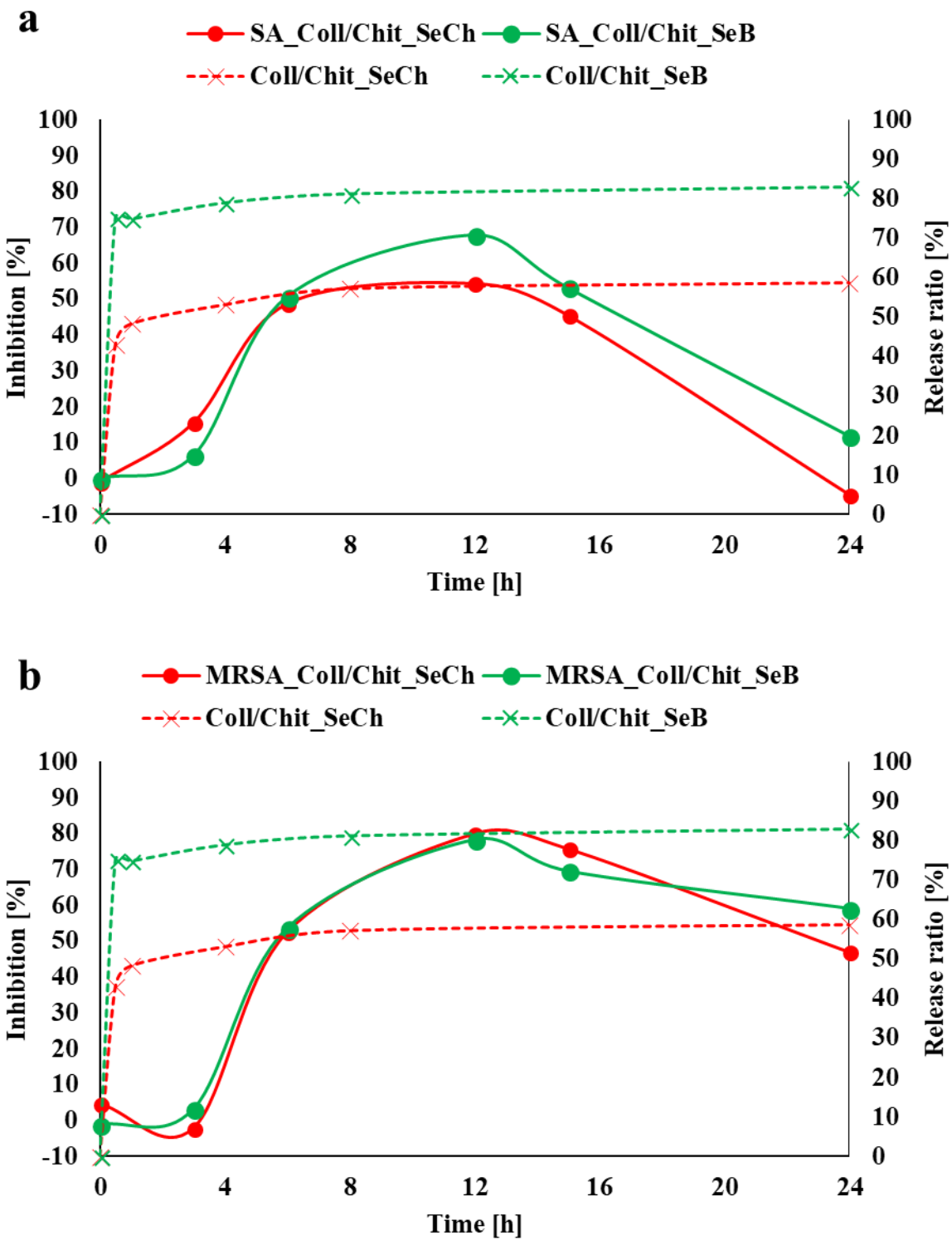

Figure 34: Combination of time-dependent bacterial inhibition profiles (full lines) and release ratio profiles of SeNPs (dashed lines). The bacterial inhibition was tested on two types of samples − Coll/Chit_SeCh (red lines) and Coll/Chit_SeB (green lines) in the presence of SA (a) and MRSA (b).

6 CONCLUSION

In the presented work 0.5% freeze-dried collagen sponges were prepared. These sponges were enriched by two types of antibacterial agents – chitosan and selenium nanoparticles. Use of nanoparticles in the biomedicine field of interest can be very controversial since metal nanoparticles have been raising the suspicion with their potential toxicity. Selenium nanoparticles could serve as a good replacement of metal nanoparticles since selenium is a biogenic element, that could be well received by the body environment. Cytocompatibility of selenium nanoparticles can be improved by binding them into the biopolymer carriers. In this work two types of selenium nanoparticles were used differing in the biopolymeric carriers – selenium nanoparticles bound in carboxymethyl-cellulose (SelenBact) and selenium nanoparticles bound in chitosan (SelenChitosan). The samples were prepared by the freeze-drying method of fabrication in an ultrapure water. Through the freeze-drying procedure 3D porous structure was achieved. Collagen-chitosan blends were prepared by addition of chitosan into the disintegrated collagen suspension. The samples enriched with selenium nanoparticles were prepared using two different procedures of preparation – *in situ* (addition of SeNPs before crosslinking) and *ex situ* (addition of SeNPs after crosslinking).

The EDX analysis was carried out for the purpose of selenium nanoparticles detection and evaluation of their homogeneous distribution it the samples. The summarization of the EDX elemental mapping showed a very low efficiency of binding selenium nanoparticles into the *in situ* samples comparing to the *ex situ* and the non-crosslinked samples. After the evaluation of elemental mapping, the *in situ* samples were not used for further characterization. The EDX distribution of selenium element in the *ex situ*-prepared samples showed homogenous distribution of selenium nanoparticles.

The SEM analysis was carried out to gain an insight into the microstructure of the porous scaffolds. The freeze-drying procedure created porous 3D structure within the samples. The additives significantly changed the microstructure visually. The pore size distribution analysis showed that the average pore sizes decreased in the following order – Coll ≈ Coll/Chit > Coll_SeCh > Coll/Chit_SeCh ≈ Coll_SeB > Coll/Chit_SeB. The largest pores possessed pure collagen sample (the average pore size value – 179±19 μm) and the smallest pores possessed Coll/Chit_SeB (the average pore size value – 94±13 μm). The samples did not exhibit homogenous pore size distribution. The pore size distribution should be taken into the consideration when creating a material for regenerative medicine, since the addition of antibacterial agents could change the morphology of microstructure. If the change would have a positive or negative effect on the cells viability is hard to predict, since there are a lot of papers with different results. A further complex study on how the change in the microstructure after addition of antibacterial agents influence the viability of cells is highly recommended. Change in the microstructure can influence the proliferation and differentiation of cells. Porosity was measured using Archimedes principle and the trends of porosity followed the order: Coll > Coll/Chit > Coll_SeB > Coll/Chit_SeB > Coll_SeCh > Coll/Chit_SeCh, where Coll sample possesed the highest porosity.

The stability of the samples in a water environment was gravimetrically evaluated. All samples were stable during the whole process of swelling and degradation measurements (up to 35 days in a water environment). The stability was improved by the EDC/NHS treatment. Pure collagen samples exhibited the highest swelling ratios. The addition of antibacterial agents decreased the swelling ratios to lower values, following the order – Coll > Coll/Chit ≈ Coll/SeB > Coll/Chit_SeB > Coll_SeCH > Coll/Chit_SeCh. The order corresponded to the porosity data, suggesting that the swelling ratios are influenced by porosity. The water content values followed the same trend as swelling ratios – the pure collagen sample absorbed the highest amount of water (85.7±1.1 %) and the collagen sample enriched with chitosan and SeCh nanoparticles absorbed the least amount of water (38.8±7.0 %). The range of the water content values corresponded to the range of *in vivo* water content in human skin. The samples remained stable for the 35 days, with a maximal weight loss of 2.6 %. During the 35 days, no significant difference in the degradation rate between the samples was observed.

As expected the degradation rate of the samples in the presence of collagenase and lysozyme, separately, was higher than in a water environment. The faster degradation rate should be taken into the consideration when fabricating scaffolds with matching degradation rate to the normal tissue. Both collagenase and lysozyme enzymatic degradations were performed in the course of 6 days. In the presence of collagenase, the collagen samples enriched only with the nanoparticles disintegrated fully within 6 day, despite the fact the pure collagen samples remained stable during the whole measurement. Complete disintegration of the collagen-chitosan samples enriched with selenium nanoparticles in the presence of lysozyme was also observed (at both pH). These results might suggest the positive effect of selenium nanoparticles on the enzymatic activity of both collagenase and lysozyme.

The ATR-FTIR analysis was carried out to determine how the additives interacted with the collagen-specific groups. The pure collagen sample displayed characteristics bands related to the Amide A, B, I, II and III bands, which are characteristic for the collagen peptide bonds. The lower position of Amide A band might be related to the relatively high content of hydrogen bonds represented in the sample. Observing the collagen-chitosan blends, the bands belonging to the polysaccharidic structure of chitosan added up to the spectrum of the pure collagen. The slight shifts of collagenous bands could be the implication of changes in the content of hydrogen bonds, since collagen and chitosan may bind together through them. Selenium nanoparticles were not visible in the ATR-FTIR spectra, however small changes in the bands positions were observed. The triple helix ratio was 1.00 in all of the samples, meaning that the triple helical structure of the collagen did not lose its integrity during the process of samples preparation.

The release kinetics of selenium nanoparticles was carried out on ICP-OES. The samples exhibited a burst release of selenium nanoparticles in the first 30 minutes (values ranged from 41.4±8.5 to 75.2±6.1 %). After 8 hours, the release rate set on a constant value, meaning no or a minimum amount of selenium nanoparticles were further released. The highest values of percentage release were observed in the samples enriched with chitosan and selenium nanoparticles type SeB, leading us to believe there is a connection between the pore sizes and release rate – the smaller the sizes, the higher the release rate. The overall lower values of the amounts of selenium nanoparticles released form the samples, suggesting that a certain amount of nanoparticles was incorporated deeper into the structure and did not release at all.

The whole experiment was set up in the environment of ultrapure water. To achieve better results concerning a better simulation of physiological conditions and a higher release rate of incorporated nanoparticles, revision of experiment in a presence of enzymes is highly suggested.

The samples exhibited a better antibacterial activity in the liquid environment of the macrodilution method than in a relatively dry environment of the agar diffusion disk method. Even though the samples enriched with chitosan exhibited better antibacterial activity compared to the pure collagen samples, selenium nanoparticles stood behind the main contribution to the bacterial inhibition. The samples were tested on gram-negative (*E. coli*) and gram-positive (*Staphylococcus aureus*, Methicillin-resistant *Staphylococcus aureus*) bacterial strains. The inhibition of the bacterial growth was observed only in the gram-positive cultures. It is worth mentioning that the samples enriched with the selenium nanoparticles showed an antibacterial effect against Methicillin-resistant *Staphylococcus aureus*. Satisfactory bacterial inhibition was observed only in the samples with the maximal concentration of selenium nanoparticles (5 ppm). The results obtained from the live/dead assay showed that *SA* and *MRSA* did not overgrow within the samples showing antibacterial activity. Comparing the trends of bacterial inhibition over time with the trends of release kinetics of selenium nanoparticles a delay in the bacterial inhibition was observed. The results also shown better and prolonged antibacterial effect of selenium nanoparticles towards MRSA compared to SA and EC.

Based on the presented results, collagenous matrices enriched with chitosan and selenium nanoparticles are good candidates for the further use in the field of regenerative medicine. Both chitosan and selenium nanoparticles showed satisfactory antibacterial activity regarding to noncytotoxic concentrations. Although further studies on how the scaffolds enriched with these additives would interact with a biological environment are needed.

7 REFERENCES

[1] Organ Donation Statistics. *Organdonor.gov* [online]. Health Resources & Services Administration [cit. 2017-12-10].

[2] BÖTTCHER-HABERZETH, Sophie, Thomas BIEDERMANN a Ernst REICHMANN. Tissue engineering of skin. *Burns*. 2010, **36**(4), 450−460.

[3] KATARI, Ravi S., Andrea PELOSO a Giuseppe ORLANDO. Tissue Engineering. *Advances in Surgery*. 2014, **48**(1), 137−154.

[4] GARG, Tarun, Onkar SINGH, Saahil ARORA a R. S. R. MURTHY. Scaffold: a Novel Carrier for Cell and Drug Delivery. *Critical Reviews™ in Therapeutic Drug Carrier Systems*. 2012, **29**(1), 1−63.

[5] KUMBAR, Sangamesh G., Cato T. LAURENCIN a Meng DENG, ed. *Natural and synthetic biomedical polymers*. Burlington: Elsevier, 2014. ISBN 978−0−12−396983−5.

[6] Gene and Cell Therapy Defined. *American Society of Gene & Cell Therapy* [online]. Milwaukee: American Society of Gene & Cell Therapy [cit. 2018−04−07].

[7] DIECKMANN, Christina, Regina RENNER, Linda MILKOVA a Jan C. SIMON. Regenerative medicine in dermatology: biomaterials, tissue engineering, stem cells, gene transfer and beyond. *Experimental Dermatology*. 2010, **19**(8), 697−706.

[8] MAYET, Naeema, Yahya E. CHOONARA, Pradeep KUMAR, Lomas K. TOMAR, Charu TYAGI, Lisa C. DU TOIT a Viness PILLAY. a Comprehensive Review of Advanced Biopolymeric Wound Healing Systems. *Journal of Pharmaceutical Sciences*. 2014, **103**(8), 2211−2230.

[9] ABOU NEEL, Ensanya A., Laurent BOZEC, Jonathan C. KNOWLES, Omaer SYED, Vivek MUDERA, Richard DAY a Jung Keun HYUN. Collagen – Emerging collagen based therapies hit the patient. *Advanced Drug Delivery Reviews*. 2013, **65**(4), 429−456.

[10] RAMANATHAN, Giriprasath, Sivakumar SINGARAVELU, Thangavelu MUTHUKUMAR, Sitalakshmi THYAGARAJAN, Paramasivan Thirumalai PERUMAL a Uma Tiruchirapalli SIVAGNANAM. Design and characterization of 3D hybrid collagen matrixes as a dermal substitute in skin tissue engineering. *Materials Science and Engineering: C*. 2017, 72, 359−370.

[11] RAJENDRAN, Naresh Kumar, Sathish Sundar Dhilip KUMAR, Nicolette Nadene HOURELD a Heidi ABRAHAMSE. a review on nanoparticle based treatment for wound healing. *Journal of Drug Delivery Science and Technology*. 2018, 44, 421−430.

[12] YANNAS, Ioannis V., Dimitrios S. TZERANIS a Peter T.C. SO. Regeneration mechanism for skin and peripheral nerves clarified at the organ and molecular scales. *Current Opinion in Biomedical Engineering*. 2018, 6, 1−7.

[13] JEON, Eun Young, Bong-Hyuk CHOI, Dooyup JUNG, Byeong Hee HWANG a Hyung Joon CHA. Natural healing-inspired collagen-targeting surgical protein glue for accelerated scarless skin regeneration. *Biomaterials*. 2017, 134, 154−165.

[14] GAUGLITZ, Gerd a Hans KORTING. Hypertrophic Scarring and Keloids: Pathomechanisms and Current and Emerging Treatment Strategies. *Molecular Medicine*. 2010, **17**(1-2), 113−125.

[15] O'BRIEN, Fergal J. Biomaterials and scaffolds for tissue engineering. *Materials Today*. 2011, **14**(3), 88−95.

[16] CHEUNG, Hoi-Yan, Kin-Tak LAU, Tung-Po LU a David HUI. A critical review on polymer-based bio-engineered materials for scaffold development. *Composites Part B: Engineering*. 2007, **38**(3), 291−300.
[17] GODAVITARNE, Charles, Alastair ROBERTSON, Jonathan PETERS a Benedict ROGERS. Biodegradable materials. *Orthopaedics and Trauma*. 2017, **31**(5), 316−320.
[18] LIU, Xing, Lie MA, Zhengwei MAO a Changyou GAO. Chitosan-Based Biomaterials for Tissue Repair and Regeneration. *Chitosan for Biomaterials II*. 2011, 244, 81−127.
[19] LOH, Qiu Li a Cleo CHOONG. Three-Dimensional Scaffolds for Tissue Engineering Applications: Role of Porosity and Pore Size. *Tissue Engineering Part B: Reviews*. 2013, **19**(6), 485−502.
[20] NEVES, Nuno N., Rui CAMPOS, Adriano J. PREDRO a Rui L. REIS. Patterning of polymer nanofiber meshes by electrospinning for biomedical applications. *International Journal of Nanomedicine*. 2007, **2**(3), 433−448.
[21] EL-SHERBINY, Ibrahim M. a Magdi H. YACOUB. Hydrogel scaffolds for tissue engineering: Progress and challenges. *Global Cardiology Science and Practice*. 2013, 3, 1−27.
[22] GUPTA, Vineet, Yusuf KHAN, Cory J. BERKLAND, Cato T. LAURENCIN a Michael S. DETAMORE. Microsphere-Based Scaffolds in Regenerative Engineering. *Annual Review of Biomedical Engineering*. 2017, **19**(1), 135−161.
[23] LIN, Yunfeng, ed. *Osteogenesis*. London: InTech, 2012. ISBN 978-953-51-0030-0.
[24] KHANG, Gilson, Moon Suk KIM a Hai Bang LEE, ed. *A manual for biomaterials: scaffold fabrication technology*. New Jersey: World Scientific, 2007. ISBN 978-981-270-595-2.
[25] LU, Tingli, Yuhui LI a Tao CHEN. Techniques for fabrication and construction of three-dimensional scaffolds for tissue engineering. *International Journal of Nanomedicine*. 2013, 337−350.
[26] CHASE, George G., Jackapon S. VARABHAS a Darell H. RENEKER. New Methods to Electrospin Nanofibers. *Journal of Engineered Fibers and Fabrics*. 2011, **6**(3), 32−38.
[27] SHOULDERS, Matthew D. a Ronald T. RAINES. Collagen Structure and Stability. *Annual Review of Biochemistry*. 2009, **78**(1), 929−958.
[28] LI, Qing, Lanlan MU, Fenghua ZHANG, Yue SUN, Quan CHEN, Cuicui XIE a Hongmei WANG. a novel fish collagen scaffold as dural substitute. *Materials Science and Engineering: C*. 2017, **80**, 346−351.
[29] ELANGO, Jeevithan, Jingyi ZHANG, Bin BAO, Krishnamoorthy PALANIYANDI, Shujun WANG, Wu WENHUI a Jeya Shakila ROBINSON. Rheological, biocompatibility and osteogenesis assessment of fish collagen scaffold for bone tissue engineering. *International Journal of Biological Macromolecules*. 2016, **91**, 51−59.
[30] BARBOSA, Mário A. *Peptides and proteins as biomaterials for tissue regeneration and repair*. Duxford: Woodhead Publishing, 2018. ISBN 978-008-1008-034.
[31] FRIESS, Wolfgang. Collagen – biomaterial for drug delivery. *European Journal of Pharmaceutics and Biopharmaceutics*. 1998, **45**(2), 113−136.
[32] WEGST, Ulrike G. K., Hao BAI, Eduardo SAIZ, Antoni P. TOMSIA a Robert O. RITCHIE. Bioinspired structural materials. *Nature Materials*. 2015, **14**(1), 23−36.
[33] GLOWACKI, Julie a Shuichi MIZUNO. Collagen scaffolds for tissue engineering. *Biopolymers*. 2008, **89**(5), 338−344.

[34] LAUER-FIELDS, Janelle L., Darius JUSKA a Gregg B. FIELDS. Matrix metalloproteinases and collagen catabolism. *Biopolymers*. 2002, **66**(1), 19−32.
[35] CHATTOPADHYAY, Sayani, Ronald T. RAINES a Gary D. GLICK. Review collagen-based biomaterials for wound healing. *Biopolymers*. 2014, **101**(8), 821−833.
[36] PARENTEAU-BAREIL, Rémi, Robert GAUVIN a François BERTHOD. Collagen-Based Biomaterials for Tissue Engineering Applications. *Materials*. 2010, **3**(3), 1863−1887.
[37] DAVIDENKO, N., C.F. SCHUSTER, D.V. BAX, N. RAYNAL, R.W. FARNDALE, S.M. BEST a R.E. CAMERON. Control of crosslinking for tailoring collagen-based scaffolds stability and mechanics. *Acta Biomaterialia*. 2015, **25**, 131−142.
[38] WEADOCK, Kevin S., Edward J. MILLER, Lisa D. BELLINCAMPI, Joseph P. ZAWADSKY a Michael G. DUNN. Physical crosslinking of collagen fibers: Comparison of ultraviolet irradiation and dehydrothermal treatment. *Journal of Biomedical Materials Research*. 1995, **29**(11), 1373−1379.
[39] HUA, Jiachuan, Zheng LI, Wen XIA, Ning YANG, Jixian GONG, Jianfei ZHANG a Changsheng QIAO. Preparation and properties of EDC/NHS mediated crosslinking poly (gamma-glutamic acid)/epsilon-polylysine hydrogels. *Materials Science and Engineering: C*. 2016, **61**, 879−892.
[40] ZEEMAN, Raymond, Pieter J. DIJKSTRA, Pauline B. VAN WACHEM, Marja J.A. VAN LUYN, Marc HENDRIKS, Patrick T. CAHALAN a Jan FEIJEN. Successive epoxy and carbodiimide cross-linking of dermal sheep collagen. *Biomaterials*. 1999, **20**(10), 921−931.
[41] GRABAREK, Zenon a John GERGELY. Zero-length crosslinking procedure with the use of active esters. *Analytical Biochemistry*. 1990, **185**(1), 131−135.
[42] OLDE DAMINK, L.H.H., P.J. DIJKSTRA, M.J.A. VAN LUYN, P.B. VAN WACHEM, P. NIEUWENHUIS a J. FEIJEN. Cross-linking of dermal sheep collagen using a water-soluble carbodiimide. *Biomaterials*. 1996, **17**(8), 765−773.
[43] Carbodiimide Crosslinker Chemistry. *Thermo Fisher Scientific* [online]. Paisley (UK): Thermo Fisher [cit. 2018-04-07].
[44] PENSALFINI, Marco, Alexander E. EHRET, Silvia STÜDELI, Daniela MARINO, Andres KAECH, Ernst REICHMANN a Edoardo MAZZA. Factors affecting the mechanical behavior of collagen hydrogels for skin tissue engineering. *Journal of the Mechanical Behavior of Biomedical Materials*. 2017, 69, 85−97.
[45] BROWN, Robert A. in the beginning there were soft collagen-cell gels: towards better 3D connective tissue models? *Experimental Cell Research*. 2013, **319**(16), 2460−2469.
[46] FENG, Zhonggang, Yusuke WAGATSUMA, Masato KIKUCHI, et al. The mechanisms of fibroblast-mediated compaction of collagen gels and the mechanical niche around individual fibroblasts. *Biomaterials*. 2014, **35**(28), 8078−8091.
[47] GEORGE, Joseph, Jun ONODERA a Teruo MIYATA. Biodegradable honeycomb collagen scaffold for dermal tissue engineering. *Journal of Biomedical Materials Research Part A*. 2008, **87**(4), 1103−1111.
[48] GAUTAM, Sneh, Chia-Fu CHOU, Amit K. DINDA, Pravin D. POTDAR a Narayan C. MISHRA. Surface modification of nanofibrous polycaprolactone/gelatin composite scaffold by collagen type I grafting for skin tissue engineering. *Materials Science and Engineering: C*. 2014, 34, 402−409.

[49] AHSAN, Saad M., Mathai THOMAS, Kranthi K. REDDY, Sujata Gopal SOORAPARAJU, Amit ASTHANA a Ira BHATNAGAR. Chitosan as biomaterial in drug delivery and tissue engineering. *International Journal of Biological Macromolecules*. 2017, **104**.

[50] ORYAN, Ahmad a Sonia SAHVIEH. Effectiveness of chitosan scaffold in skin, bone and cartilage healing. *International Journal of Biological Macromolecules*. 2017, 104, 1003−1011.

[51] VARAN, Nilufer Y. The Use of Titration Technique and FTIR Bands to Determine the Deacetylation Degree of Chitosan Samples. *Journal of Textile Science & Engineering.* 2017, **7**(2).

[52] WIEGAND, C., D. WINTER a U.-C. HIPLER. Molecular-Weight-Dependent Toxic Effects of Chitosans on the Human Keratinocyte Cell Line HaCaT. *Skin Pharmacology and Physiology*. 2010, **23**(3), 164−170.

[53] FREIER, Thomas, Hui Shan KOH, Karineh KAZAZIAN a Molly S. SHOICHET. Controlling cell adhesion and degradation of chitosan films by N-acetylation. *Biomaterials*. 2005, **26**(29), 5872−5878.

[54] CHATELET, C. Influence of the degree of acetylation on some biological properties of chitosan films. *Biomaterials*. 2000, **22**(3), 261−268.

[55] CROISIER, Florence a Christine JÉRÔME. Chitosan-based biomaterials for tissue engineering. *European Polymer Journal*. 2013, **49**(4), 780−792.

[56] DAI, Tianhong, Masamitsu TANAKA, Ying-Ying HUANG a Michael R HAMBLIN. Chitosan preparations for wounds and burns: antimicrobial and wound-healing effects. *Expert Review of Anti-infective Therapy*. 2014, **9**(7), 857−879.

[57] HUANG, Shuya, Baoqin HAN, Kai SHAO, Miao YU a Wanshun LIU. Analgesis and wound healing effect of chitosan and carboxymethyl chitosan on scalded rats. *Journal of Ocean University of China*. 2014, **13**(5).

[58] LIU, Haifeng, Jinshu MAO, Kangde YAO, Guanghui YANG, Lei CUI a Yilin CAO. a study on a chitosan-gelatin-hyaluronic acid scaffold as artificial skin *in vitro* and its tissue engineering applications. *Journal of Biomaterials Science, Polymer Edition*. 2004, **15**(1), 25−40.

[59] SANAD, Rania Abdel-Basset a Hend Mohamed ABDEL-BAR. Chitosan–hyaluronic acid composite sponge scaffold enriched with Andrographolide-loaded lipid nanoparticles for enhanced wound healing. *Carbohydrate Polymers*. 2017, **173**, 441−450.

[60] AL-BAYATY, Fouad Hussain, Mahmood Ameen ABDULLA, Mohamed Ibrahim Abu HASSAN a Hapipah Mohd ALI. Effect of Andrographis paniculata leaf extract on wound healing in rats. *Natural Product Research*. 2012, **26**(5), 423−429.

[61] AGARWAL, Tarun, Rajan NARAYAN, Somnath MAJI, et al. Gelatin/Carboxymethyl chitosan based scaffolds for dermal tissue engineering applications. *International Journal of Biological Macromolecules*. 2016, **93**, 1499−1506.

[62] PATEL, Satish, Shikha SRIVASTAVA, Manju Rawat SINGH a Deependra SINGH. Preparation and optimization of chitosan-gelatin films for sustained delivery of lupeol for wound healing. *International Journal of Biological Macromolecules*. 2017.

[63] SALEEM, Mohammad. Lupeol, a novel anti-inflammatory and anti-cancer dietary triterpene. *Cancer Letters*. 2009, **285**(2), 109−115.

[64] HAJIPOUR, Mohammad J., Katharina M. FROMM, Ali AKBAR ASHKARRAN, et al. Antibacterial properties of nanoparticles. *Trends in Biotechnology*. 2012, **30**(10), 499−511.

[65] *GLOBAL TUBERCULOSIS REPORT 2017*. Geneva: World Health Organization 2017, 2017. ISBN 978-92-4-156551-6.

[66] BAEK, Yong-Wook, Youn-Joo AN, Patricia A. WILEY, Lisa WEN, J. Scott MCCONNELL a Baohong ZHANG. Microbial toxicity of metal oxide nanoparticles (CuO, NiO, ZnO, and Sb2O3) to Escherichia coli, Bacillus subtilis, and Streptococcus aureus. *Science of The Total Environment*. 2011, **409**(8), 1603−1608.

[67] MANESS, Pin-Ching, Sharon SMOLINSKI, Daniel M. BLAKE, Zheng HUANG, Edward J. WOLFRUM a William A. JACOBY. Bactericidal Activity of Photocatalytic TiO2 Reaction: toward an Understanding of Its Killing Mechanism. *Applied and environmental microbiology*. 1999, **65**(9), 4094−4098.

[68] BUI, Vu, Duckshin PARK a Young-Chul LEE. Chitosan Combined with ZnO, TiO2 and Ag Nanoparticles for Antimicrobial Wound Healing Applications: A Mini Review of the Research Trends. Polymers. 2017, 9(12), 21−45.

[69] BROWN, MICHAEL R. W., DAVID G. ALLISON a PETER GILBERT. Resistance of bacterial biofilms to antibiotics a growth-rate related effect. *Journal of Antimicrobial Chemotherapy*. 1988, **22**(6), 777−780.

[70] BANIN, Ehud, ALEXANDRA FRIEDMAN, ROXANNE LAHMI a AHARON GEDANKEN. Antibiofilm surface functionalization of catheters by magnesium fluoride nanoparticles. *International Journal of Nanomedicine*. 2012, **7**, 1175−1188.

[71] PARK, Hongsuk, Hee-Jin PARK, Jeong Ah KIM, Seung Hwan LEE, Jong Hyo KIM, Jeyong YOON a Tai Hyun PARK. Inactivation of Pseudomonas aeruginosa PA01 biofilms by hyperthermia using superparamagnetic nanoparticles. *Journal of Microbiological Methods*. 2011, **84**(1), 41−45.

[72] AHMAD, Bashir, Nabia HAFEEZ, Shumaila BASHIR, Abdur RAUF a MUJEEB-UR-REHMAN. Phytofabricated gold nanoparticles and their biomedical applications. *Biomedicine & Pharmacotherapy*. 2017, **89**, 414−425.

[73] JIA, Yan-Peng, Bu-Yun MA, Xia-Wei WEI a Zhi-Yong QIAN. The *in vitro* and *in vivo* toxicity of gold nanoparticles. *Chinese Chemical Letters*. 2017, **28**(4), 691−702.

[74] PITCHAIMANI, Arunkumar, Tuyen Duong Thanh NGUYEN, Mukund KOIRALA, Yuntao ZHANG a Santosh ARYAL. Impact of cell adhesion and migration on nanoparticle uptake and cellular toxicity. *Toxicology in Vitro*. 2017, **43**, 29−39.

[75] PAN, Yu, Sabine NEUSS, Annika LEIFERT, et al. Size-Dependent Cytotoxicity of Gold Nanoparticles. *Small*. 2007, **3**(11), 1941−1949.

[76] DURÁN, Nelson, Marcela DURÁN, Marcelo Bispo DE JESUS, Amedea B. SEABRA, Wagner J. FÁVARO a Gerson NAKAZATO. Silver nanoparticles: a new view on mechanistic aspects on antimicrobial activity. *Nanomedicine: Nanotechnology, Biology and Medicine*. 2016, **12**(3), 789−799.

[77] RESHI, Mohd S., , Deepa YADAV, Chhavi UTHRA, Sadhana SHRIVASTAVA, Jatinder S. ARORA a Sangeeta SHUKLA. Pure silver nanoparticles showed potential anticancer effect on colon and breast cancer cell lines. *Octa Journal of Biosciences*. 2016, **4**(2), 46−48.

[78] YUE, Yang, Xiaomei LI, Laura SIGG, Marc J-F SUTER, Smitha PILLAI, Renata BEHRA a Kristin SCHIRMER. Interaction of silver nanoparticles with algae and fish cells: a side by side comparison. *Journal of Nanobiotechnology*. 2017, **15**(1), 1−11.

[79] VRČEK, Ivana Vinković, Irena ŽUNTAR, Roberta PETLEVSKI, Ivan PAVIČIĆ, Maja DUTOUR SIKIRIĆ, Marija ĆURLIN a Walter GOESSLER. Comparison of *in vitro* toxicity of silver ions and silver nanoparticles on human hepatoma cells. *Environmental Toxicology*. 2016, **31**(6), 679−692.

[80] SOKOŁOWSKA, Paulina, Kamila BIAŁKOWSKA, Małgorzata SIATKOWSKA, Marcin ROSOWSKI, Magdalena KUCIŃSKA, Piotr KOMOROWSKI, Krzysztof MAKOWSKI a Bogdan WALKOWIAK. Human brain endothelial barrier cells are distinctly less vulnerable to silver nanoparticles toxicity than human blood vessel cells. *Nanomedicine: Nanotechnology, Biology and Medicine*. 2017, **13**(7), 2127−2130.

[81] STHIJNS, Mireille M.J.P.E., Waluree THONGKAM, Catrin ALBRECHT, Bryan HELLACK, Aalt BAST, Guido R.M.M. HAENEN a Roel P.F. SCHINS. Silver nanoparticles induce hormesis in A549 human epithelial cells. *Toxicology in Vitro*. 2017, **40**, 223−233.

[82] CHAUDHARY, Savita, Ahmad UMAR a S.K. MEHTA. Selenium nanomaterials: an overview of recent developments in synthesis, properties and potential applications. *Progress in Materials Science*. 2016, **83**(1), 270−329.

[83] WADHWANI, Sweety A., Utkarsha U. SHEDBALKAR, Richa SINGH a Balu A. CHOPADE. Biogenic selenium nanoparticles: current status and future prospects. *Applied Microbiology and Biotechnology*. 2016, **100**(6), 2555−2566.

[84] MONSEN, ELAINE R. Dietary Reference Intakes for The Antioxidant Nutrients. *Journal of the American Dietetic Association*. 2000, **100**(6), 637−640.

[85] WADHWANI, Sweety A., Utkarsha U. SHEDBALKAR, Richa SINGH a Balu A. CHOPADE. Biogenic selenium nanoparticles: current status and future prospects. *Applied Microbiology and Biotechnology*. 2016, **100**(6), 2555−2566.

[86] YIP, Joanne, Liwei LIU, Ka-Hing WONG, Polly H. M. LEUNG, Chun-Wah Marcus YUEN a Mei-Chun CHEUNG. Investigation of antifungal and antibacterial effects of fabric padded with highly stable selenium nanoparticles. *Journal of Applied Polymer Science*. 2014, **131**(17), 1−8.

[87] BEHESHTI, Nasibeh, Saied SOFLAEI, Mojtaba SHAKIBAIE, Mohammad Hossein YAZDI, Fatemeh GHAFFARIFAR, Abdolhossein DALIMI a Ahmad Reza SHAHVERDI. Efficacy of biogenic selenium nanoparticles against Leishmania major: *in vitro* and *in vivo* studies. *Journal of Trace Elements in Medicine and Biology*. 2013, **27**(3), 203−207.

[88] GUISBIERS, Grégory, Humberto H. LARA, Ruben MENDOZA-CRUZ, Guillermo NARANJO, Brandy A. VINCENT, Xomalin G. PERALTA a Kelly L. NASH. Inhibition of Candida albicans biofilm by pure selenium nanoparticles synthesized by pulsed laser ablation in liquids. *Nanomedicine: Nanotechnology, Biology, and Medicine*. 2017, **13**(3), 1095−1103.

[89] SHAKIBAIE, Mojtaba, Hamid FOROOTANFAR, Yaser GOLKARI, Tayebe MOHAMMADI-KHORSAND a Mohammad Reza SHAKIBAIE. Anti-biofilm activity of biogenic selenium nanoparticles and selenium dioxide against clinical isolates of Staphylococcus aureus, Pseudomonas aeruginosa, and Proteus mirabilis. *Journal of Trace Elements in Medicine and Biology*. 2015, **29**, 235−241.

[90] WANG, Qi a Thomas J. WEBSTER. Selenium Nanoparticles Inhibit Various Bacterial Growth on Paper Towels. *MRS Proceedings*. 2014, **1626**.

[91] HUANG, Xiaoquan, Xu CHEN, Qingchang CHEN, Qianqian YU, Dongdong SUN a Jie LIU. Investigation of functional selenium nanoparticles as potent antimicrobial agents against superbugs. *Acta Biomaterialia*. 2016, **30**, 397−407.

[92] TRAN, Phong a a Thomas J WEBSTER. Antimicrobial selenium nanoparticle coatings on polymeric medical devices. Nanotechnology. 2013, 24(15), 155101−155105.

[93] CHUDOBOVA, Dagmar, Kristyna CIHALOVA, Simona DOSTALOVA, et al. Comparison of the effects of silver phosphate and selenium nanoparticles on Staphylococcus aureus growth reveals the potential for selenium particles to prevent infection. *FEMS Microbiology Letters*. 2014, **351**(2), 195−201.

[94] NGUYEN, Trang H.D., Bongkosh VARDHANABHUTI, Mengshi LIN a Azlin MUSTAPHA. Antibacterial properties of selenium nanoparticles and their toxicity to Caco-2 cells. *Food Control*. 2017, **77**, 17−24.

[95] HEGEROVA, Dagmar, Radek VESELY, Kristyna CIHALOVA, et al. Antimicrobial Agent Based on Selenium Nanoparticles and Carboxymethyl Cellulose for the Treatment of Bacterial Infections. *Journal of Biomedical Nanotechnology*. 2017, **13**(7), 767−777.

[96] Komplex biopolymerní látky s nanočásticemi selenu a antibiotickými léčivy s antibakteriálním účinkem. 2014. The Czech Republic. CZ 26981 U1. Registrated 26.5.2014.

[97] ARAHIRA, Takaaki a Mitsugu TODO. Effects of Proliferation and Differentiation of Mesenchymal Stem Cells on Compressive Mechanical Behavior of Collagen/β-TCP Composite Scaffold. *Journal of the Mechanical Behavior of Biomedical Materials*. 2014, **39**, 218−230.

[98] BAUER, E. A., T. W. COOPER, J. S. HUANG, J. ALTMAN a T. F. DEUEL. Stimulation of *in vitro* human skin collagenase expression by platelet-derived growth factor. *Proceedings of the National Academy of Sciences*. 1985, **82**(12), 4132−4136.

[99] AINE, ESKO a PERTTI MÖRSKY. Lysozyme concentration in tears-assessment of reference values in normal subjects. *Acta Ophthalmologica*. 1984, **62**(6), 932−938.

[100] O'BRIEN, F. J., B.A. HARLEY, I.V. YANNAS a L.J. The effect of pore size on cell adhesion in collagen-GAG scaffolds. *Biomaterials*. 2005, **26**(4), 433−441.

[101] YANG, CHUNRONG. Enhanced physicochemical properties of collagen by using EDC/NHS-crosslinking. *Bulletin of Materials Science*. 2012, **35**(5), 913−918.

[102] BABRNÁKOVÁ, J. *The effect of biologically active substances on the structure and properties of collagenous substrates*. Brno, 2016. 108 p. Diploma thesis, Brno university of Technology, Faculty of Chemistry, Institute of Materials Science. Supervisor doc. Ing. Lucy Vojtová, Ph.D.

[103] KACZMAREK, Beata, Alina SIONKOWSKA a Anna Maria OSYCZKA. Scaffolds based on chitosan and collagen with glycosaminoglycans cross-linked by tannic acid. *Polymer Testing*. 2018, **65**, 163−168.

[104] EGAWA, Mariko, Hidenobu ARIMOTO, Tetsuji HIRAO, Motoji TAKAHASHI a Yukihiro OZAKI. Regional Difference of Water Content in Human Skin Studied by Diffuse-Reflectance Near-Infrared Spectroscopy: Consideration of Measurement Depth. *Applied Spectroscopy*. 2016, **60**(1), 24−28.
[105] HILL, Kristina E., Gary W. MCCOLLUM, Martha E. BOEGLIN a Raymond F. BURK. Thioredoxin Reductase Activity Is Decreased by Selenium Deficiency. *Biochemical and Biophysical Research Communications*. 1997, **234**(2), 293−295.
[106] BRODERIUS, M. A., P. D. WHANGER a P. H. WESWIG. Collagenase Activity in Tissues of Selenium Responsive Myopathic Lambs. *Experimental Biology and Medicine*. 1973, **143**(1), 297−299.
[107] YANG, Bin, Jianwu WANG, Bo TANG, et al. Characterization of Bioactive Recombinant Human Lysozyme Expressed in Milk of Cloned Transgenic Cattle. *PLoS ONE*. 2011, **6**(3).
[108] SCHNEIDER, Lars Alexander, Andreas KORBER, Stephan GRABBE a Joachim DISSEMOND. Influence of pH on wound-healing: a new perspective for wound-therapy?. *Archives of Dermatological Research*. 2007, **298**(9), 413−420.
[109] PAPINI, M., S. SIMONETTI, S. FRANCESCHINI, L. SCARINGI a M. BINAZZI. Lysozyme distribution in healthy human skin. *Archives of Dermatological Research*. 1981, **272**(1-2), 167−170.
[110] DOYLE, Barbara Brodsky, E. G. BENDIT a Elkan R. BLOUT. Infrared spectroscopy of collagen and collagen-like polypeptides. *Biopolymers*. 1975, **14**(5), 937−957.
[111] ABE, Yasuaki a S. KRIMM. Normal vibrations of crystalline polyglycine I. *Biopolymers*. 1972, **11**(9), 1817−1839.
[112] NAGAI, Takeshi, Nobutaka SUZUKI, Yasuhiro TANOUE a Norihisa KAI. Collagen from Tendon of Yezo Sika Deer as By-Product. *Food and Nutrition Sciences*. 2012, **3**(1), 72−79.
[113] FERNANDES, Ligia L., Cristiane X. RESENDE, Débora S. TAVARES, Gloria A. SOARES, Letícia O. CASTRO a Jose M. GRANJEIRO. Cytocompatibility of chitosan and collagen-chitosan scaffolds for tissue engineering. Polímeros. 2011, 21(1), 1−6.
[114] JÚNIOR, Zenildo Santos Silva, Sergio Brossi BOTTA, Patricia Aparecida ANA, Cristiane Miranda FRANÇA, Kristianne Porta Santos FERNANDES, Raquel Agnelli MESQUITA-FERRARI, Alessandro DEANA a Sandra Kalil BUSSADORI. Effect of papain-based gel on type I collagen - spectroscopy applied for microstructural analysis. *Scientific Reports*. 2015, **5**(1).
[115] BUTNARIU, Monica. The study of infrared spectrum of chitin and chitosan extract as potential sources of biomass. *Digest Journal of Nanomaterials and Biostructures*. 2015, **10**(4). 1129−1138.

8 LIST OF FIGURES

9 LIST OF TABLES

10 LIST OF ABBREVIATIONS

3D	Three-dimensional
ATR-FTIR	Fourier-transformed infrared spectroscopy with attenuated total reflectance
Coll	Collagen
DDA	Degree of deacetylation
DLS	Dynamic light scattering
DNA	Deoxyribonucleic acid
EC	*Escherichia coli*
ECM	Extracellular matrix
EDC	1-ethyl-3-(3-dimethylaminopropyl)-carbodiimide
EDTA	Ethylenediaminetetraacetic acid
EDX	Energy dispersive x-ray optical analysis
Chit	Chitosan
ICP-OES	Optical emission spectroscopy with inductively coupled plasma
MMPs	Matrix metalloproteinases
MRSA	Methicillin-resistant *Staphylococcus aureus*
NHS	N-hydroxysuccinimide
NPs	Nanoparticles
PBS	Phosphate-buffered saline
PCL	Polycaprolactone
PPII	Polyproline II-type
PU	Polyurethane
PVC	Polyvinylchloride
RM	Regenerative medicine
RNA	Ribonucleic acid
ROS	Reactive oxygen species
SA	*Staphylococcus aureus*
Se	Selenium
SeB	Selenium nanoparticles type SelenBact
SeCh	Selenium nanoparticles type SelenChitosan

SEM	Scanning electron microscopy
SeNPs	Selenium nanoparticles
TEM	Transmission electron microscopy
UV	Ultra-violent

11 LIST OF APPENDICES

12 APPENDICES

12.1 Samples

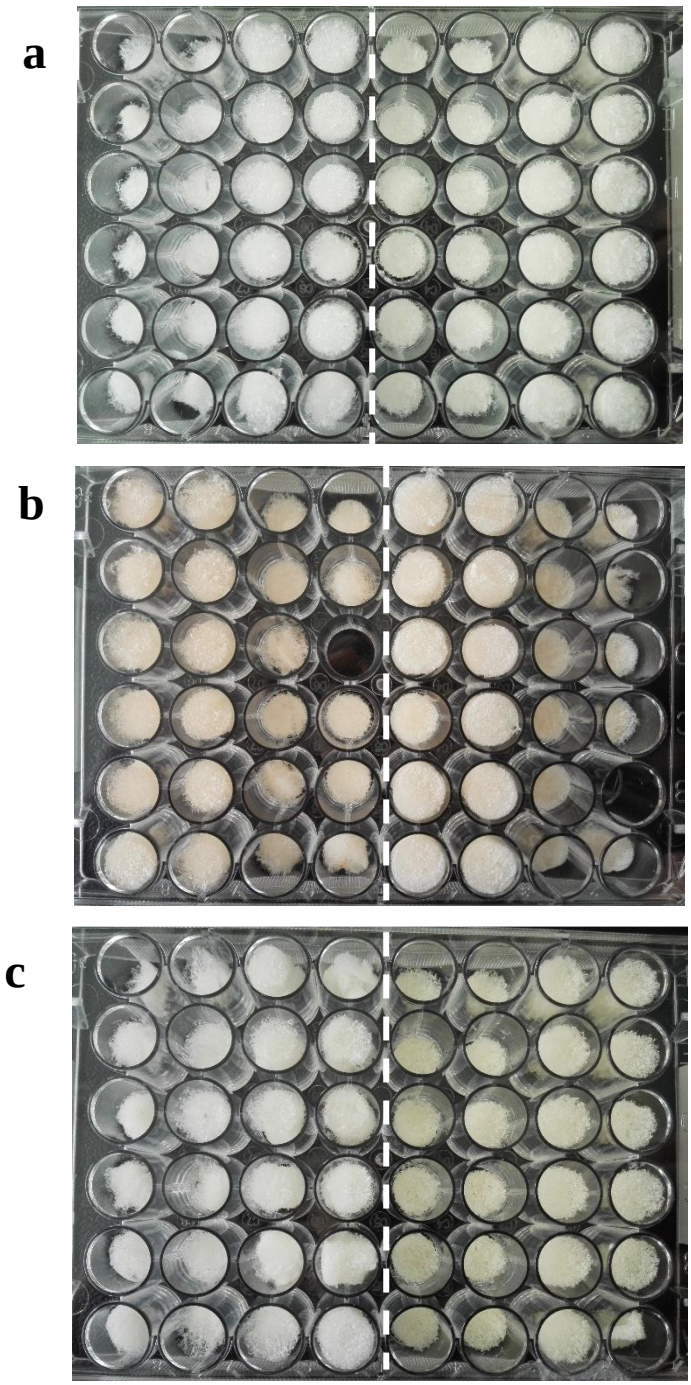

Appendix 1: The first serie of the samples – (a) Coll samples on the left side, Coll/Chit samples on the right side, (b) Coll_SeCh samples on the left side, Coll/Chit_SeCh samples on the right side, (c) Coll_SeB samples on the left side, Coll/Chit_SeB samples on the right side, divided by dashed lines.

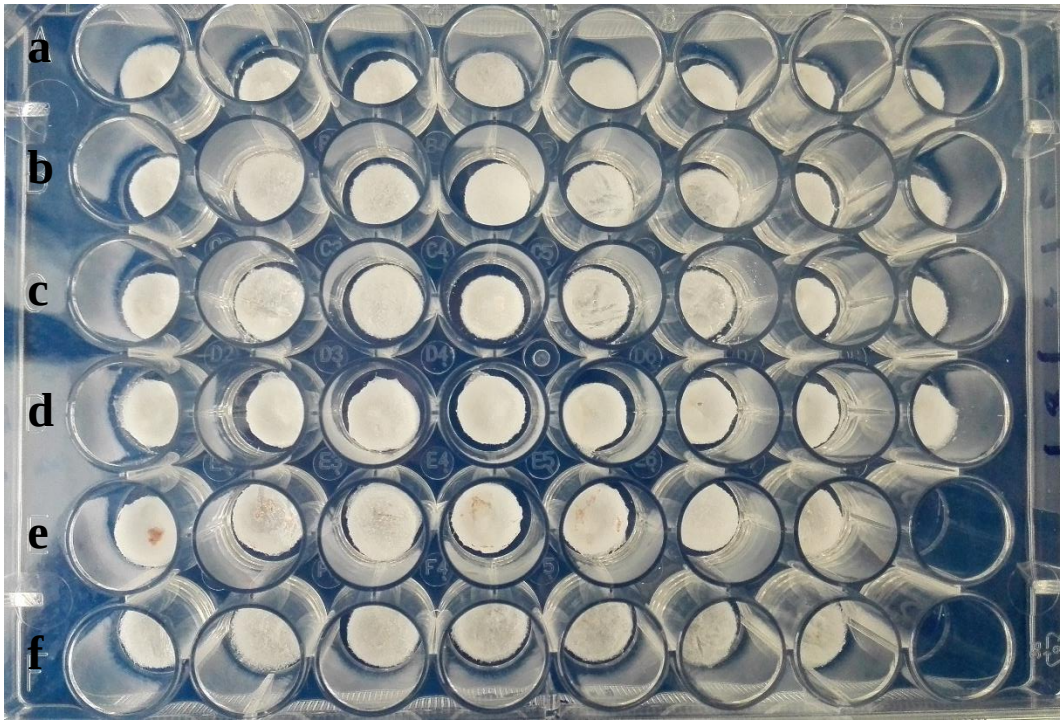

Appendix 2: The second serie of the samples, where each line contains the same type of samples – Coll (a), Coll/Chit (b), 1_Coll/Chit_SeCh (c), 1_Coll/Chit_SeB (d), 5_Coll/Chit_SeCh (e), 5_Coll/Chit_SeB (f).

12.2 EDX Elemental Distribution Mapping

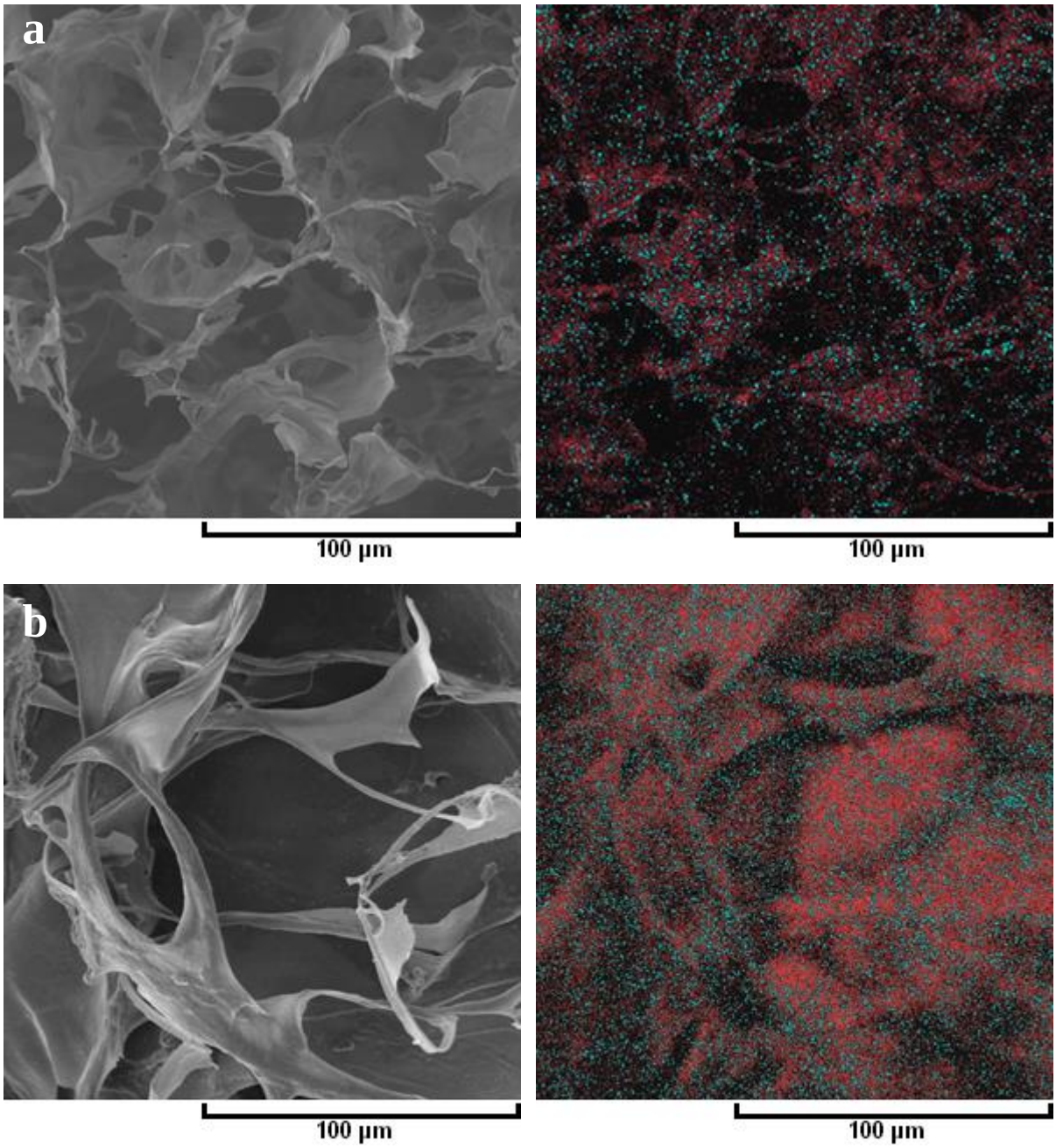

Appendix 3: SEM images (left) and EDX elemental distribution (right) of carbon (red) and selenium (blue) in the samples Coll_SeCh (a) and Coll/Chit_SeCh (b).

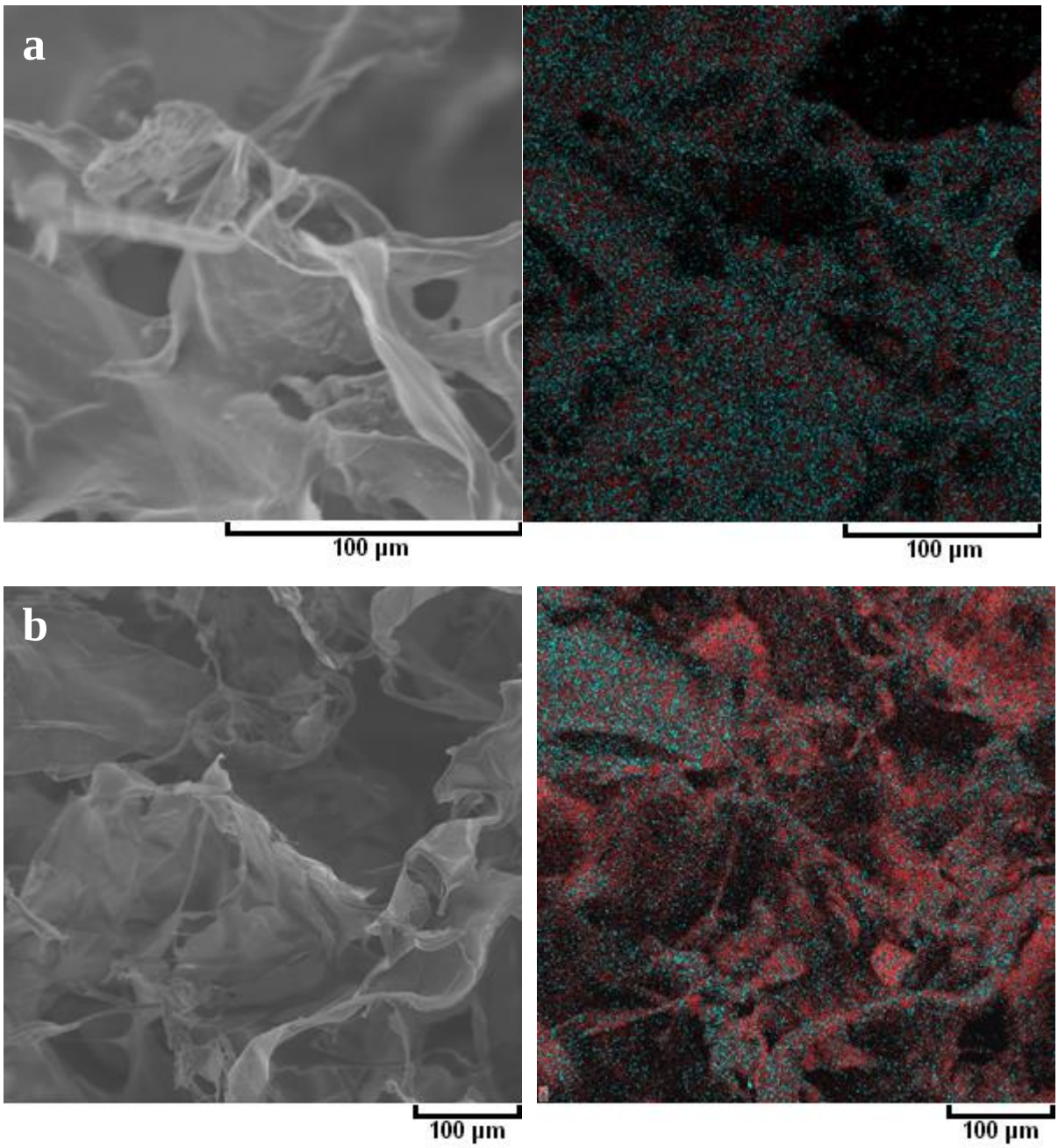

Appendix 4: SEM images (left) and EDX elemental distribution (right) of carbon (red) and selenium (blue) in the samples Coll_SeB (a) and Coll/Chit_SeB (b).

12.3 Pore Size Distribution

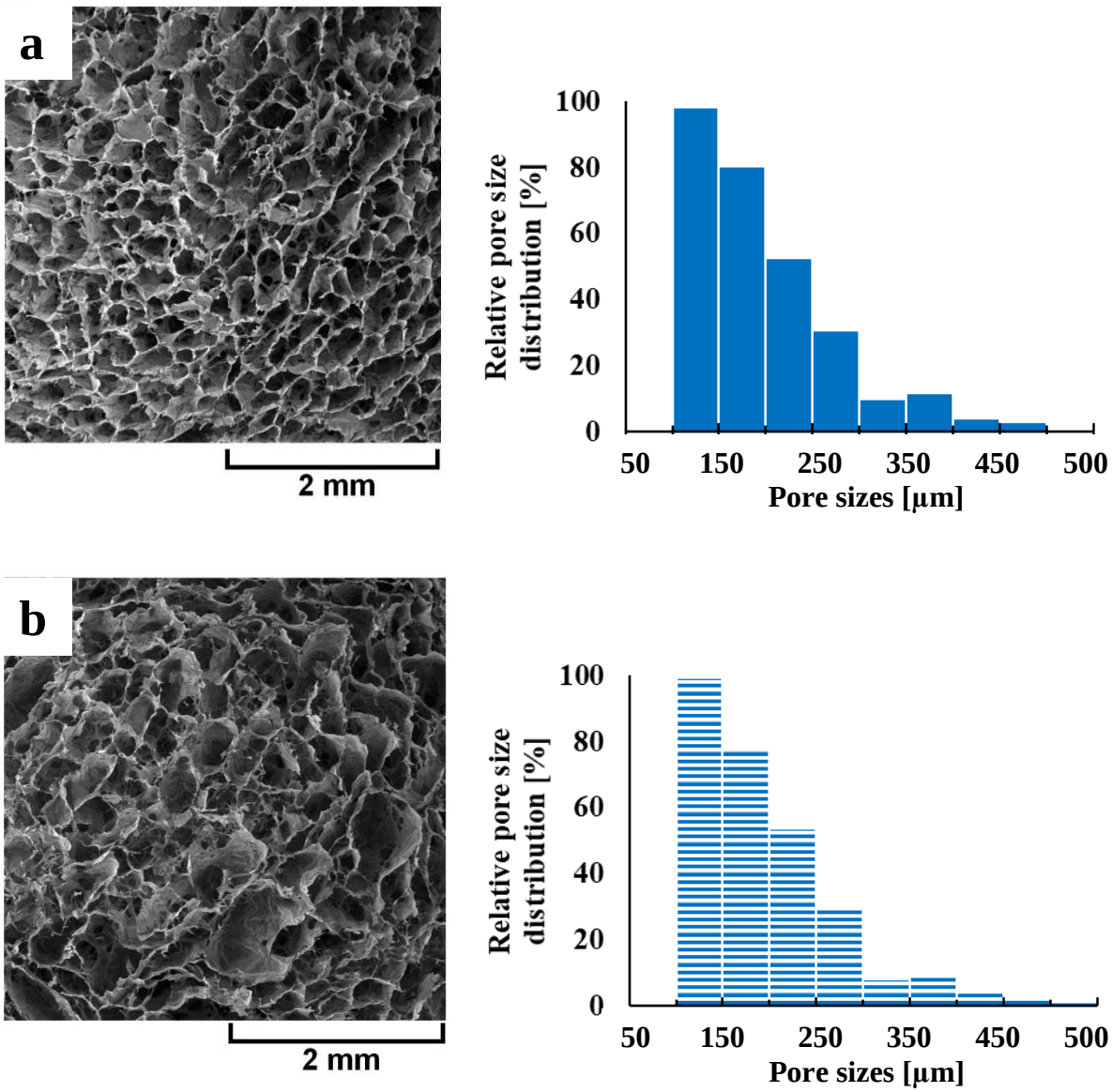

Appendix 5: SEM image (left) and corresponding pore size distribution histogram of the samples – Coll (a), Coll/Chit (b).

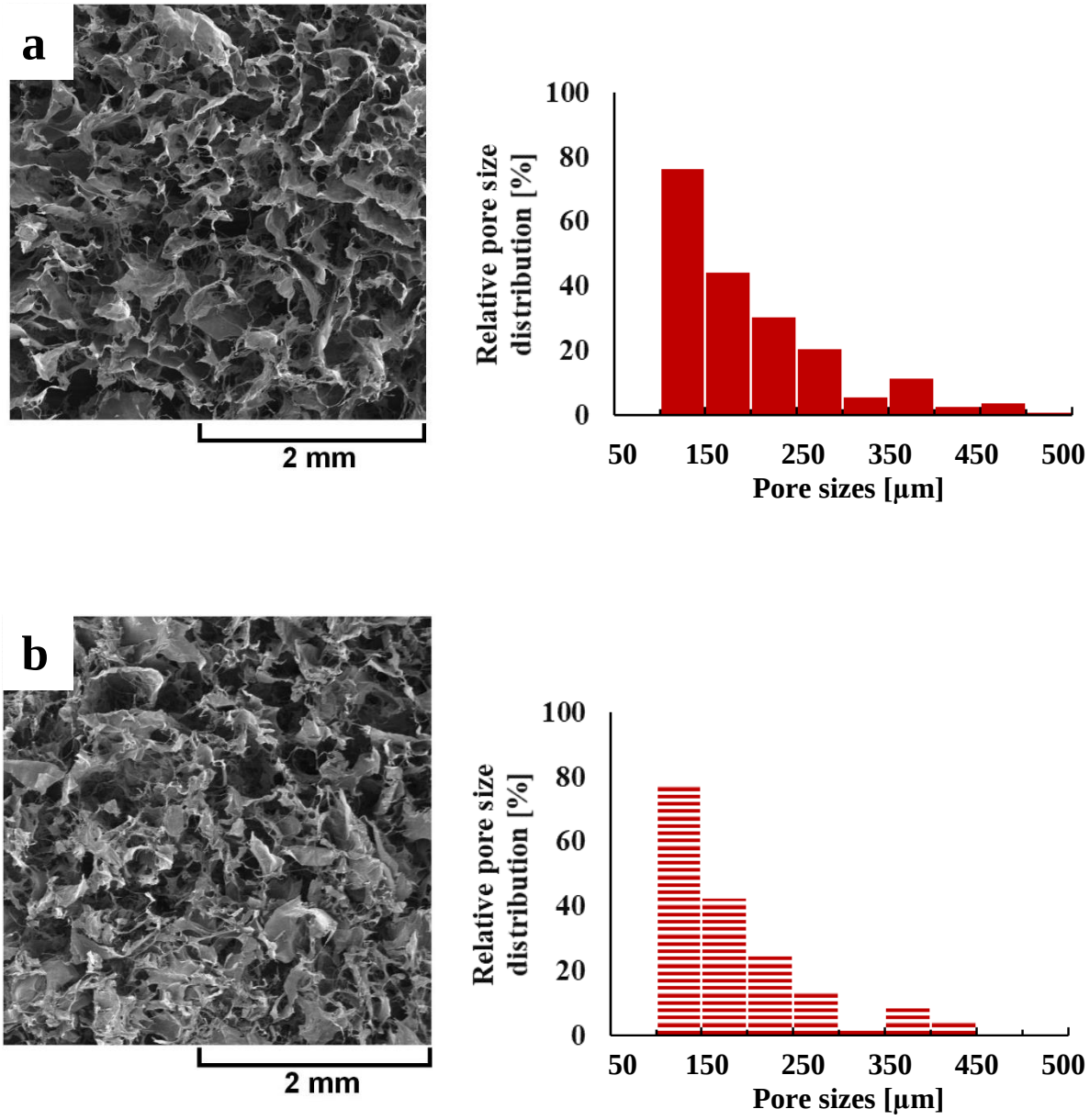

Appendix 6: SEM image (left) and corresponding pore size distribution histogram of the samples – Coll_SeCh (a), Coll/Chit_SeCh (b).

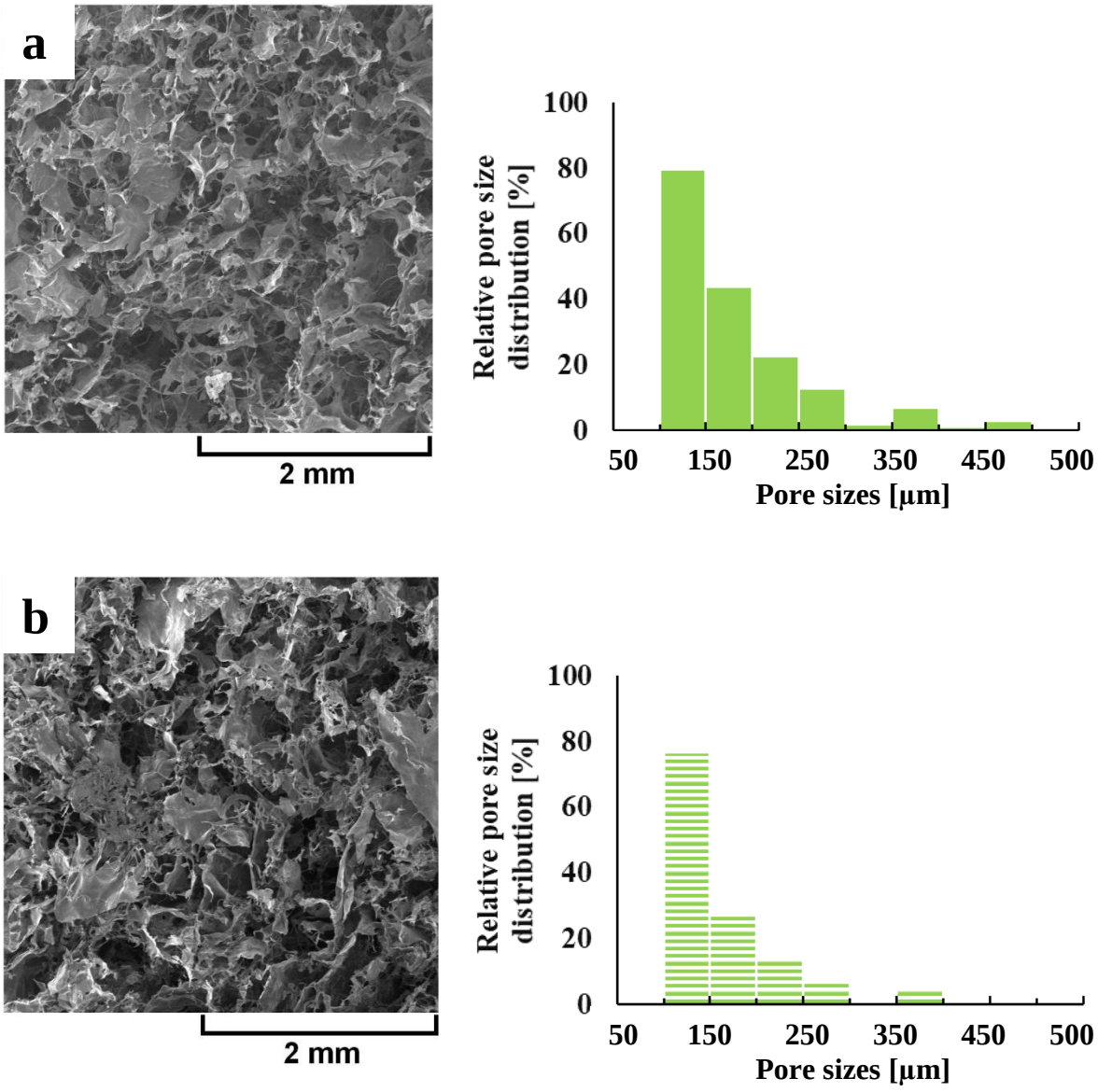

Appendix 7: SEM image (left) and corresponding pore size distribution histogram of the samples – Coll_SeB (a), Coll/Chit_SeB (b).

12.4 Degradation *in vitro*

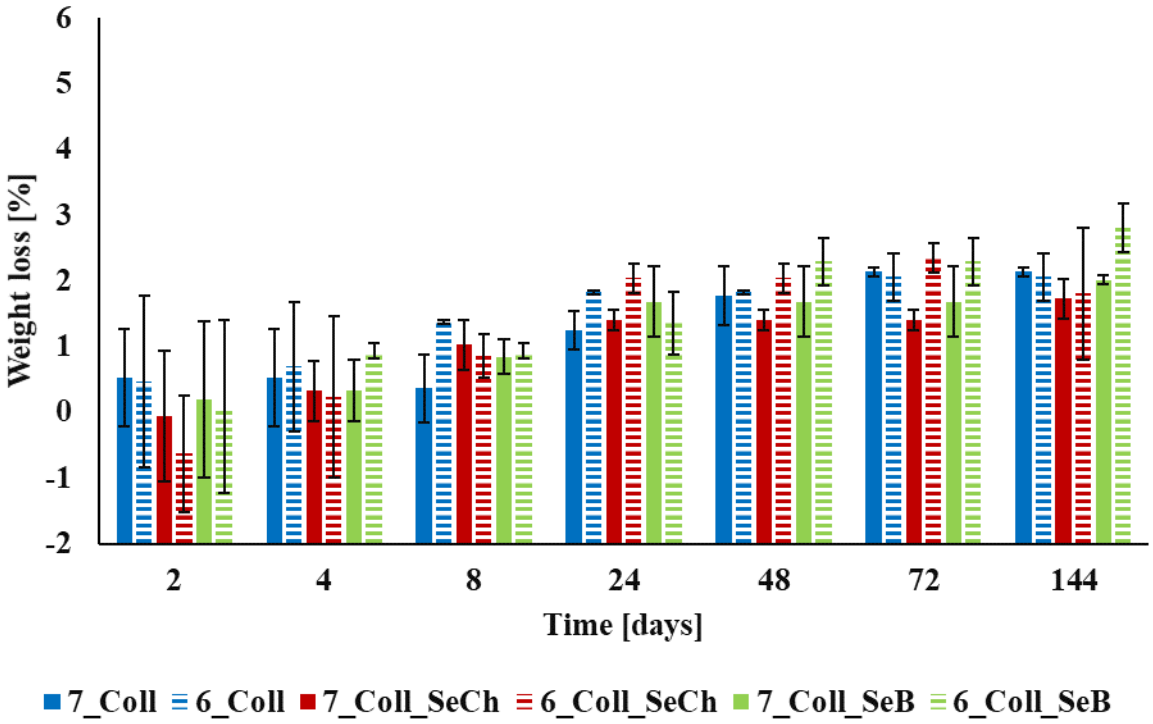

Appendix 8: Enzymatic degradation of collagenous samples enriched with selenium nanoparticles without chitosan in the presence of lysozyme. PBS was used as an environment with pH 7.4 (full column) and pH 6.0 (dashed column).

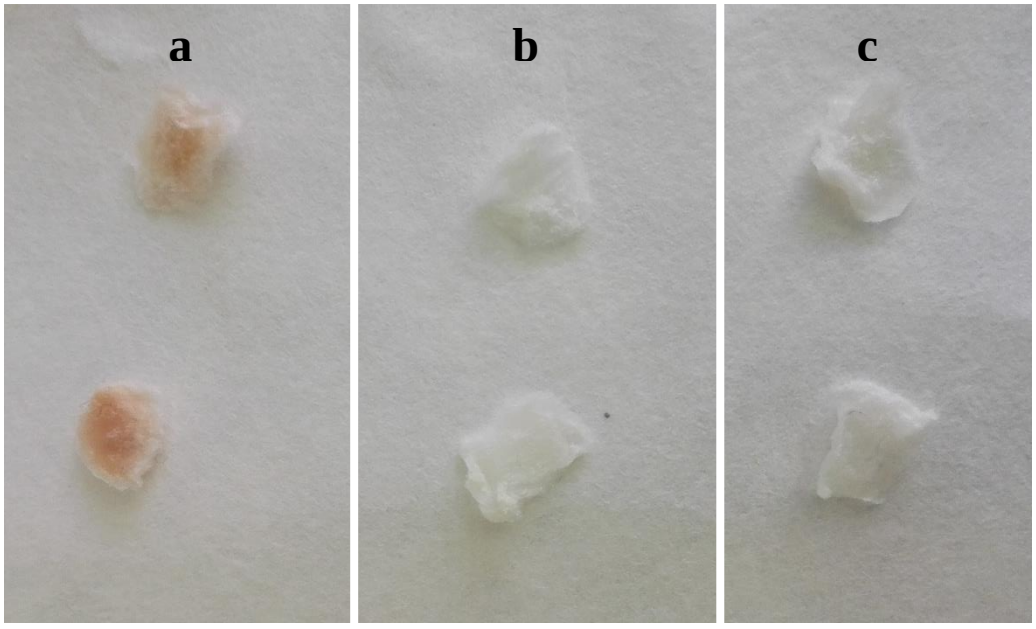

Appendix 9: Orange colouring degradation of selenium nanoparticles type SelenChitosan – (a) the samples in the presence of collagenase – no change, (b) samples in the presence of lysozyme (pH 7.4), (c) samples in the presence of lysozyme (pH 6.0).

12.5 Antibacterial Activity Assay

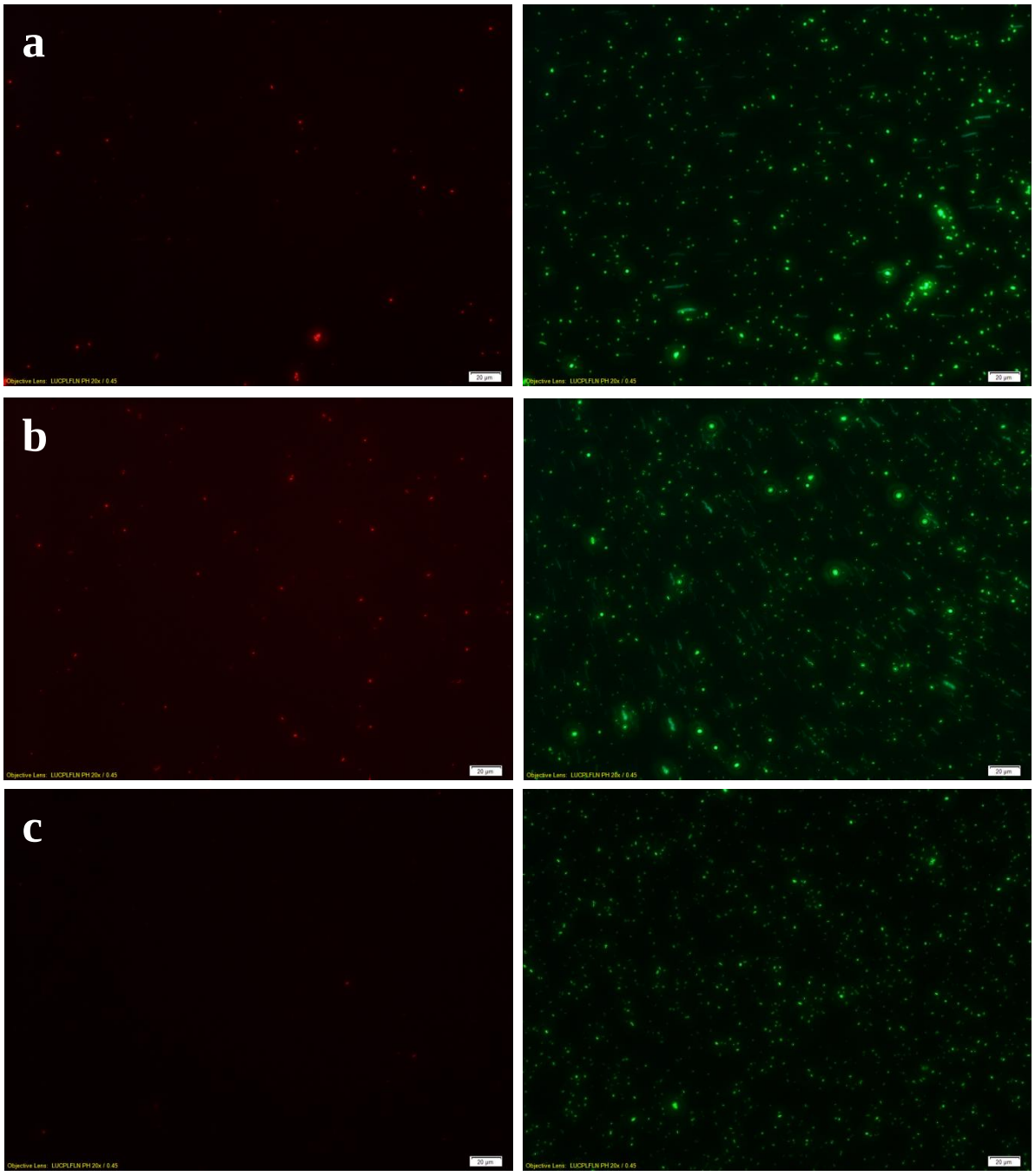

Appendix 10: Live/dead assay images of Coll/Chit (a), Coll/Chit_SeCh (b) and Coll/Chit_SeB (c) samples after their removal from the agar plate covered with E. Coli.

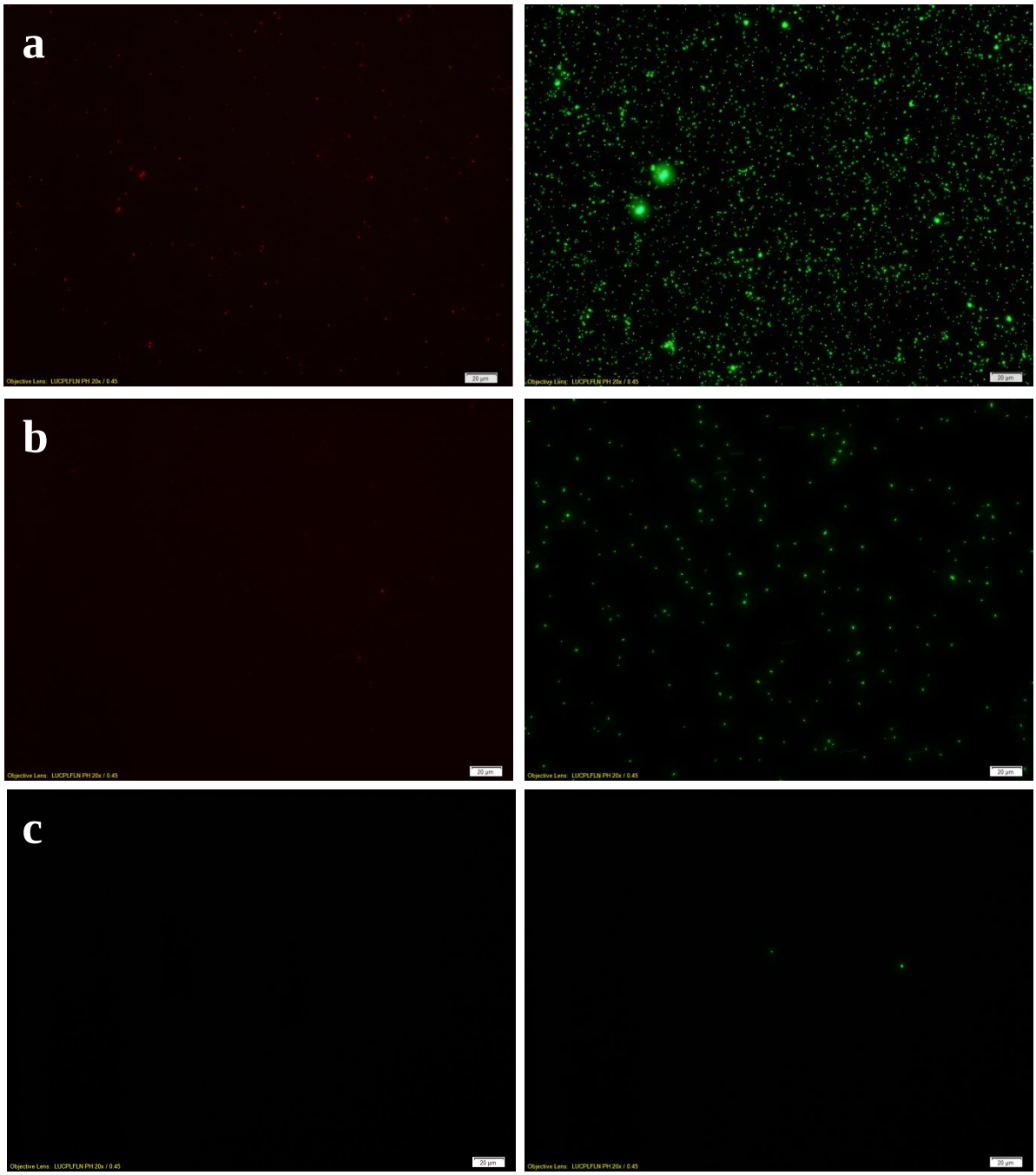

Appendix 11: Live/dead assay images of Coll/Chit (a), Coll/Chit_SeCh (b) and Coll/Chit_SeB (c) samples after their removal from the agar plate covered with SA.

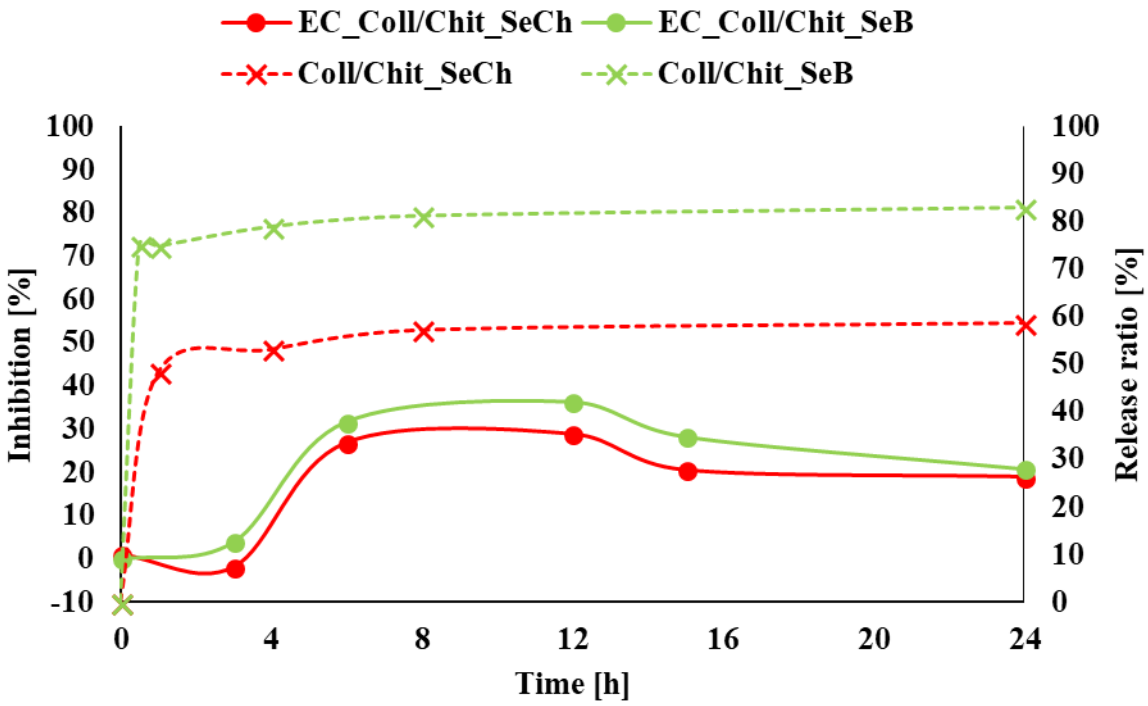

Appendix 12: Combination of time-dependent bacterial inhibition profiles of EC (full lines) and release ratio profiles of SeNPs (dashed lines).

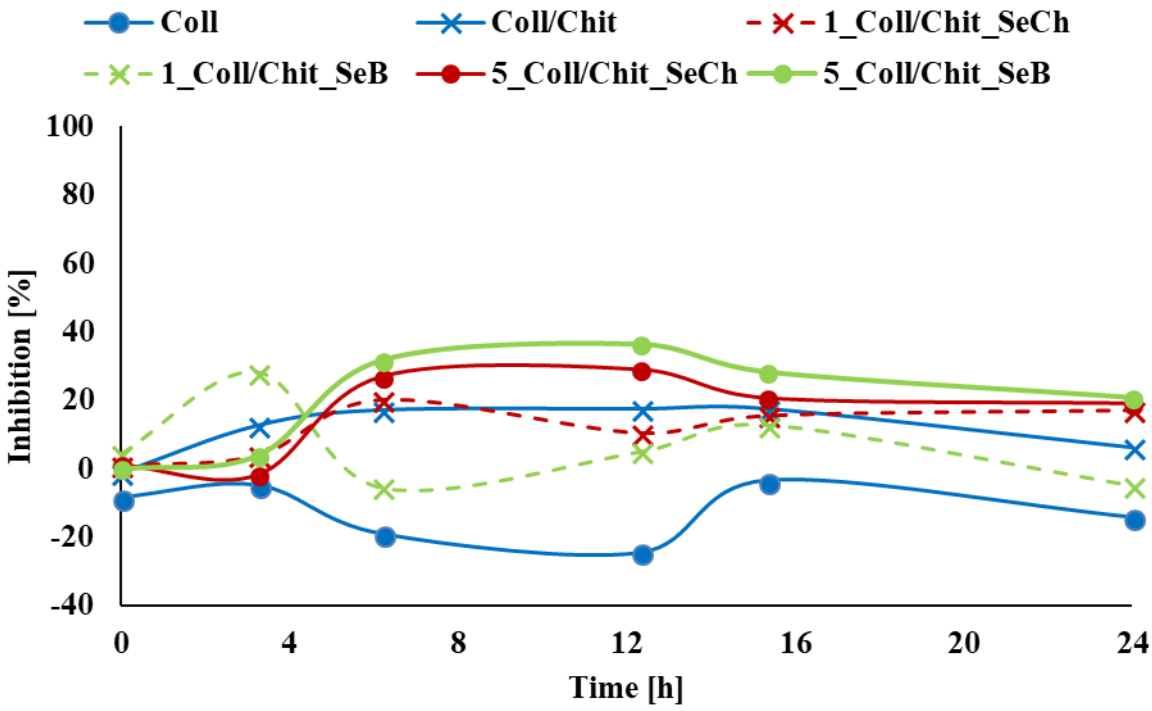

Appendix 13: Time dependence evaluation of bacterial inhibition of EC.

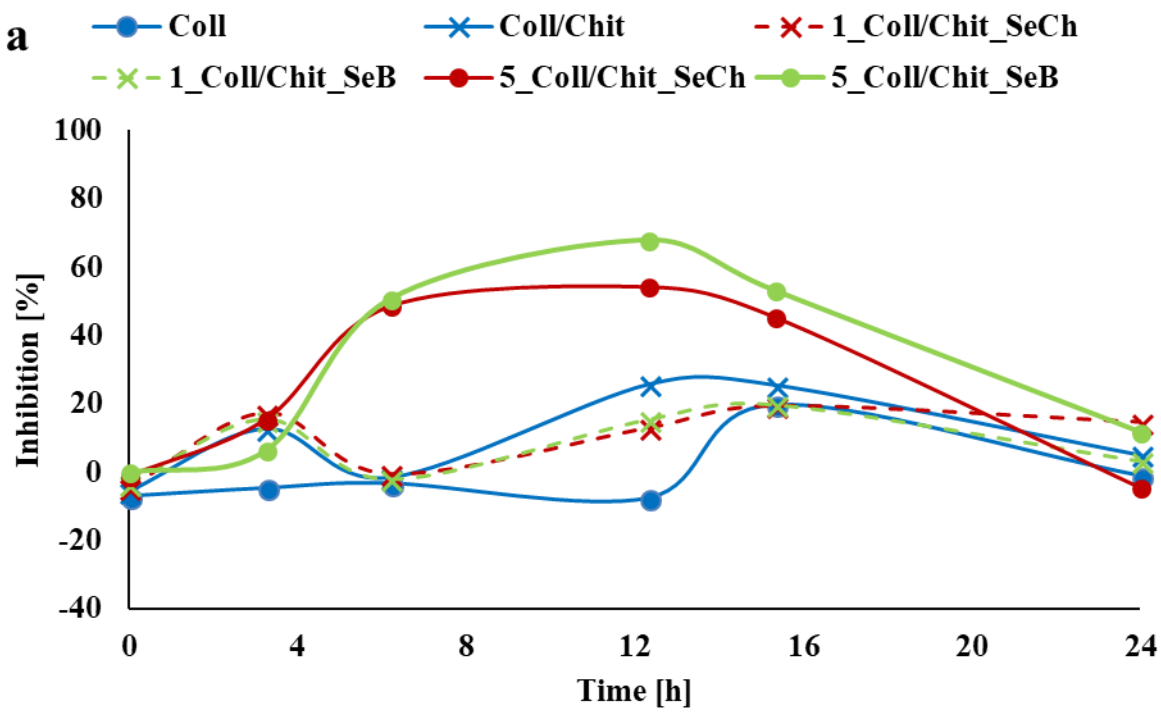

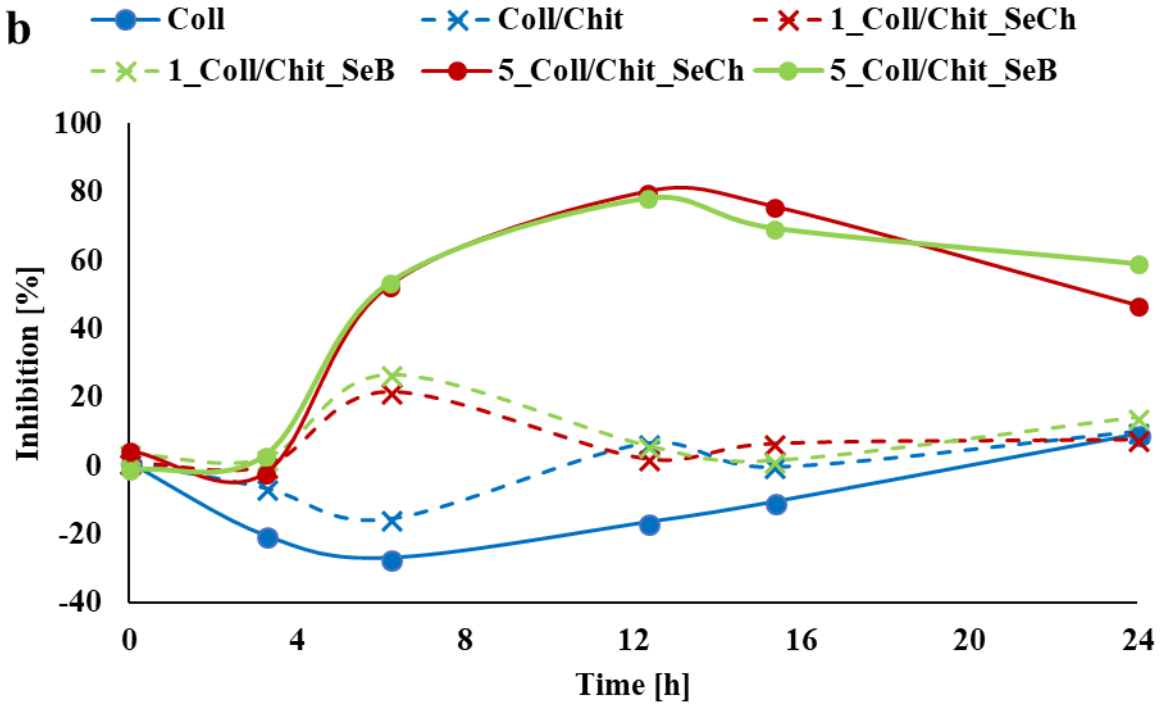

Appendix 14: Time dependence evaluation of bacterial inhibition of SA (a) and MRSA (b).